ANALYSIS OF METAL MATRIX COMPOSITE STRUCTURES USING A MICROMECHANICAL CONSTITUTIVE THEORY

by

Robert Thomas Arenburg

Dissertation submitted to the Faculty of the

Virginia Polytechnic Institute and State University

in partial fulfillment of the requirements for the degree of

DOCTOR OF PHILOSOPHY

in

Engineering Mechanics

APPROVED:

J. N. Reddy, Chairman

J. Aboudi

S. L. Hendricks

E. G. Henneke

E. R. Johnson

D. T. Mook

December, 1988

Blacksburg, Virginia

Analysis of Metal Matrix Composite Structures Using a Micromechanics Constitutive Theory

by

Robert Thomas Arenburg

J. N. Reddy, Chairman

Engineering Mechanics

(ABSTRACT)

The nonlinear behavior of continuous-fiber-reinforced metal-matrix composite structures is examined using a micromechanical constitutive theory. Effective lamina and laminate constitutive relations based on the Aboudi micromechanics theory are presented. The inelastic matrix behavior is modeled by the unified viscoplasticity theory of Bodner and Partom. The laminate constitutive relations are incorporated into a first-order shear deformation plate theory. The resulting boundary value problem is solved by utilizing the finite element method. Computational aspects of the numerical solution, such as the temporal integration of the inelastic strains and the spatial integration of bending moments are addressed. Numerical results are presented which illustrate the nonlinear response of metal matrix composites subjected to extensional and bending loads. Experimental data from available literature are in good agreement with the numerical results.

ACKNOWLEDGEMENTS

I wish to thank my advisor, Dr. J. N. Reddy for his support and advice throughout my graduate studies here at Virginia Tech. Dr. Reddy has extended to me his kindness, understanding and friendship, and for this I am very grateful.

I would also like to extend my appreciation to Drs. S. L. Hendricks, E. G. Henneke, E. R. Johnson and D. T. Mook for the many hours spent serving on my advisory committee. Additionally, I would like to thank Dr. J. Aboudi for his always cheerful personality and our many conversations which proved to be invaluable during the course of this research.

I also wish to acknowledge the support of the Boeing Company provided by their 1987 summer fellowship awarded through the Center for Composite Materials and Structures.

A special thanks to all my friends at Virginia Tech for their help, encouragement and support. Although I have not thanked them individually, their kind friendship is regarded highly.

For her expert typing of the manuscript many thanks go to Mrs. Vanessa McCoy.

Finally, I am most grateful to my parents and family for their continual love, support and encouragement without which this degree would not have been possible. May this be my last degree.

To

for her love, understanding and support

TABLE OF CONTENTS

TABLE OF CONTENTS (CONTINUED)

LIST OF FIGURES

LIST OF FIGURES (CONTINUED)

LIST OF FIGURES (CONTINUED)

LIST OF FIGURES (CONTINUED)

LIST OF TABLES

1. INTRODUCTION

1.1 Motivation

The demanding requirements of high-performance aerospace vehicles in recent years have spurred a new interest in metal matrix composites. These materials offer several distinct advantages over the more common organic polymer matrix composites such as: high thermal/electrical conductivity, no moisture absorption and higher operating temperatures. One aspect of these materials which has hampered their use is the inability to analyze the inherent nonlinear load-displacement response. Efforts by several researchers have focused on the development of constitutive models suitable for metal matrix composites. Few of these, however, have been utilized for structural analysis.

Before metal matrix composite structural components can be seriously considered for aerospace applications, an adequate understanding of their complex behavior is essential. In order to facilitate the investigation of these components, suitable analysis methods are required which can account for the nonlinear behavior characteristic of metal matrix composites. The current need for these analysis methods is the motivation for this research.

In the section which follows, a review of several nonlinear constitutive theories for composite materials is presented. Based on this review, the most promising constitutive theory will be selected for incorporation into an analysis capability suitable for metal matrix structures. In the closing section of this chapter, an overview of the proposed analysis methodology is presented.

1.2 Review of Constitutive Theories

Constitutive theories can be broadly classified by the manner in which the characteristic material inhomogeneities are addressed. For composite materials, microscopic theories examine a representative volume element composed of discrete homogeneous fiber and matrix phases. By the application of mechanics principles the local stress and deformation fields of the volume element can be established. If the scale of the inhomogeneity is small compared to the characteristic dimension of the problem, then the local fields can be averaged to produce effective or equivalent homogeneous lamina properties. This field of mechanics is typically referred to as micromechanics. Alternately, macroscopic theories address the behavior of the composite material wherein the material is presumed homogeneous on a lamina scale. As a result, the macroscopic theories provide no information with regards to the state of the individual constituent phases.

In this section representative microscopic and macroscopic constitutive theories will be reviewed. The purpose of this is to identify the current state of constitutive models suitable for metal matrix composites.

1.2.1 Microscopic Theories

In the field of micromechanics, the behavior of linear elastic and viscoelastic composites is well documented [1,2]. The elastic-plastic behavior characteristic of metal matrix composites, however, has not provided many tractable solutions.

Hill [3,4] is generally recognized as the first to provide a framework for the evaluation of effective moduli of fiber reinforced materials with elastic-plastic phases. Incremental stress-strain expressions in conjunction with a self-consistent micromechanics scheme were used to obtain instantaneous moduli. Bounds were obtained for the overall modulus and the flow stress. The only rigorous solution obtained was for the axisymmetric loading of a transversely isotropic composite cylinder.

An elastic-plastic continuum model for fiber reinforced composites was developed by Mulhern, Rogers and Spencer [5]. Their model regards the composite as transversely isotropic with inextensible fibers and a rigid-perfectly plastic matrix. The yield surface was formulated in terms of invariants, characteristic of the transversely isotropic geometry. The extension of an elastic fiber with an elastic-perfectly plastic coating was considered in Mulhern et al. [6]. The stages of development of the plastic zone in the fiber coating was examined. These were compared to the results obtained by Hill [3]. Hill's solution differed from that of Mulhern et al. in that the fiber coating yielded instantaneously. A comparison of the results from these two solutions showed an insignificant difference. In a later publication [7], the authors generalized their earlier continuum theory [5]. These extensions included incorporation of an elastic fiber and an elastic-perfectly plastic matrix. The assumed yield function was unaffected by normal stress in the fiber direction which eliminated the hysteresis loops found in their earlier work [6].

The assumptions incorporated by Mulhern, Rogers and Spencer [5] made their model easily adaptable to various applications. Spencer [8] extended the theory to a composite reinforced by two families of fibers. This was useful in studying the behavior of composite laminates. The same model was the basis for other applications such as the dynamic analysis of composite beams [9] and large deformation of composite structures [10,11].

Adams and others [12-19] solved various micromechanics problems using numerical techniques. Most of the analyses were based on finite element methods. Typically matrix nonlinearities were modeled by using an incremental plasticity theory. Various effects were addressed such as temperature, moisture and crack propagation. The work performed by Adams and Crane [19] is of particular interest. The inelastic stress-strain behavior of a cross-ply laminate was determined using a finite element micromechanics model for the constitutive relation. While the results presented showed good agreement with experimental tests, the formulation was not presented in a systematic manner which could be applied to general laminates.

Dvorak and his colleagues [20-29] have spent many years researching the behavior of metal matrix composites. One of their earlier works [20] used the finite element method to establish the initial yield surface of a metal matrix composite assuming a hexagonal fiber array. These results were later generalized [20] by introducing a set of stress invariants characteristic of the transversely isotropic geometry. The initial yield surface was found to be an irregular ellipsoid with its longest axis inclined toward the hydrostatic stress axis. Their analy-

sis showed that matrix yielding generally starts at the fiber-matrix interface. The yielding was influenced in the fiber direction by the fiber to matrix moduli ratio and the fiber volume fraction. Transverse to the fiber, the initial yielding was controlled by the matrix yield stress. Hydrostatic stress was shown to cause yielding and volume changes, unlike typical metal behavior. Relatively small temperature changes were shown to produce matrix yielding. Values as small as 70°F were shown to cause initial yielding for a boron/aluminum composite with a 10,000 psi matrix yield stress. Based upon their investigation of initial yield surfaces, Dvorak and Rao [22] developed a simple but accurate continuum plasticity theory for axisymmetric deformation of unidirectional fibrous composites. Assuming elastic fibers with a nonhardening matrix, a simple hardening rule and associated flow rule were formulated. In comparison with a composite cylinder model evaluated by the finite element method for a complex load history, the continuum theory showed very good agreement. Their axisymmetric theory was also applied to analyze uniform temperature changes in a metal matrix composite with considerable success [23].

The elastic-plastic behavior of fibrous composites was explored by Dvorak and Bahei-El-Din [24] using the self-consistent micromechanics scheme [4]. The authors modified the self-consistent scheme to alleviate the problems reported by Hutchinson who observed high estimates of initial yield stress and low plastic strains in the early stages of deformation [30]. To correct this problem, Dvorak and Bahei-El-Din replaced the elastic inclusion by the composite cylinder model from Dvorak and Rao [22]. For the case of axisymmetric mechanical loading,

the modified self-consistent scheme produced similar results predicted by the unmodified self-consistent scheme and the composite cylinder model. For case of initial yielding due to longitudinal shear loading, the modified self-consistent scheme performed well while the unmodified self-consistent scheme encountered some difficulties. Calculations of longitudinal shear loads produced an initial yield stress which was substantially higher than the matrix yield stress. This contradicted the initial yield estimates obtained by finite element analysis [21], which showed the initial yield stress well below the matrix yield stress. While modifications to the self-consistent model were found to improve the performance, their implementation was prohibitively difficult for nonsymmetric loading.

To obtain a general constitutive model and retain computational simplicity, Dvorak and Bahei-El-Din [24,31] introduced a simple micromechanics model, which they called the Vanishing Fiber Diameter Model. This model assumed each of the fibers to have a vanishing diameter while the fiber volume fraction in the composite remained finite. The assumptions resulted in equal fiber and matrix stresses in all directions but the axial direction. In the axial direction, the fiber imposes a deformation constraint on the matrix which produces equal axial normal strains in the fiber and matrix. The simplicity of this model allows for the easy incorporation of any matrix material nonlinearity. Bahei-El-Din [30,26-29] incorporated the Vanishing Fiber Diameter Model with a Mises-type matrix material which obeys the Prager-Ziegler kinematic hardening rule. This constitutive model was used in classical lamination theory and in a three-dimensional finite element analysis code,

PAC78. In order to obtain good correlation with experimental results, Bahei-El-Din used in situ matrix properties since the unreinforced matrix properties yielded poor results. Initial yield surfaces computed for a cross-ply laminate showed reasonable agreement when compared to results obtained by the finite element method from Rao [32]. Experimental results for an axially loaded laminate were compared to the results from PAC78 [27]. The predicted strains in the load direction showed very good agreement, however, the strains in the transverse direction were overestimated. The authors suggested this discrepancy could be a result of neglecting the fiber-matrix interaction in the transverse direction.

Min and Crossman [33] used a plane stress mechanics of materials model for the elastoplastic deformation analysis of unidirectional composites subjected to both thermal and mechanical loading. The model explicitly accounts for the microstresses and the thermal residual stresses but only for a nonhardening matrix. The model of Min and Crossman was extended by Min and Flaggs [34,35] who added a White-Besseling plasticity model [36] for the matrix material. The deformations induced by thermal cycling of a unidirectionally reinforced graphite/magnesium composite were examined by Wolf, Min and Kural [40]. The authors used the mechanics of materials model developed by Min and Flaggs [34,35] to analyze the complex thermal load history. The comparison between this analysis and experimental data was poor. The authors attributed the difference to temperature dependence of the matrix yield stress and matrix creep which were ignored in the analysis.

Ruffin, Rimbos and Bigelow [41] developed an elastic-plastic point stress laminate analysis program called MLAP. Their program was formulated using the Vanishing Fiber Diameter Model and a kinematic hardening Mises-type matrix material based upon Dvorak and Bahei-El-Din [26,29]. Comparison of experimental results and predictions by the MLAP program showed fair agreement. The MLAP program over predicted the transverse strains which seems to be characteristic of the Vanishing Fiber Diameter Model.

Aboudi, in a series of investigations [39-48], presented a micromechanics model based on a higher-order continuum theory. The theory is very versatile in that it can account for:

1) particulate, short or continuous fiber reinforcement,
2) general mechanical and thermal load histories,
3) quasi-static or dynamic impact loading rates, and
4) damage in the form of fiber-matrix debonding.

Aboudi [43] modeled fiber reinforced metal matrix composites as transversely isotropic fibers of rectangular cross section arranged in a doubly periodic array. The matrix surrounding the fibers was modeled as an isotropic viscoplastic material by using the unified viscoplastic theory of Bodner and Partom [49]. Due to the periodic fiber/matrix arrangement only a representative unit cell need to be considered. The representative cell was subdivided into four rectangular subcells, one for the fiber and the remaining three for the matrix material. This allowed the displacement field to be expanded in terms of an n^{th} order Legendre series within each of the subcells. Displacement continuity relations were developed by requiring the displacements to be continuous

at the subcell interfaces in an average sense. The governing differential equations for the n^{th}-order continuum theory were obtained by taking moments of the equations of motion. Consequently, field quantities such as stresses were replaced by moments of stresses. Solutions are obtained by solving the higher-order equations of motion, the displacement continuity relations and appropriate traction boundary conditions.

In order to predict average behavior of a composite only a first-order displacement expansion was required. Results for the first-order theory showed good agreement with other micromechanics solutions and experimental data. Comparisons of the inelastic behavior were made to conventional finite element solutions by Foye [50] and Hashin and Humphreys [51]. These indicate good agreement, especially in the transverse direction.

In this section a broad overview of various micromechanically based constitutive theories is presented. Many of the theories have certain limitations while others are more complete. The following list provides some of the highlights of the theories reviewed in this section:

- Rigid fibers assumed [5]
- Nonhardening matrix behavior [5,33]
- Restricted loading conditions [6,22,23]
- Numerical solution accounting for various effects [12-19]
- Based on simple closed-form micromechanics formulation [26], includes nonisothermal behavior [35,38]
- Rectangular fiber cross section assumed, includes viscoplastic matrix and thermal effects [39,40,42,45]

1.1.2 Macroscopic Theories

One of the first attempts to analyze the nonlinear behavior of composites at the macro level was performed by Petit and Waddoups [52]. The authors considered uncoupled nonlinearities in the longitudinal, transverse and shear directions which acted independently during combined loading. Failure of individual plies was determined by a maximum-strain criterion. The authors made certain assumptions about the behavior of the failed plies. Transverse ply failure implied that load could still be carried in the longitudinal or shear directions. Similarly, shear failure implied that load could still be carried in the longitudinal or transverse directions. Longitudinal failure, however, implied a total ply failure and no further load carrying capability. The authors incorporated these principles into a lamination analysis program. The plies were allowed successive failures until the laminate ultimately failed. The correlation with experimental results for stress-strain response was fair to good, but the failure predictions were generally poor.

Hahn and Tsai [53] modeled nonlinear shear response of a composite by introducing a complimentary elastic energy density function. A polynomial expansion of the complementary elastic energy density function was performed. In addition to the second-order terms which describe the linear elastic behavior, one fourth-order term was retained to describe the nonlinear shear behavior. The application of this model to unidirectional [53] and multidirectional composite systems [54] produced fair results.

Hashin, Bagchi and Rosen [55] used a Ramberg-Osgood representation of lamina transverse and shear stress-strain curves in conjunction with a deformation theory to describe the nonlinear laminate behavior. The lamina was assumed to be linear elastic in the fiber direction. The inelastic compliance was assumed to be a function of the transverse and shear stresses only. Comparison with experimental results provided fair results for the stress-strain behavior.

Jones and Nelson [56], using a deformation theory of plasticity, developed a nonlinear model to describe the biaxial softening behavior of ATJ-S graphite. The authors used a generalization of the Ramberg-Osgood stress-strain relations to represent the material properties. A strain energy density function was introduced to relate the uniaxial material properties to the multiaxial stress state. Biaxial test data showed good correlation with model predictions. The theory was later adapted to unidirectional laminates [57] with limited success.

The anisotropic plasticity theory of Hill [58,59] has influenced many subsequent researchers. Hill originally proposed his theory to model the weakly orthotropic behavior typically found in cold-rolled metals. The theory assumed yielding was independent of hydrostatic stress and plastic flow was incompressible, which are standard assumptions for metals. A generalization of the von Mises yield criterion was formulated in which the yield criterion was not expressed in terms of stress invariants. As a result of this, the criterion was defined only with respect to the principle axes of anisotropy.

Several authors have suggested extensions to Hill's theory. Hu [60] and Jensen et al. [61] proposed work hardening rules. Dubey and

Hillier [62] developed a more general yield criterion and associated flow rule based upon invariant principles. Shih and Lee [63] formulated a simple extension which allows distortion of the yield surface and variations of the anisotropic yield parameters during deformation.

Pifko, Levine and Armen [64] developed a three-dimensional finite element program for the inelastic analysis of composites. Heuristic arguments were used to develop a simple normality condition and kinematic hardening rule.

Chou and Chou [65] developed a plastic flow rule for laminated composites within the context of a three-dimensional lamination theory [66]. The authors used a generalization of the Mises yield criterion. In addition, a Henchy stress-strain expression [59] was incorporated to describe the evolution of the plastic strain components. Proportional loading of a composite with a bilinear stress-strain relation was examined. These assumptions allowed the development of analytical expressions for the response of the composite without resorting to numerical evaluation. The authors stated that their theory was general enough to be incorporated into an incremental formulation but the resulting nonlinear equations for the overall stresses would require a numerical solution.

Renieri and Herakovich [67] used quasi three-dimensional finite element analysis to examine the thermomechanical response of composite laminates. In their analysis, nonlinear material behavior was introduced by a Ramberg-Osgood expression for material properties, but no stress interaction was assumed.

Griffin [68] developed a three-dimensional finite element program for the analysis of composite materials. An incremental approach was used which incorporated Hill's anisotropic theory of plasticity and second-order thermal effects. Analysis of unidirectional off-axis laminates showed generally good agreement with experimental data. As a result of the three-dimensional formulation, the variety of laminates and structural configurations examined were limited by the available computer resources.

Chandrashekhara [69], using the finite element method, introduced a version of Hill's anisotropic plasticity model into a geometrically nonlinear shell theory. The author demonstrated the versatility of the finite element method by solving a large variety of static and dynamic problems. Unfortunately, the lack of available experimental data made it impossible to determine the accuracy of the modified Hill plasticity model used in the analysis.

Pindera and Herakovich [70] extended Valanis' endochronic theory of plasticity [71] to transversely isotropic media. Their theory was based on the internal variable formalism employed within the context of classical irreversible thermodynamics. The authors demonstrated the accuracy of their theory by modeling various phenomena such as dissipative response in the shear and the transverse directions, permanent strain accumulation, nonlinear loading and reloading and stress interaction effects.

Russian researchers, Zinov'ev and Sarbaev [72] presented a generalization of the endochronic theory. Incremental stress-strain relations were presented in which the total strain tensor was uncoupled into

elastic and inelastic strain components. The inelastic strains were characterized by a set of intrinsic time scales, characteristic of the endochronic theory. Results for proportional loading showed fair agreement. The authors did not address the incorporation of complex load histories into their model.

Recently, Wren and Allen [73] developed a constitutive model for the inelastic deformation of a metal matrix composite with damage. The model is still in the developmental stage while a suitable damage growth law is being formulated.

In this section a broad overview of various macromechanically based constitutive theories is presented. Many of the theories have certain limitations while others are more complete. The following list provides some of the highlights of the theories presented in this section:

- Nonlinear elastic analysis without stress interaction for multiaxial load conditions [52,53,67]
- Deformation theory of plasticity [55,56,57]
- Generalization of Hill's anisotropic theory of plasticity [62,63,64,68,69]
- Endochronic and other theories based upon the internal state variable formalism of irreversible thermodynamics [70,72,73]

1.2.3 Discussion of the Constitutive Theories

In order to select a constitutive model which would be suitable for structural analysis, certain minimal requirements are needed. Obviously, the theory must be valid for any general type of mechanical loading. Also, thermal loading must be included since metal matrix

composites are primarily used at elevated temperatures and for thermally stable structures. Another requirement is the capability to model complex load histories. While not as important as the first two requirements, this capability would be required for any type of dynamic analysis or thermal cycling.

In view of the previously stated requirements, the micromechanics based theories seem the most complete. Most of these theories satisfy the requirements of general mechanical and thermal loadings. General load histories could be addressed if an appropriate inelastic material model was selected for the matrix. The accuracy of the micromechanics theories have demonstrated certain problems, especially in predicting transverse material properties. The theory of Aboudi seems most promising in this regard. In addition, Aboudi's theory has been extended to include damage in the form of fiber/matrix debonding. The use of relatively conventional finite element formulations for constitutive relations, such as those of Adams and Crane [19], also must be disregarded because they would result in models which would be computationally too intensive for structural analysis.

One other advantage of a micromechanically based theory should be mentioned. In the preliminary design phase, new fiber/matrix combinations must often be evaluated prior to extensive characterization. If laminate material properties are limited, then a macroscopic model could be of little or no use. However, if the constituent materials have been characterized, then a micromechanics based theory could provide estimates of the composite behavior.

The macroscopic constitutive theories demonstrate considerable promise, most notable of these theories is the endochronic theory of Pindera and Herakovich [70]. Unfortunately, the endochronic theory has not been extended to include thermal effects. The only other macroscopic constitutive theory which would be suitable is the anisotropic theory of plasticity by Hill. This particular theory has been studied by many other researchers and further examination of it is not warranted.

1.3 Present Study

The emphasis of the present research is the development of suitable analysis methods which will accurately predict the nonlinear response of metal matrix composite structures. For this purpose the micromechanics theory of Aboudi has been selected for the composite constitutive theory. This theory has many attractive features which are responsible for its selection such as the suitability of the theory for a variety of reinforcement geometries, relatively few material parameters required for characterization, ability to account for imperfect fiber/matrix bonding and overall computational simplicity.

The various stages of the analysis are depicted in Fig. 1.1. The analysis process has two distinct aspects which are referred to as composition and decomposition. In general, composition can be defined as the progression of the analysis from smaller scales to larger scales. Decomposition is simply the composition process in reverse.

The composition process begins at the micro scale with individual homogeneous fiber and matrix phases. Micromechanics is used to evaluate

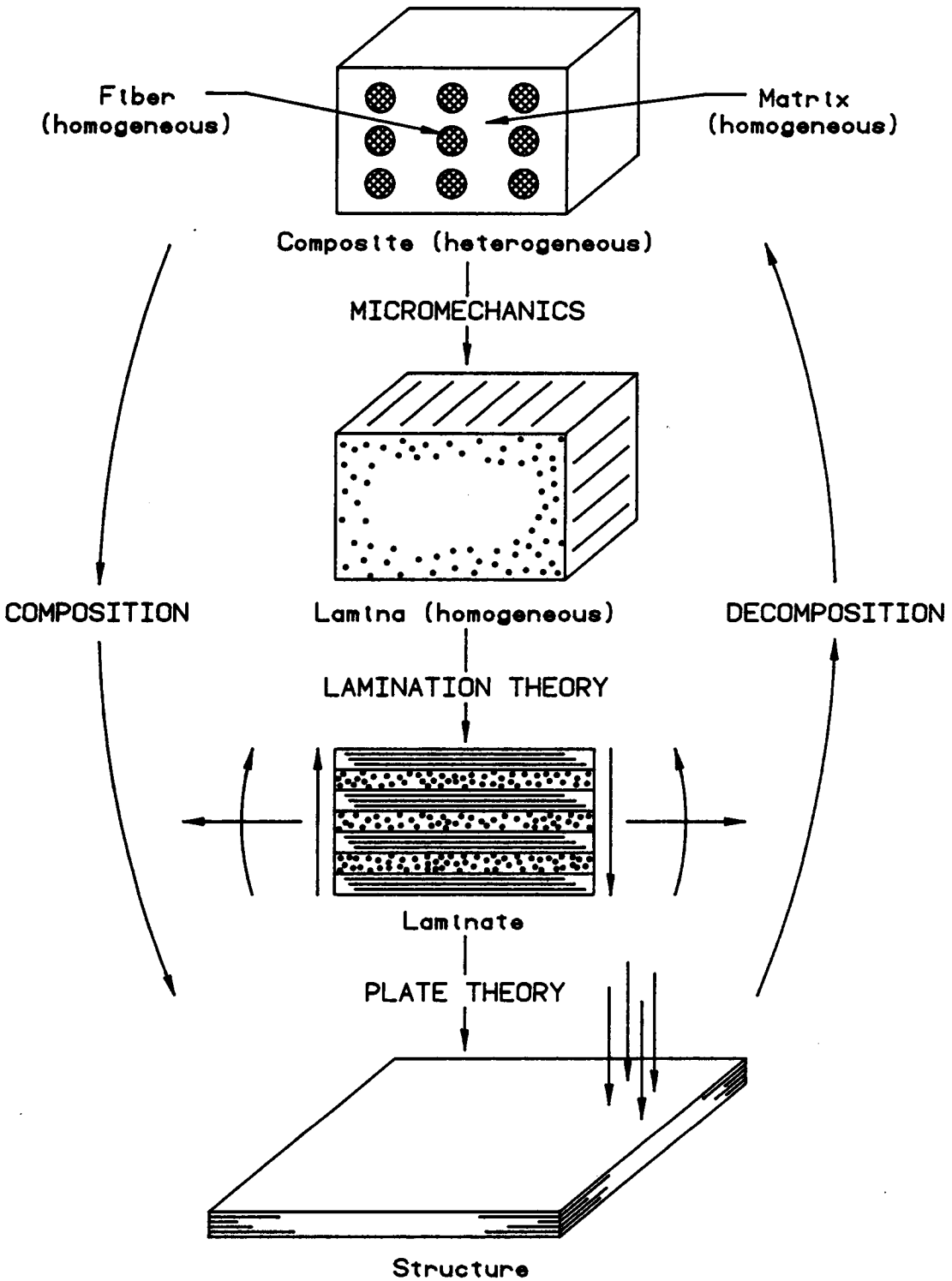

Figure 1.1. Composition/Decomposition Process

the effective homogeneous behavior of the individual phases. This results in is the first scale transition, from the micro scale to the lamina scale. In the composition process, the effect of the fiber and matrix have been averaged such that on this scale the lamina appears as a homogeneous anisotropic media.

At this point a decision is required regarding the type of structural analysis to perform. Due to the preliminary nature of this study, three-dimensional analysis was dismissed because it would be computationally too expensive. This in turn would result in limiting the type and variety of the structures which could be examined. With regards to the general types of two-dimensional theories, a laminated plate theory was selected due to its simplicity and its ability to model the geometries found in most test coupons.

The next scale transition is from the lamina to the laminate scale. This consists of assembling several lamina into a laminate via the use of lamination theory. At the laminate scale, the integrated response of all the laminae is obtained by eliminating the dependence on the thickness coordinate. Fundamentally this provides the constitutive relation for a typical differential element of the laminate. The final scale transition to the structural scale is performed through the utilization of plate theory. This transition requires the solution of a boundary value problem for the displacement field associated with the equilibrium position of the plate. The solution of the boundary value problem is performed numerically by using the finite element method.

After the displacement field is obtained for the structure, the reverse process, decomposition, is performed. From the displacement

field at the structural scale, the midplane strains, curvatures and stress resultants are obtained at the laminate scale. Next the average lamina stresses and strains are computed by using the lamina constitutive relations. Finally, the fiber and matrix stresses are established by using the micromechanics theory.

The nonlinear material response characteristic of metal matrix composites is attributed primarily to yielding in the matrix material. To account for this behavior, a viscoplastic material model is incorporated into the Aboudi micromechanics theory. Due to the inelastic behavior of the matrix material, the structural analysis is performed in an incremental fashion. For each increment the effect of the inelastic matrix strains is transformed from the micro scale to the structural scale by the composition process. At the structural scale, the plate boundary value problem is solved including the effects of the inelastic matrix strains. The decomposition process is then used to evaluate the matrix stress state at the micro scale. With the matrix stresses known, the inelastic strains are determined for the next increment in the solution where the process is repeated.

Now that the overall analysis methodology has been presented, a detailed examination of the individual components is required. In the following chapter, a review of the Aboudi micromechanics theory for continuous fiber reinforced materials is presented. The third chapter will address the development of the laminated plate constitutive relations and the solution of the laminated plate boundary value problem. The fourth chapter presents numerical results of the theory developed in

Chapter 3. The concluding chapter summarizes the findings and provides recommendations for future work.

2. MICROMECHANICS

2.1 Background

In this chapter, the micromechanics theory which is used for the analysis of continuously reinforced metal matrix composites will be presented. The chapter begins with a brief introduction to the micromechanics effective modulus theory followed by the development of the governing equations used in the Aboudi theory. These governing equations are then solved to obtain the effective lamina constitutive relations.

In general, all materials are heterogeneous. The only question which remains is the scale at which the heterogeneities are observable. Certainly one would agree that this statement is true if a material is examined at the atomic or molecular scale. In continuously reinforced composite materials, the smallest scale at which both constituent phases are observable will be referred to as the micro scale. The size of a particular scale can be defined in terms of a characteristic dimension. The mean fiber spacing is a suitable characteristic dimension for the micro scale. If the composite is examined on a scale an order of magnitude larger than the micro scale, the individual fiber and matrix phases would be indistinguishable. This scale will be referred to as the lamina scale. Since the individual phases are not readily observable, this suggests replacing the composite material with a homogeneous material which responds on average identically to the original composite. At this point, the basic problem can be stated. Utilizing an averaging process, we want to predict the equivalent homogeneous

material properties of a composite given the constituent phase material properties and phase geometries.

In order to develop the required averaging process, a mathematically rigorous approach will be abandoned in favor of a physically based development. Consider an experimentalist who is faced with the task of determining the properties of a material. Test coupons will be fabricated which are designed to produce uniform stress and strain fields within the gage section. To determine the Young's modulus of a homogeneous material, an axial load P is applied to the test coupon which results in a uniform stress σ in the gage section. Based on measurements of the deformation field, the strain is found to be uniform with a magnitude ε. From this information the Young's modulus can simply be calculated as σ/ε.

If the material was heterogeneous instead of homogeneous, then the applied load P would result in nonuniform stress and strain fields within the gage section. Since the stress and strain fields are varying spatially the Young's modulus cannot be determined directly, however, by averaging the stress and strain fields over a suitable volume the effective or average Young's modulus can be determined.

Using the previous simple example as a guide, we can generalize the averaging process by considering a suitable volume V with bounding surface S. When the body is loaded by prescribed surface tractions T_i^o on S which would result in a uniform stress field for a homogeneous material, the effective compliance $S^*_{ijk\ell}$ of a heterogeneous material can be defined through the relation

$$\bar{\varepsilon}_{ij} = S^{*}_{ijk\ell}\, \bar{\sigma}_{k\ell} \tag{2.1}$$

where the average stress is defined by

$$\bar{\sigma}_{ij} = \frac{1}{V} \int_{V} \sigma_{ij}(x_i)\, dV \tag{2.2}$$

and the average strain by

$$\bar{\varepsilon}_{ij} = \frac{1}{V} \int_{V} \varepsilon_{ij}(x_i)\, dV \tag{2.3}$$

where ε_{ij} is the infinitesimal strain tensor, and the displacement field is assumed to be single valued. Similarly, by considering a set of prescribed displacements u_i^0 on S which would result in a uniform strain field for a homogeneous material, the effective moduli $C^{*}_{ijk\ell}$ of a heterogeneous material can be defined through the relation

$$\bar{\sigma}_{ij} = C^{*}_{ijk\ell}\, \bar{\varepsilon}_{k\ell} \tag{2.4}$$

The evaluation of the effective material properties requires the formulation of a suitable boundary value problem. The domain of the problem is selected as a typical representative volume element V which is loaded either by prescribed tractions T_i^0 or displacements u_i^0 on S. These boundary conditions are selected to produce uniform stress or deformation fields in a homogeneous material. After the solution of the boundary value problem is obtained, the average stress and average strain can be determined from (2.2) and (2.3). The effective material properties are then obtained by utilizing either (2.1) or (2.4).

The solution of the boundary value problem is facilitated by various simplifying assumptions regarding the representative volume ele-

ment. The simplifications are employed in order to yield tractable solutions that still retain the fundamental characteristics of the composite. Assumptions which are typically used are: perfect fiber/matrix bonding, uniform fiber spacing and various fiber cross sections. Examples of several of these idealizations and their associated representative volume elements are presented in Fig. 2.1.

The material presented in this section was included to explain the motivation of this research and to provide a brief introduction to micromechanics theory. The material presented is by no means comprehensive, the interested reader is referred to the work by Christensen [1] and Hashin [2] for a rigorous treatment of the subject.

2.2 Development of the Aboudi First-Order Micromechanics Theory

Since the Aboudi micromechanics theory is relatively new, there is no single source where a complete presentation of the subject may be found. For this reason, the theory is reviewed in this section with considerable detail. The work presented in this section for the most part is based on Refs. [39,40,44,47,48].

2.2.1 Geometry

The geometrical idealization of the composite is illustrated in Fig. 2.2. The fibers are continuous along the x_1 axis with a uniform rectangular cross section of dimension h_1 and ℓ_1. The fibers are suspended within the matrix phase in a rectangular array, uniformly spaced at distances h_2, ℓ_2 in the x_2, x_3 directions respectively. Due to the periodic arrangement of the fibers, only the representative volume

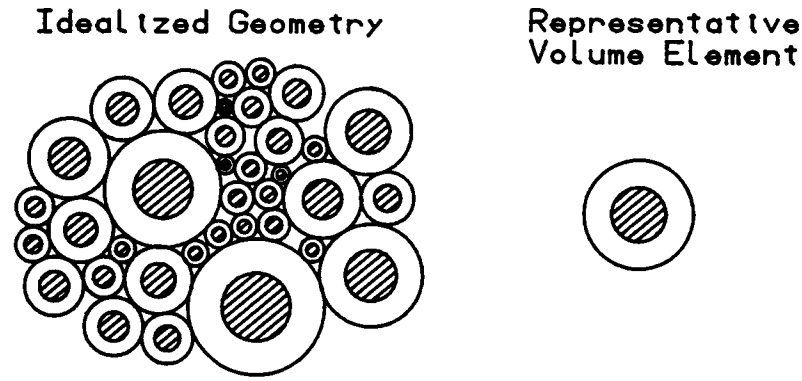

(a) Composite Cylinder Assemblage

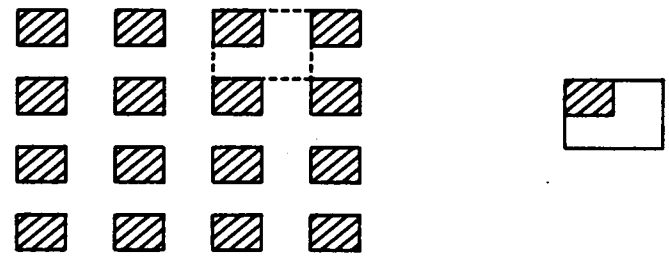

(b) Rectangular Array with Rectangular Fibers

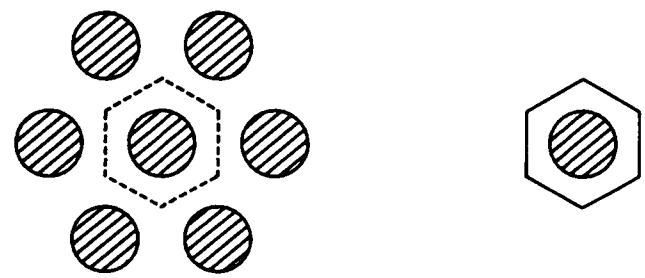

(c) Hexagonal Array with Circular Fibers

Figure 2.1. Geometrical Idealization of Fiber Reinforced Composites

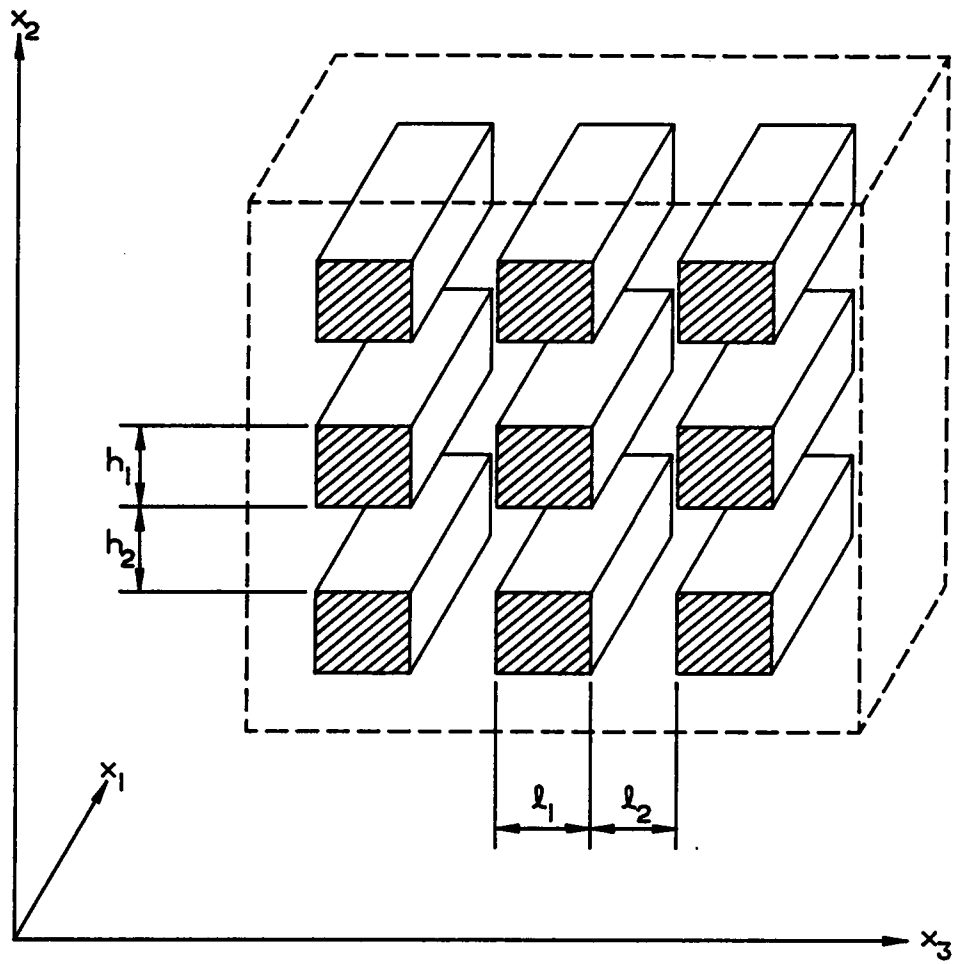

Figure 2.2. Rectangular Fiber Array

element is required for further analysis, see Fig. 2.3. The representative volume element or unit cell is subdivided into four subcells, one fiber and three matrix. Each subcell is identified by indices $\beta\gamma$, where $\beta,\gamma = 1,2$. For example the fiber subcell is indicated by $\beta\gamma = 11$. Unless stated otherwise, the summation convention will be suspended for the indices β and γ. Located at the center of each subcell is a local coordinate system $x_1, \bar{x}_2^{(\beta)}, \bar{x}_3^{(\gamma)}$.

2.2.2 Displacement Field and Continuity Relations

In order to predict the effective behavior of a composite, only a first-order displacement expansion is required. Since the desired average response of the composite is only meaningful if the heterogeneities are small, we shall eliminate all terms of $O(h_\beta^2)$ and $O(\ell_\gamma^2)$.

Within this context, the displacement field for a typical subcell can be expressed as

$$u_i^{(\beta\gamma)} = W_i^{(\beta\gamma)} + \bar{x}_2^{(\beta)}\, \phi_i^{(\beta\gamma)} + \bar{x}_3^{(\gamma)}\, \psi_i^{(\beta\gamma)} \qquad i = 1,2,3 \tag{2.5}$$

where $W_i^{(\beta\gamma)}$, $\phi_i^{(\beta\gamma)}$ and $\psi_i^{(\beta\gamma)}$ are generalized displacements which are functions of the spatial coordinate x_1 and time t only. The generalized displacements take the role of undetermined parameters which must be evaluated.

If the subcells are assumed to be perfectly bonded, the following displacement continuity relations are required:

$$u_i^{(1\gamma)}\Big|_{\bar{x}_2^{(1)} = \mp h_1/2} = u_i^{(2\gamma)}\Big|_{\bar{x}_2^{(2)} = \pm h_2/2} \tag{2.6}$$

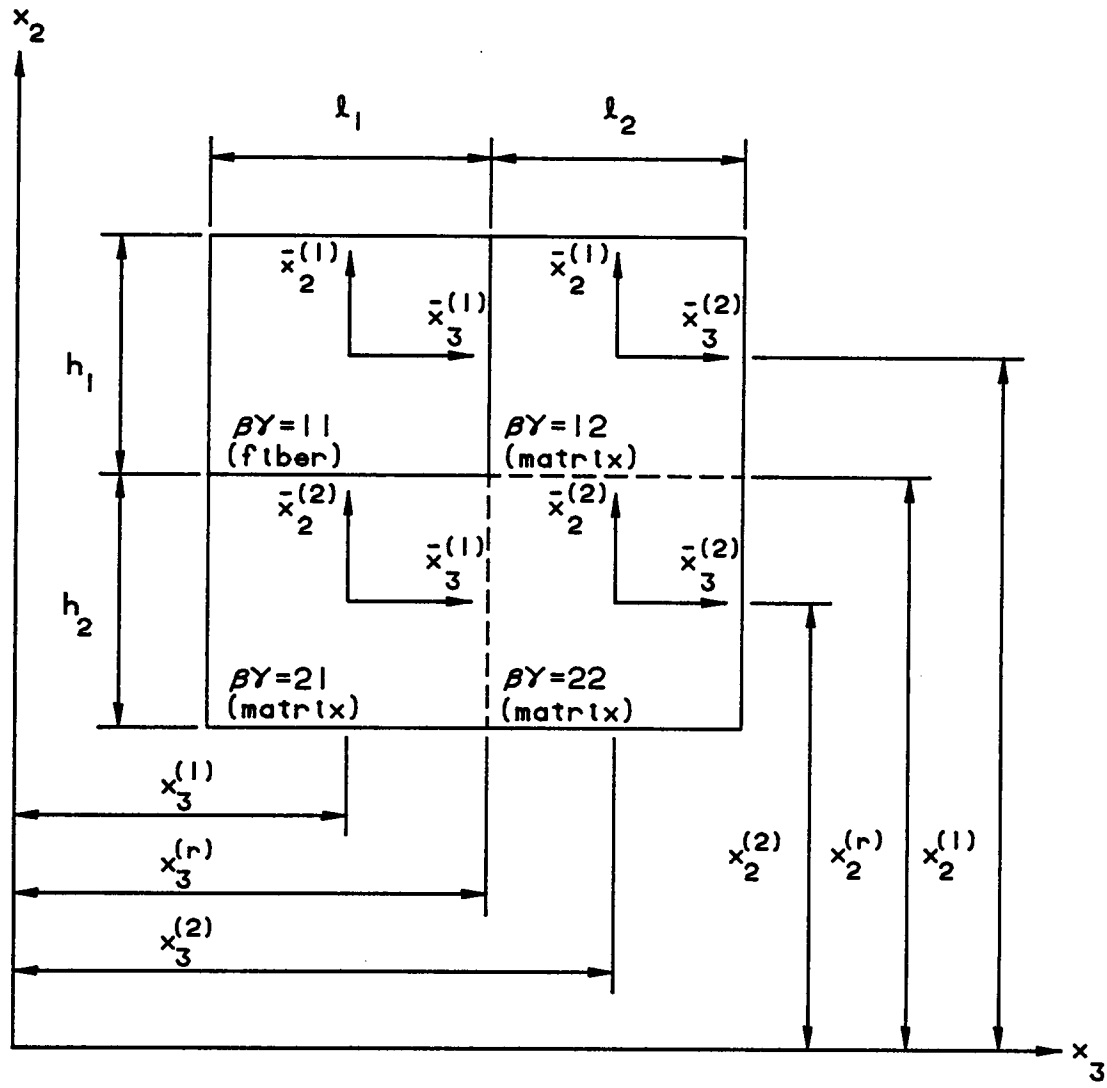

Figure 2.3. Representative Volume Element

$$u_i^{(\beta 1)}\Big|_{\bar{x}_3^{(1)} = \pm \ell_1/2} = u_i^{(\beta 2)}\Big|_{\bar{x}_3^{(2)} = \mp \ell_2/2} \tag{2.7}$$

for i = 1,2,3. These relations reflect the displacement continuity at adjacent and at periodic subcell faces within the representative cell. If an exact solution is desired, these equations would have to be satisfied in a point-wise manner. Since only the effective response of the composite is required, the continuity relations will be imposed in an average sense which yields:

$$\frac{1}{\ell_\gamma}\int_{-\ell_\gamma/2}^{+\ell_\gamma/2}\left[u_i^{(1\gamma)}\Big|_{\bar{x}_2^{(1)} = \mp h_1/2} - u_i^{(2\gamma)}\Big|_{\bar{x}_2^{(2)} = \pm h_2/2}\right]d\bar{x}_3^{(\gamma)} = 0 \tag{2.8}$$

$$\frac{1}{h_\beta}\int_{-h_\beta/2}^{+h_\beta/2}\left[u_i^{(\beta 2)}\Big|_{\bar{x}_3^{(1)} = \pm \ell_1/2} - u_i^{(\beta 1)}\Big|_{\bar{x}_3^{(2)} = \mp \ell_2/2}\right]d\bar{x}_2^{(\beta)} = 0 \tag{2.9}$$

Introducing the generalized displacements into the displacement continuity relation, we obtain

$$W_i^{(1\gamma)} \mp \frac{h_1}{2}\,\phi_i^{(1\gamma)} - W_i^{(2\gamma)} \mp \frac{h_2}{2}\,\phi_i^{(2\gamma)} = 0 \tag{2.10}$$

$$W_i^{(\beta 1)} \pm \frac{\ell_1}{2}\,\psi_i^{(\beta 1)} - W_i^{(\beta 2)} \pm \frac{\ell_2}{2}\,\phi_i^{(\beta 2)} = 0 \tag{2.11}$$

The final development of the displacement continuity relations requires the replacement of the discrete generalized displacements by globally continuous functions. Aboudi refers to this process as a "smoothing operation" [39]. By introducing the Dirac delta function $\delta(x_2,x_3)$, the generalized displacements can be expressed in terms of continuous functions $w_i^{(\beta\gamma)}$, $\phi_i^{(\beta\gamma)}$ and $\psi_i^{(\beta\gamma)}$ which are defined through

the following relations

$$W_i^{(\beta\gamma)} = w_i^{(\beta\gamma)}(x_1,x_2,x_3)\ \delta(x_2 - x_2^{(\beta)},x_3 - x_3^{(\gamma)}) \tag{2.12a}$$

$$\phi_i^{(\beta\gamma)} = \phi_i^{(\beta\gamma)}(x_1,x_2,x_3)\ \delta(x_2 - x_2^{(\beta)},x_3 - x_3^{(\gamma)}) \tag{2.12b}$$

$$\Psi_i^{(\beta\gamma)} = \psi_i^{(\beta\gamma)}(x_1,x_2,x_3)\ \delta(x_2 - x_2^{(\beta)},x_3 - x_3^{(\gamma)}) \tag{2.12c}$$

Using (2.12), the first displacement continuity relation in (2.10) can be expressed as

$$w_i^{(1\gamma)}\Big|_{P_{1\gamma}} - \frac{h_1}{2}\,\phi_i^{(1\gamma)}\Big|_{P_{1\gamma}} - w_i^{(2\gamma)}\Big|_{P_{2\gamma}} - \frac{h_2}{2}\,\phi_i^{(2\gamma)}\Big|_{P_{2\gamma}} = 0 \tag{2.13}$$

where $P_{\beta\gamma}$ indicates the location $(x_1,x_2^{(\beta)},x_3^{(\gamma)})$ with respect to the x_1,x_2,x_3 coordinate system, see Fig. 2.3. This equation contains terms which are evaluated at two different locations within the representative unit cell. The final form of the displacement continuity relations we seek, requires all the terms to be evaluated at a single common location. This is performed by expanding the terms in a Taylor series about a common subcell interface and dropping all terms $O(h_\beta^2)$ or $O(\ell_\gamma^2)$. In the case of equation (2.13), the terms are expanded about $x_2 = x_2^{(r)}$, where we obtain

$$w_i^{(1\gamma)} + \frac{h_1}{2}\frac{\partial w_i^{(1\gamma)}}{\partial x_2} - \frac{h_1}{2}\,\phi_i^{(1\gamma)} - w_i^{(2\gamma)} + \frac{h_2}{2}\frac{\partial w_i^{(2\gamma)}}{\partial x_2} - \frac{h_2}{2}\,\phi_i^{(2\gamma)} = 0 \tag{2.14}$$

where all the terms are evaluated at $x_1,x_2^{(r)},x_3^{(\gamma)}$.

The "smoothing operation" is completed by imposing (2.14) at all points in the composite instead of a single discrete location. Simi-

larly, the second equation of (2.10) can be expressed as

$$w_i^{(1\gamma)} - \frac{h_1}{2}\frac{\partial w_i^{(1\gamma)}}{\partial x_2} + \frac{h_2}{2}\phi_i^{(1\gamma)} - w_i^{(2\gamma)} - \frac{h_2}{2}\frac{\partial w_i^{(2\gamma)}}{\partial x_2} + \frac{h_2}{2}\phi_i^{(2\gamma)} = 0 \tag{2.15}$$

By adding and subtracting expressions (2.14) and (2.15) one obtains

$$w_i^{(1\gamma)} = w_i^{(2\gamma)} \tag{2.16a}$$

$$h_1\phi_i^{(1\gamma)} + h_2\phi_i^{(2\gamma)} = h_1\frac{\partial w_i^{(1\gamma)}}{\partial x_2} + h_2\frac{\partial w_i^{(2\gamma)}}{\partial x_2} \tag{2.16b}$$

Additionally, (2.11) can be manipulated to obtain results similar to (2.16). These combine to yield the displacement continuity relations in their final form

$$w_i^{(11)} = w_i^{(12)} = w_i^{(21)} = w_i^{(22)} = w_i \tag{2.17}$$

$$h_1\phi_i^{(1\gamma)} + h_2\phi_i^{(2\gamma)} = (h_1 + h_2)\frac{\partial w_i}{\partial x_2} \tag{2.18}$$

$$\ell_1\psi_i^{(\beta 1)} + \ell_2\psi_i^{(\beta 2)} = (\ell_1 + \ell_2)\frac{\partial w_i}{\partial x_3} \tag{2.19}$$

In equation (2.17), the twelve field variables $w_i^{(\beta\gamma)}$ have been reduced to three w_i. These represent the "gross" deformation of the composite. The remaining field variables $\phi_i^{(\beta\gamma)}$ and $\psi_i^{(\beta\gamma)}$ represent the "local" deformations within the individual subcells. Although equations (2.18) and (2.19) will typically be referred to as displacement continuity relations, these really form constraint equations on w_i, $\phi_i^{(\beta\gamma)}$ and $\psi_i^{(\beta\gamma)}$ since they are not totally independent variables. Using (2.12) and (2.17), the subcell displacement field (2.5) can be expressed as

$$u_i^{(\beta\gamma)} = w_i + \bar{x}_2^{(\beta)}\phi_i^{(\beta\gamma)} + \bar{x}_3^{(\gamma)}\psi_i^{(\beta\gamma)} \tag{2.20}$$

Considering the temperature field within the composite, the subcell temperature $T^{(\beta\gamma)}$ can be expressed in a similar fashion as the displacement field starting with (2.5). By imposing the same subcell continuity as the displacements, the subcell temperatures can be expressed as

$$T^{(\beta\gamma)} = T + \bar{x}_2^{(\beta)}\phi_T^{(\beta\gamma)} + \bar{x}_3^{(\gamma)}\psi_T^{(\beta\gamma)} \tag{2.21}$$

which is the analogue to (2.20). In this expression T represents the "gross" temperature and the "local" temperature variations are represented by $\phi_T^{(\beta\gamma)}$ and $\psi_T^{(\beta\gamma)}$.

In a later section the displacement continuity relations will be modified in order to relax the assumption of perfect bonding between the subcells. This modification will allow the analysis of debonding between the fiber and matrix phases.

2.2.3 Traction Continuity Conditions

The stresses within the individual subcell are required to satisfy both the equations of motion and traction continuity conditions between the subcells. The equations of motion for a typical subcell neglecting body forces are

$$\partial_i \sigma_{ij}^{(\beta\gamma)} = \rho_{\beta\gamma}\ddot{u}_j^{(\beta\gamma)} \tag{2.22}$$

where $\rho_{\beta\gamma}$ is the subcell mass density, the dots refer to temporal differentiation, and ∂_i implies: $\partial_1 = \partial/\partial x_1$, $\partial_2 = \partial/\partial \bar{x}_2^{(\beta)}$ and $\partial_3 = \partial/\partial \bar{x}_3^{(\gamma)}$. The required traction continuity relations can then be

stated as

$$\sigma_{2i}^{(1\gamma)}\Big|_{\bar{x}_2^{(1)} = \mp h_1/2} = \sigma_{2i}^{(2\gamma)}\Big|_{\bar{x}_2^{(2)} = \pm h_2/2} \tag{2.23a}$$

$$\sigma_{3i}^{(\beta 1)}\Big|_{\bar{x}_3^{(1)} = \pm \ell_1/2} = \sigma_{3i}^{(\beta 2)}\Big|_{\bar{x}_3^{(2)} = \mp \ell_2/2} \tag{2.23b}$$

To develop the effective homogeneous response of the composite it will be advantageous to perform an order of magnitude analysis of the stress field. This is facilitated by expanding the subcell stress components in a Legendre series as follows

$$\sigma_{ij}^{(\beta\gamma)}(\bar{x}_2,\bar{x}_3) = V_{\beta\gamma} \sum_{m=0}^{\infty} \sum_{n=0}^{\infty} S_{ij(m,n)}^{(\beta\gamma)} \bar{P}_m\left(\frac{2\bar{x}_2}{h_\beta}\right) \bar{P}_n\left(\frac{2\bar{x}_3}{\ell_\gamma}\right) \tag{2.24}$$

where

$$S_{ij(m,n)}^{(\beta\gamma)} = \frac{1}{V_{\beta\gamma}} \int_{-\ell_\gamma/2}^{+\ell_\gamma/2} \int_{-h_\beta/2}^{+h_\beta/2} \sigma_{ij}^{(\beta\gamma)} \bar{P}_m\left(\frac{2\bar{x}_2}{h_\beta}\right) \bar{P}_n\left(\frac{2\bar{x}_3}{\ell_\gamma}\right) d\bar{x}_2^{(\beta)} d\bar{x}_3^{(\gamma)} \tag{2.25}$$

$$\bar{P}_n(x) = \sqrt{\frac{2n+1}{2}}\, P_n(x) \tag{2.26}$$

$$V_{\beta\gamma} = h_\beta \ell_\gamma \tag{2.27}$$

The functions $P_n(x)$ are Legendre polynomials which can be evaluated using Rodrigues formula

$$P_n(x) = \frac{1}{(2^n)\ n!} \frac{d^n}{dx^n} (x^2 - 1)^n \tag{2.28}$$

From this formula the first three polynomials are

$$P_0 = 1$$

$$P_1 = x$$

$$P_2 = \tfrac{1}{2}\left(\tfrac{1}{3} - x^2\right)$$

The polynomials $\bar{P}_n(x)$ form an orthonormal basis over [-1,1] with respect to the inner product

$$(\bar{P}_m,\bar{P}_n) = \int_{-1}^{+1} \bar{P}_m(x)\ \bar{P}_n(x)\ dx \tag{2.29}$$

The parameters $S^{(\beta\gamma)}_{ij(m,n)}$ in (2.26) are generalized stress components, where $S^{(\beta\gamma)}_{ij(0,0)}$ can be recognized as the average subcell stress. It should be noted in (2.24) the stress field $\sigma^{(\beta\gamma)}_{ij}$ is constant in the x_1 direction (along the length of the fiber). This can be proven by considering the average stress $\bar{\sigma}_{ij}$ in (2.2). Since the stress is non-zero within the composite in general and the fibers are infinitely long, the only way $\bar{\sigma}_{ij}$ can remain finite when integrated in the x_1 direction is for the stress to be constant along the length of the fiber. Similar arguments can be used to show that the strain $\varepsilon^{(\beta\gamma)}_{ij}$ is also constant along the fiber.

Using (2.24), the average stress $\bar{\sigma}_{ij}$ can be expressed as

$$\bar{\sigma}_{ij} = \frac{1}{V} \sum_{\beta\gamma=1}^{2} V_{\beta\gamma}\ S^{(\beta\gamma)}_{ij(0,0)} \tag{2.30}$$

where $V = (h_1 + h_2)\ (\ell_1 + \ell_2)$. Since the average stress is only a function of the average subcell stress, the higher-order generalized stress components ($S^{(\beta\gamma)}_{ij(m,n)}$ for $m \neq 0$ and $n \neq 0$) will be neglected. To simplify the notation in subsequent sections we shall denote the average subcell stress as

$$S^{(\beta\gamma)}_{ij} = S^{(\beta\gamma)}_{ij(0,0)} = \frac{1}{V_{\beta\gamma}} \int_{-\ell_\gamma/2}^{+\ell_\gamma/2} \int_{-h_\beta/2}^{+h_\beta/2} \sigma^{(\beta\gamma)}_{ij}\ d\bar{x}_2 d\bar{x}_3 \tag{2.31}$$

By neglecting the higher-order generalized stress components the equations of motion (2.22) are trivially satisfied. Additionally, the

traction continuity conditions (2.23) reduce to

$$S_{2i}^{(1\gamma)} = S_{2i}^{(2\gamma)} \tag{2.32}$$

$$S_{3i}^{(\beta 1)} = S_{3i}^{(\beta 2)} \tag{2.33}$$

Since the required effective homogeneous composite response requires the computation of $\bar{\sigma}_{ij}$ which is a function of only $S_{ij}^{(\beta\gamma)}$, the need to solve a boundary value problem for the local stress field has been avoided. In a later section, we shall show that these simplifications have reduced the micromechanics effective modulus theory to a relatively simple algebraic problem.

2.2.4 Imperfect Bonding

The displacement continuity relations (2.17)-(2.19), which assumed perfect bonding between the fiber and matrix phases, will be modified to allow varying degrees of adhesion. Based on the work of Jones and Whittier [74], the displacement continuity relation will be replaced by jump conditions at the subcell interface.

The jump conditions can be expressed for a general interface I with normal vector $\underset{\sim}{n}$ and traction vector $\underset{\sim}{t}$ as

$$[\underset{\sim}{u}_n]_I = R_n \underset{\sim}{T}_n \tag{2.34a}$$

$$[\underset{\sim}{u}_t]_I = R_t \underset{\sim}{T}_t \tag{2.34b}$$

where

$$\underset{\sim}{u}_n = (\underset{\sim}{u}\cdot\underset{\sim}{n})\underset{\sim}{n}$$

$$\underset{\sim}{u}_t = \underset{\sim}{u} - \underset{\sim}{u}_n$$

$$\underset{\sim}{T}_n = (\underset{\sim}{t}\cdot\underset{\sim}{n})\underset{\sim}{n}$$

$$\underset{\sim}{T}_t = \underset{\sim}{t} - \underset{\sim}{T}_n$$

$$t_i = \sigma_{ij} n_j$$

In the above expression

$[\cdot]_I$ = jump in the enclosed quantity across the interface I

$\underset{\sim}{u}_n, \underset{\sim}{u}_t$ = normal and tangential displacement vectors

$\underset{\sim}{T}_n, \underset{\sim}{T}_t$ = normal and tangential traction vectors

R_n, R_t = normal and tangential bonding parameters

The scalar parameters R_n and R_t are introduced to describe the state or condition of the interface. When $R_n = R_t = 0$, perfect bonding of the interface is obtained. When $R_n = 0$ and $R_t \to \infty$, perfectly lubricated contact ($T_n \neq 0$, $T_t = 0$) is obtained. Complete debonding is obtained when $R_n \to \infty$ and $R_t \to \infty$.

Incorporating the jump conditions (2.34) into the current micromechanics formulation we obtain

$$u_i^{(1\gamma)}\Big|_{\bar{x}_2^{(1)} = \pm h_1/2} - u_i^{(2\gamma)}\Big|_{\bar{x}_2^{(2)} = \mp h_2/2} = \mp R_{i2}^{\gamma}\, \sigma_{i2}^{(1\gamma)}\Big|_{\bar{x}_2^{(1)} = \pm h_1/2} \tag{2.35}$$

$$u_i^{(\beta 1)}\Big|_{\bar{x}_3^{(1)} = \mp \ell_1/2} - u_i^{(\beta 2)}\Big|_{\bar{x}_3^{(2)} = \pm \ell_2/2} = \pm R_{i3}^{\beta}\, \sigma_{i3}^{(\beta 1)}\Big|_{\bar{x}_3^{(1)} = \mp \ell_1/2} \tag{2.36}$$

where R_{i2}^{γ} and R_{i3}^{β} are generalizations of the bonding parameters introduced in (2.34) and no sum is implied on the index i.

Due to the similarity of the jump conditions and the displacement continuity relations (2.6) and (2.7), the development will proceed in an analogous manner. The jump conditions are imposed in an average sense at the subcell interface. After introducing the continuous generalized displacements (2.16) we obtain

$$w_i^{(1\gamma)} \mp \frac{h_1}{2}\phi_i^{(1\gamma)} - w_i^{(2\gamma)} \mp \frac{h_2}{2}\phi_i^{(2\gamma)} = \mp R_{i2}^{\gamma} S_{i2}^{(1\gamma)} \tag{2.37}$$

$$w_i^{(\beta 1)} \pm \frac{\ell_1}{2}\psi_i^{(\beta 1)} - w_i^{(\beta 2)} \pm \frac{\ell_2}{2}\psi_i^{(\beta 2)} = \pm R_{i3}^{\beta} S_{i3}^{(\beta 1)} \tag{2.38}$$

where the integral of the surface tractions is replaced by the average stresses. This is motivated by the development of the traction continuity relations in the previous section.

Smoothing is performed by expanding the jump conditions about their respective subcell interface. The resulting equations are then imposed throughout the composite to complete the process. At this point, the development is identical to the displacement continuity conditions. Due to the similarity with the displacement continuity relations, we will only state the resulting imperfect bonding conditions which are

$$w_i^{(11)} = w_i^{(12)} = w_i^{(21)} = w_i^{(22)} = w_i \tag{2.39}$$

$$h_1\phi_i^{(1\gamma)} + h_2\phi_i^{(2\gamma)} + 2R_{i2}^{\gamma} S_{i2}^{(1\gamma)} = (h_1 + h_2)\frac{\partial w_i}{\partial x_2} \tag{2.40}$$

$$\ell_1\psi_i^{(\beta 1)} + \ell_2\psi_i^{(\beta 2)} + 2R_{i3}^{\beta} S_{i3}^{(\beta 1)} = (\ell_1 + \ell_2)\frac{\partial w_i}{\partial x_3} \tag{2.41}$$

where no sum is implied on the index i.

In (2.40) and (2.41), the most general case of imperfect bonding is considered. This allows the degree of bonding to be specified between each of the subcells. This capability provides a means to simulate the effects of a flaw within the composite. Considering debonding at the fiber/matrix interface only, the generalized bonding parameters can be related to the normal and tangential bonding parameters by the following

$$R_{2i}^{\gamma} = \begin{cases} R_n, & \gamma = 1,\ i = 2 \\ R_t, & \gamma = 1,\ i \neq 2 \\ 0, & \gamma = 2 \end{cases} \tag{2.42}$$

$$R_{3i}^{\beta} = \begin{cases} R_n, & \beta = 1,\ i = 3 \\ R_t, & \beta = 1,\ i \neq 3 \\ 0, & \beta = 2 \end{cases} \tag{2.43}$$

2.2.5 Average Strain Relations

The evaluation of the average strains must reflect the possibility of discontinuities in the displacement field [75]. The expression for the average strain $\bar{\varepsilon}_{ij}$ given by (2.3) requires suitable modification to reflect the possibility of imperfect bonding given by

$$\bar{\varepsilon}_{ij} = \frac{1}{V} \sum_{\beta\gamma=1}^{2} V_{\beta\gamma} E_{ij}^{(\beta\gamma)} - \frac{1}{2V} \int_I ([u_i]_I\, n_j + [u_j]_I\, n_i)\, dI \tag{2.44}$$

where $E_{ij}^{(\beta\gamma)}$ is the subcell average strain defined as

$$E_{ij}^{(\beta\gamma)} = \frac{1}{V_{\beta\gamma}} \int_{-\ell_\gamma/2}^{+\ell_\gamma/2} \int_{-h_\beta/2}^{+h_\beta/2} \varepsilon_{ij}^{(\beta\gamma)}\, d\bar{x}_2^{(\beta)} d\bar{x}_2^{(\gamma)} \tag{2.45a}$$

$$\varepsilon_{ij}^{(\beta\gamma)} = \frac{1}{2} \left(\partial_i u_j^{(\beta\gamma)} + \partial_j u_i^{(\beta\gamma)}\right) \tag{2.45b}$$

$$\partial_i = \{\partial/\partial x_1,\ \partial/\partial \bar{x}_2^{(\beta)},\ \partial/\partial \bar{x}_3^{(\gamma)}\} \tag{2.45c}$$

and $[u_i]_I$ is the jump in the displacement across the interface I with normal n_i. When the displacements are continuous across the interface I, the integral over the interface vanishes in (2.44) and expression (2.3) is obtained.

The average subcell strains $E_{ij}^{(\beta\gamma)}$ can be evaluated by using (2.20) with (2.45) to produce

$$E_{11}^{(\beta\gamma)} = \frac{\partial w_1}{\partial x_1} \tag{2.46a}$$

$$E_{22}^{(\beta\gamma)} = \phi_2^{(\beta\gamma)} \tag{2.46b}$$

$$E_{33}^{(\beta\gamma)} = \psi_3^{(\beta\gamma)} \tag{2.46c}$$

$$2E_{12}^{(\beta\gamma)} = \phi_1^{(\beta\gamma)} + \frac{\partial w_2}{\partial x_1} \tag{2.46d}$$

$$2E_{13}^{(\beta\gamma)} = \psi_1^{(\beta\gamma)} + \frac{\partial w_3}{\partial x_1} \tag{2.46e}$$

$$2E_{23}^{(\beta\gamma)} = \phi_3^{(\beta\gamma)} + \psi_2^{(\beta\gamma)} \tag{2.46f}$$

The evaluation of the average strains will be performed by considering $\bar{\varepsilon}_{22}$, from (2.44) and (2.46b) we have

$$\bar{\varepsilon}_{22} = \frac{1}{V} \sum_{\beta,\gamma=1}^{2} V_{\beta\gamma}\, \phi_2^{(\beta\gamma)} - \frac{1}{V} \int_I [u_2] n_2 \, dI \tag{2.47}$$

Using the jump conditions in (2.35), the second integral becomes

$$\int_I [u_2] n_2 \, dI = \sum_{\gamma=1}^{2} R_{22}^{\gamma} \int_{-\ell_\gamma/2}^{+\ell_\gamma/2} \sigma_{22}^{(1\gamma)}\Big|_{\bar{x}_2^{(1)} = +h_1/2} \, d\bar{x}_3^{(\gamma)}$$

$$+ \sum_{\gamma=1}^{2} R_{22}^{\gamma} \int_{-\ell_\gamma/2}^{+\ell_\gamma/2} \sigma_{22}^{(1\gamma)}\Big|_{\bar{x}_2(1)} = -h_1/2 \; d\bar{x}_3^{(\gamma)} \qquad (2.48)$$

Neglecting the higher-order generalized stress components, $\sigma_{22}^{(1\gamma)}$ is replaced with $S_{22}^{(1\gamma)}$. Performing the indicated integration one obtains

$$\int_I [u_2] n_2 \, dI = 2\ell_1 \, R_{22}^{1} \, S_{22}^{(11)} + 2\ell_2 \, R_{22}^{2} \, S_{22}^{(12)} \qquad (2.49)$$

The jump conditions (2.40) can be used to express the above integral in terms of the generalized displacements. Consider (2.40) for the case $\gamma = 1$ multiplied by ℓ_1 and for the case $\gamma = 2$ multiplied by ℓ_2. Adding the two resulting equations together we obtain

$$2\ell_1 \, R_{22}^{1} \, S_{22}^{(11)} + 2\ell_2 \, R_{22}^{2} \, S_{22}^{(12)} = V \frac{\partial w_i}{\partial x_2} - \sum_{\beta,\gamma=1}^{2} V_{\beta\gamma} \, \phi_i^{(\beta\gamma)} \qquad (2.50)$$

Substitution of (2.49) and (2.50) into (2.47) yields

$$\bar{\varepsilon}_{22} = \frac{\partial w_2}{\partial x_2} \qquad (2.51)$$

Similarly the remaining components can be evaluated to obtain

$$\bar{\varepsilon}_{ij} = \frac{1}{2} \left(\frac{\partial w_i}{\partial x_j} + \frac{\partial w_j}{\partial x_i} \right) \qquad (2.52)$$

2.2.6 Subcell Constitutive Relations

The subcell strain tensor (2.45b) is assumed to be composed of elastic, plastic and thermal components such that

$$\varepsilon_{ij}^{(\beta\gamma)} = \varepsilon_{ij}^{E(\beta\gamma)} + \varepsilon_{ij}^{P(\beta\gamma)} + \varepsilon_{ij}^{T(\beta\gamma)} \qquad (2.53)$$

Introducing contracted notation, the stress with a typical subcell can be expressed as

$$\underset{\sim}{\sigma}^{(\beta\gamma)} = \underset{\sim}{C}^{(\beta\gamma)}(\underset{\sim}{\varepsilon}^{(\beta\gamma)} - \underset{\sim}{\varepsilon}^{P(\beta\gamma)} - \Delta T^{(\beta\gamma)}\underset{\sim}{\alpha}^{(\beta\gamma)}) \tag{2.54}$$

where

$$\underset{\sim}{\sigma}^{(\beta\gamma)} = \{\sigma_{11}^{(\beta\gamma)},\sigma_{22}^{(\beta\gamma)},\sigma_{33}^{(\beta\gamma)},\sigma_{12}^{(\beta\gamma)},\sigma_{13}^{(\beta\gamma)},\sigma_{23}^{(\beta\gamma)}\}^T,$$

$$\underset{\sim}{\varepsilon}^{(\beta\gamma)} = \{\varepsilon_{11}^{(\beta\gamma)},\varepsilon_{22}^{(\beta\gamma)},\varepsilon_{33}^{(\beta\gamma)},2\varepsilon_{12}^{(\beta\gamma)}2\varepsilon_{13}^{(\beta\gamma)},2\varepsilon_{23}^{(\beta\gamma)}\}^T,$$

$$\underset{\sim}{\varepsilon}^{P(\beta\gamma)} = \{\varepsilon_{11}^{P(\beta\gamma)},\varepsilon_{22}^{P(\beta\gamma)},\varepsilon_{33}^{P(\beta\gamma)},2\varepsilon_{12}^{P(\beta\gamma)},2\varepsilon_{13}^{P(\beta\gamma)},2\varepsilon_{23}^{P(\beta\gamma)}\}^T,$$

$$\underset{\sim}{\alpha}^{(\beta\gamma)} = \{\alpha_1^{(\beta\gamma)},\alpha_2^{(\beta\gamma)},\alpha_3^{(\beta\gamma)},0,0,0\}^T$$

and

$$\underset{\sim}{C}^{(\beta\gamma)} = \begin{bmatrix} C_{11}^{(\beta\gamma)} & C_{12}^{(\beta\gamma)} & C_{13}^{(\beta\gamma)} & 0 & 0 & 0 \\ C_{12}^{(\beta\gamma)} & C_{22}^{(\beta\gamma)} & C_{23}^{(\beta\gamma)} & 0 & 0 & 0 \\ C_{13}^{(\beta\gamma)} & C_{23}^{(\beta\gamma)} & C_{33}^{(\beta\gamma)} & 0 & 0 & 0 \\ 0 & 0 & 0 & C_{44}^{(\beta\gamma)} & 0 & 0 \\ 0 & 0 & 0 & 0 & C_{55}^{(\beta\gamma)} & 0 \\ 0 & 0 & 0 & 0 & 0 & C_{66}^{(\beta\gamma)} \end{bmatrix}$$

The thermal strains are given by the term $\Delta T^{(\beta\gamma)}\underset{\sim}{\alpha}^{(\beta\gamma)}$ where $\Delta T^{(\beta\gamma)}$ is the change in the temperature $T^{(\beta\gamma)}$ from the stress-free reference temperature and $\underset{\sim}{\alpha}^{(\beta\gamma)}$ is the vector of coefficients of thermal expansion. The general nature of (2.54) is selected since it can be specialized to reflect the desired behavior of the fiber or matrix. Using (2.31), (2.45), (2.21) and (2.53) the average subcell stress can be expressed as

$$\underset{\sim}{S}^{(\beta\gamma)} = \underset{\sim}{C}^{(\beta\gamma)}(\underset{\sim}{E}^{(\beta\gamma)} - \underset{\sim}{L}^{(\beta\gamma)} - \Delta T\underset{\sim}{\alpha}^{(\beta\gamma)}) \tag{2.55}$$

where the vectors representing the average subcell stress and strain are

$$\underset{\sim}{S}^{(\beta\gamma)} = \{S_{11}^{(\beta\gamma)}, S_{22}^{(\beta\gamma)}, S_{33}^{(\beta\gamma)}, S_{12}^{(\beta\gamma)}, S_{13}^{(\beta\gamma)}, S_{23}^{(\beta\gamma)}\}^T$$

$$\underset{\sim}{E}^{(\beta\gamma)} = \{E_{11}^{(\beta\gamma)}, E_{22}^{(\beta\gamma)}, E_{33}^{(\beta\gamma)}, 2E_{12}^{(\beta\gamma)}, 2E_{13}^{(\beta\gamma)}, 2E_{23}^{(\beta\gamma)}\}^T$$

and the average plastic strains are

$$\underset{\sim}{L}^{(\beta\gamma)} = \{L_{11}^{(\beta\gamma)}, L_{22}^{(\beta\gamma)}, L_{33}^{(\beta\gamma)}, 2L_{12}^{(\beta\gamma)}, 2L_{13}^{(\beta\gamma)}, 2L_{23}^{(\beta\gamma)}\}^T$$

The development of the plastic strains within the subcells is governed by a suitable plasticity theory. The unified theory of Bodner and his coworkers will be used in this study. A review of this work may be found in [76]. The theory does not use a yield surface typical of classical theories. This feature eliminates the need to monitor loading/unloading conditions. Instead the theory is defined by a system of ordinary differential equations which assumes inelastic strains always exist. These equations produce linear elastic behavior by predicting negligible small inelastic strains. The theory does not uncouple the inelastic strains into plastic and creep strain components, as a result the theory is termed unified.

The evolution of the plastic strains is given by the Prandtl-Reuss flow rule

$$\dot{L}_{ij}^{(\beta\gamma)} = \Lambda^{(\beta\gamma)} \hat{S}_{ij}^{(\beta\gamma)} \tag{2.56}$$

where $\dot{L}_{ij}^{(\beta\gamma)}$ is the average subcell plastic strain rate, $\Lambda^{(\beta\gamma)}$ is the subcell flow function and $\hat{S}_{ij}^{(\beta\gamma)}$ is the average subcell stress deviator

$$\hat{S}_{ij}^{(\beta\gamma)} = S_{ij}^{(\beta\gamma)} - S_{kk}^{(\beta\gamma)} \delta_{ij} \tag{2.57}$$

Initially, at t = 0 the subcell plastic strains are zero, thus,

$$L_{ij}^{(\beta\gamma)}(0) = 0$$

The flow function $\Lambda^{(\beta\gamma)}$ is given by

$$\Lambda^{(\beta\gamma)} = \frac{D_o^{(\beta\gamma)}}{\sqrt{J_2^{(\beta\gamma)}}} \text{EXP}\left[-\frac{n^{(\beta\gamma)}+1}{2}\left(\frac{\left(z^{(\beta\gamma)}\right)^2}{3J_2^{(\beta\gamma)}}\right)^{n^{(\beta\gamma)}}\right] \tag{2.58}$$

where $J_2^{(\beta\gamma)}$ is the second invariant of the stress deviator

$$J_2^{(\beta\gamma)} = \frac{1}{2}\hat{S}_{ij}^{(\beta\gamma)}\hat{S}_{ij}^{(\beta\gamma)} \tag{2.59}$$

$z^{(\beta\gamma)}$ is a state variable and $D_o^{(\beta\gamma)}$, $n^{(\beta\gamma)}$ are material parameters. The effect of the load history is introduced through the internal variable z. For isotropic hardening, the evolution of z is given by

$$\dot{z}^{(\beta\gamma)} = m^{(\beta\gamma)}(z_1^{(\beta\gamma)} - z)\,\dot{W}_p^{(\beta\gamma)}/z_o^{(\beta\gamma)} \tag{2.60}$$

$$z^{(\beta\gamma)}(0) = z_o^{(\beta\gamma)}$$

where $\dot{W}_p$ is the rate of plastic work

$$\dot{W}_p^{(\beta\gamma)} = S_{ij}^{(\beta\gamma)}\dot{L}_{ij}^{(\beta\gamma)} = 2\Lambda^{(\beta\gamma)}J_2^{(\beta\gamma)} \tag{2.61}$$

$$W_p^{(\beta\gamma)}(0) = 0$$

and $m^{(\beta\gamma)}$, $z_1^{(\beta\gamma)}$ are additional material parameters. When the material parameters are constant, (2.60) can be integrated directly to obtain

$$z^{(\beta\gamma)} = z_1^{(\beta\gamma)} + (z_o^{(\beta\gamma)} - z_1^{(\beta\gamma)})\text{EXP}[-m^{(\beta\gamma)}\,W_p^{(\beta\gamma)}/z_o^{(\beta\gamma)}] \tag{2.62}$$

The inelastic behavior is characterized by z_0, z_1, m, n and D_0. The parameters z_0 and z_1 are proportional to the yield stress and ultimate stress, respectively. The rate of work hardening is specified by m. The sensitivity of the material to the loading rate is controlled through the parameter n. Experience indicates for n = 10, the material response is essentially rate independent for strain rates less than 10/sec. The limiting strain rate of the material is prescribed using D_0. Typically this is arbitrarily set to $D_0 = 10^4$ sec^{-1}.

In this section, the fundamental relations required for the micromechanic theory have been presented. In the next section, these relations will be employed to develop the effective constitutive relations for a metal matrix composite.

2.3 Composite Constitutive Relations

Utilizing the theory presented in the previous section, the effective composite constitutive relations are established. These relations are given by Aboudi in Ref. [77,78]. An alternate development for the normal stress-strain response is presented which is easily programmed and readily validated.

The fiber behavior is assumed to be orthotropic linear elastic. It is convenient to express (2.55) for the fiber phase ($\beta\gamma$ = 11) as follows:

$$\begin{Bmatrix} \sigma_{11}^{(11)} \\ \sigma_{22}^{(11)} \\ \sigma_{33}^{(11)} \\ \sigma_{12}^{(11)} \\ \sigma_{13}^{(11)} \\ \sigma_{23}^{(11)} \end{Bmatrix} = \begin{bmatrix} C_{11}^{(f)} & C_{12}^{(f)} & C_{13}^{(f)} & 0 & 0 & 0 \\ C_{12}^{(f)} & C_{22}^{(f)} & C_{23}^{(f)} & 0 & 0 & 0 \\ C_{13}^{(f)} & C_{23}^{(f)} & C_{33}^{(f)} & 0 & 0 & 0 \\ 0 & 0 & 0 & G_{12}^{(f)} & 0 & 0 \\ 0 & 0 & 0 & 0 & G_{13}^{(f)} & 0 \\ 0 & 0 & 0 & 0 & 0 & G_{23}^{(f)} \end{bmatrix} \begin{Bmatrix} \varepsilon_{11}^{(11)} \\ \varepsilon_{22}^{(11)} \\ \varepsilon_{33}^{(11)} \\ 2\varepsilon_{12}^{(11)} \\ 2\varepsilon_{13}^{(11)} \\ 2\varepsilon_{23}^{(11)} \end{Bmatrix} - \Delta T \begin{Bmatrix} b_1^{(f)} \\ b_2^{(f)} \\ b_3^{(f)} \\ 0 \\ 0 \\ 0 \end{Bmatrix} \tag{2.63}$$

where

$$b_1^{(f)} = C_{11}^{(f)}\ \alpha_1^{(f)} + C_{12}^{(f)}\ \alpha_2^{(f)} + C_{13}^{(f)}\ \alpha_3^{(f)}$$

$$b_2^{(f)} = C_{12}^{(f)}\ \alpha_1^{(f)} + C_{22}^{(f)}\ \alpha_2^{(f)} + C_{23}^{(f)}\ \alpha_3^{(f)}$$

$$b_3^{(f)} = C_{13}^{(f)}\ \alpha_1^{(f)} + C_{23}^{(f)}\ \alpha_2^{(f)} + C_{33}^{(f)}\alpha_3^{(f)}$$

The matrix is assumed to be isotropic elastoplastic. Assuming plastic incompressibility, the stress-strain relation (2.54) for the matrix phase ($\beta\gamma \neq 11$) will be expressed as:

$$\begin{Bmatrix} \sigma_{11}^{(\beta\gamma)} \\ \sigma_{22}^{(\beta\gamma)} \\ \sigma_{33}^{(\beta\gamma)} \\ \sigma_{12}^{(\beta\gamma)} \\ \sigma_{13}^{(\beta\gamma)} \\ \sigma_{23}^{(\beta\gamma)} \end{Bmatrix} = \begin{bmatrix} \mu & \lambda & \lambda & 0 & 0 & 0 \\ \lambda & \mu & \lambda & 0 & 0 & 0 \\ \lambda & \lambda & \mu & 0 & 0 & 0 \\ 0 & 0 & 0 & G^{(m)} & 0 & 0 \\ 0 & 0 & 0 & 0 & G^{(m)} & 0 \\ 0 & 0 & 0 & 0 & 0 & G^{(m)} \end{bmatrix} \begin{Bmatrix} \varepsilon_{11}^{(\beta\gamma)} \\ \varepsilon_{22}^{(\beta\gamma)} \\ \varepsilon_{33}^{(\beta\gamma)} \\ 2\varepsilon_{12}^{(\beta\gamma)} \\ 2\varepsilon_{13}^{(\beta\gamma)} \\ 2\varepsilon_{23}^{(\beta\gamma)} \end{Bmatrix} - 2G^{(m)} \begin{Bmatrix} \varepsilon_{11}^{P(\beta\gamma)} \\ \varepsilon_{22}^{P(\beta\gamma)} \\ \varepsilon_{33}^{P(\beta\gamma)} \\ \varepsilon_{12}^{P(\beta\gamma)} \\ \varepsilon_{13}^{P(\beta\gamma)} \\ \varepsilon_{23}^{P(\beta\gamma)} \end{Bmatrix}$$

$$- \Delta T \begin{Bmatrix} b^{(m)} \\ b^{(m)} \\ b^{(m)} \\ 0 \\ 0 \\ 0 \end{Bmatrix} \tag{2.64}$$

where

$$\lambda = \frac{E^{(m)}\nu^{(m)}}{(1 + \nu^{(m)})(1 - 2\nu^{(m)})}$$

$$\mu = \lambda + 2G^{(m)}$$

$$b^{(m)} = \frac{\alpha^{(m)}E^{(m)}}{1 - 2\nu^{(m)}}$$

In (2.63) and (2.64) the superscripts f and m are introduced to identify fiber and matrix quantities, respectively. The inelastic matrix behavior is characterized by the five Bodner parameters z_0, z_1, m, n and D_0. Superscripts are omitted from these parameters with the understanding that they apply only to the matrix subcells ($\beta\gamma \neq 11$).

In this section and those which follow, the dimensions h_β and ℓ_γ will be replaced by the normalized quantities:

$$h_\beta \leftarrow \frac{h_\beta}{h_1 + h_2} \tag{2.65a}$$

$$\ell_\gamma \leftarrow \frac{\ell_\gamma}{\ell_1 + \ell_2} \tag{2.65b}$$

Using the normalized dimensions, the fiber and matrix volume fractions become

$$V_f = V_{11} = h_1 \ell_1 \tag{2.66}$$

$$V_m = h_1 \ell_2 + h_2 \ell_1 + h_2 \ell_2 \tag{2.66}$$

Due to the assumed orthotropy of the composite, the normal and shear responses are uncoupled. This allows the solution of the normal response to be obtained independently from the shear response.

2.3.1 Average Normal Stress-Strain Relations

The objective of this section is to develop the average normal stress-strain relations in the following form

$$\underset{\sim}{\bar{\sigma}}_N = \underset{\sim}{C}^*_N \underset{\sim}{\bar{\varepsilon}}_N - \sum_{\substack{\beta,\gamma=1 \\ \beta\gamma\neq 1}}^{2} \underset{\sim}{C}^{*(\beta\gamma)}_N \underset{\sim}{L}^{(\beta\gamma)}_N - \Delta T \, \underset{\sim}{C}^{*(T)} \tag{2.68}$$

where

$$\underset{\sim}{\bar{\sigma}}_N = \{\bar{\sigma}_{11}, \bar{\sigma}_{22}, \bar{\sigma}_{33}\}^T$$

$$\underset{\sim}{\bar{\varepsilon}}_N = \{\bar{\varepsilon}_{11}, \bar{\varepsilon}_{22}, \bar{\varepsilon}_{33}\}^T$$

$$\underset{\sim}{L}^{(\beta\gamma)}_N = \{L^{(\beta\gamma)}_{11}, L^{(\beta\gamma)}_{22}, L^{(\beta\gamma)}_{33}\}^T$$

The matrices $\underset{\sim}{C}^*_N$, $\underset{\sim}{C}^{*(\beta\gamma)}_N$ and $\underset{\sim}{C}^{*(T)}$ are introduced to characterize the effective homogeneous response of the composite to the total strains, matrix plastic strains and thermal deformations, respectively. The effective properties of the composite are obtained from $\underset{\sim}{C}^*_N$ by noting the following:

$$(C_N^*)^{-1} = \begin{bmatrix} \frac{1}{E_1^*} & \frac{\nu_{21}^*}{E_2^*} & \frac{\nu_{31}^*}{E_3^*} \\ \frac{\nu_{12}^*}{E_1^*} & \frac{1}{E_2^*} & \frac{\nu_{32}^*}{E_3^*} \\ \frac{\nu_{13}^*}{E_1^*} & \frac{\nu_{23}^*}{E_2^*} & \frac{1}{E_3^*} \end{bmatrix} \tag{2.69}$$

and

$$(C_N^*)^{-1}\, C^*(T) = \begin{Bmatrix} \alpha_1^* \\ \alpha_2^* \\ \alpha_3^* \end{Bmatrix} \tag{2.70}$$

where E_i^* is the effective Young's modulus, ν_{ij}^* is the effective Poisson's ratio, and α_i^* is the effective coefficient of thermal expansion.

Similarly, the average normal subcell stresses will be expressed as

$$\underset{\sim}{S}_N = \overline{\underset{\sim}{D}}_N\, \overline{\underset{\sim}{\varepsilon}}_N - \sum_{\substack{\beta,\gamma=1 \\ \beta\gamma\neq 1}}^{2} \overline{\underset{\sim}{D}}_N^{(\beta\gamma)}\, \underset{\sim}{L}_N^{(\beta\gamma)} - \Delta T\, \overline{\underset{\sim}{D}}^T \tag{2.71}$$

where

$$\underset{\sim}{S}_N = \{\underset{\sim}{S}_N^{(11)},\ \underset{\sim}{S}_N^{(12)},\ \underset{\sim}{S}_N^{(21)},\ \underset{\sim}{S}_N^{(22)}\}^T$$

$$\underset{\sim}{S}_N^{(\beta\gamma)} = \{S_{11}^{(\beta\gamma)},\ S_{22}^{(\beta\gamma)},\ S_{33}^{(\beta\gamma)}\}^T$$

Using (2.46), (2.52), (2.54), (2.63) and (2.64), the average normal subcell stresses can be expressed as

$$\underset{\sim}{S}_N = \underset{\sim\sim}{E}\underset{\sim}{e} + \underset{\sim\sim}{F}\underset{\sim}{w} \tag{2.72}$$

where

$$\underset{\sim}{e} = \{\overline{\underset{\sim}{\varepsilon}}_N,\ -\underset{\sim}{L}_N^{(12)},\ -\underset{\sim}{L}_N^{(21)},\ -\underset{\sim}{L}_N^{(22)},\ -\Delta T\}^T$$

$$\underset{\sim}{w} = \{\phi_2^{(11)},\ \psi_3^{(11)},\ \phi_2^{(12)},\ \psi_3^{(12)},\ \phi_2^{(21)},\ \psi_3^{(21)},\ \phi_2^{(22)},\ \psi_3^{(22)}\}^T$$

where matrix $\underset{\sim}{E}$ is

$$
\begin{bmatrix}
C_{11}^{(f)} & 0 & 0 & 0 & 0 & 0 & 0 & 0 & 0 & 0 & 0 & 0 & b_1^{(f)} \\
C_{12}^{(f)} & 0 & 0 & 0 & 0 & 0 & 0 & 0 & 0 & 0 & 0 & 0 & b_2^{(f)} \\
C_{13}^{(f)} & 0 & 0 & 0 & 0 & 0 & 0 & 0 & 0 & 0 & 0 & 0 & b_3^{(f)} \\
\mu & 0 & 0 & 2G^{(m)} & 0 & 0 & 0 & 0 & 0 & 0 & 0 & 0 & b^{(m)} \\
\lambda & 0 & 0 & 0 & 2G^{(m)} & 0 & 0 & 0 & 0 & 0 & 0 & 0 & b^{(m)} \\
\lambda & 0 & 0 & 0 & 0 & 2G^{(m)} & 0 & 0 & 0 & 0 & 0 & 0 & b^{(m)} \\
\mu & 0 & 0 & 0 & 0 & 0 & 2G^{(m)} & 0 & 0 & 0 & 0 & 0 & b^{(m)} \\
\lambda & 0 & 0 & 0 & 0 & 0 & 0 & 2G^{(m)} & 0 & 0 & 0 & 0 & b^{(m)} \\
\lambda & 0 & 0 & 0 & 0 & 0 & 0 & 0 & 2G^{(m)} & 0 & 0 & 0 & b^{(m)} \\
\mu & 0 & 0 & 0 & 0 & 0 & 0 & 0 & 0 & 2G^{(m)} & 0 & 0 & b^{(m)} \\
\lambda & 0 & 0 & 0 & 0 & 0 & 0 & 0 & 0 & 0 & 2G^{(m)} & 0 & b^{(m)} \\
\lambda & 0 & 0 & 0 & 0 & 0 & 0 & 0 & 0 & 0 & 0 & 2G^{(m)} & b^{(m)}
\end{bmatrix}
$$

(12 x 13)

$$\underset{\sim}{F} = \begin{bmatrix} C_{12}^{(f)} & C_{13}^{(f)} & 0 & 0 & 0 & 0 & 0 & 0 \\ C_{22}^{(f)} & C_{23}^{(f)} & 0 & 0 & 0 & 0 & 0 & 0 \\ C_{23}^{(f)} & C_{33}^{(f)} & 0 & 0 & 0 & 0 & 0 & 0 \\ 0 & 0 & \lambda & \lambda & 0 & 0 & 0 & 0 \\ 0 & 0 & \mu & \lambda & 0 & 0 & 0 & 0 \\ 0 & 0 & \lambda & \mu & 0 & 0 & 0 & 0 \\ 0 & 0 & 0 & 0 & \lambda & \lambda & 0 & 0 \\ 0 & 0 & 0 & 0 & \mu & \lambda & 0 & 0 \\ 0 & 0 & 0 & 0 & \lambda & \mu & 0 & 0 \\ 0 & 0 & 0 & 0 & 0 & 0 & \lambda & \lambda \\ 0 & 0 & 0 & 0 & 0 & 0 & \mu & \lambda \\ 0 & 0 & 0 & 0 & 0 & 0 & \lambda & \mu \end{bmatrix}$$

(12 x 8)

The vector $\underset{\sim}{w}$ can be eliminated from (2.72) by imposing the required displacement and traction continuity. This is performed by organizing equations (2.32), (2.40) and (2.42) with i = 2 along with equations (2.33), (2.41) and (2.43) with i = 3 into the following form

$$\underset{\sim\sim}{G}\underset{\sim}{w} = \underset{\sim\sim}{H}\underset{\sim}{e} \tag{2.73}$$

where

$$\underset{\sim}{G} = \begin{bmatrix} h_1+2R_nC_{22}^{(f)} & 2R_cC_{23}^{(f)} & 0 & 0 & h_2 & 0 & 0 & 0 \\ 0 & 0 & h_1 & 0 & 0 & 0 & h_2 & 0 \\ 2R_nC_{23}^{(f)} & \ell_1+2R_nC_{33}^{(f)} & 0 & \ell_2 & 0 & 0 & 0 & 0 \\ 0 & 0 & 0 & 0 & 0 & \ell_1 & 0 & \ell_2 \\ C_{22}^{(f)} & C_{23}^{(f)} & 0 & 0 & -\mu & -\lambda & 0 & 0 \\ 0 & 0 & -\mu & \lambda & 0 & 0 & -\mu & -\lambda \\ C_{23}^{(f)} & C_{33}^{(f)} & -\lambda & -\mu & 0 & 0 & 0 & 0 \\ 0 & 0 & 0 & 0 & \lambda & \mu & -\lambda & -\mu \end{bmatrix}$$

(8 x 8)

$$\underset{\sim}{H} = \begin{bmatrix} -2R_nC_{12}^{(f)} & 1 & 0 & 0 & 0 & 0 & 0 & 0 & 0 & 0 & 0 & 0 & -2R_nb_2^{(f)} \\ 0 & 1 & 0 & 0 & 0 & 0 & 0 & 0 & 0 & 0 & 0 & 0 & 0 \\ -2R_nC_{13}^{(f)} & 0 & 1 & 0 & 0 & 0 & 0 & 0 & 0 & 0 & 0 & 0 & -2R_nb_3^{(f)} \\ 0 & 0 & 1 & 0 & 0 & 0 & 0 & 0 & 0 & 0 & 0 & 0 & 0 \\ \lambda - C_{12}^{(f)} & 0 & 0 & 0 & 0 & 0 & 0 & 2G & 0 & 0 & 0 & 0 & b^{(m)}-b_2^{(f)} \\ 0 & 0 & 0 & 0 & -2G & 0 & 0 & 0 & 0 & 0 & 2G & 0 & 0 \\ \lambda - C_{13}^{(f)} & 0 & 0 & 0 & 0 & 2G & 0 & 0 & 0 & 0 & 0 & 0 & b^{(m)}-b_3^{(f)} \\ 0 & 0 & 0 & 0 & 0 & 0 & 0 & 0 & -2G & 0 & 0 & 2G & 0 \end{bmatrix}$$

(8 x 13)

In matrix $\underset{\sim}{H}$, G is the shear modulus of the matrix.

Substituting (2.73) into (2.71), the average normal subcell stresses can be expressed as

$$\underset{\sim}{S}_N = \overline{\underset{\sim}{D}}\underset{\sim}{e} \tag{2.74a}$$

where

$$\overline{\underset{\sim}{D}} = \underset{\sim}{E} + \underset{\sim}{F}\underset{\sim}{G}^{-1}\underset{\sim}{H} \tag{2.74b}$$

By examination of (2.71) and (2.72), it is observed that

$$\underset{\sim}{\bar{D}} = \left[\underset{\sim}{\bar{D}}_N \,|\, \underset{\sim}{\bar{D}}_N^{(12)} \,|\, \underset{\sim}{\bar{D}}_N^{(21)} \,|\, \underset{\sim}{\bar{D}}_N^{(22)} \,|\, \underset{\sim}{\bar{D}}^{(T)}\right] \tag{2.75}$$

Using (2.31), the average normal stress vector $\underset{\sim}{\sigma}_N$ can be expressed in the following form as

$$\underset{\sim}{\sigma}_N = \underset{\sim\sim}{A}\underset{\sim}{S}_N \tag{2.76}$$

where

$$\underset{\sim}{A} = \left[V_{11}\underset{\sim}{I} \,|\, V_{12}\underset{\sim}{I} \,|\, V_{21}\underset{\sim}{I} \,|\, V_{22}\underset{\sim}{I}\right],$$

$V_{\beta\gamma}$ is defined in (2.27) and $\underset{\sim}{I}$ is a (3 x 3) identity matrix. Substitution of (2.74) into (2.76), yields the required expression for the average normal stresses

$$\bar{\underset{\sim}{\sigma}}_N = \underset{\sim\sim}{\bar{C}}\underset{\sim}{e} \tag{2.77}$$

where

$$\underset{\sim\sim}{\bar{C}} = \underset{\sim\sim}{A}\underset{\sim\sim}{\bar{D}} = \left[\underset{\sim}{C}_N^{*} \,|\, \underset{\sim}{C}_N^{*(12)} \,|\, \underset{\sim}{C}_N^{*(12)} \,|\, \underset{\sim}{C}_N^{*(22)} \,|\, \underset{\sim}{C}^{*(T)}\right]$$

At this point, the required matrix formulation for the average normal stress-strain relations is completed. From a computation aspect, the most difficult operation is forming the term $G^{-1}H$ in (2.74b). Since the G matrix is of dimension (8 x 8) the effort involved is minimal.

2.3.2 Longitudinal Shear

The longitudinal shear response in the 12 direction is evaluated by considering $\bar{\sigma}_{12} \neq 0$ and all other stress components $\bar{\sigma}_{ij} = 0$. From (2.32), (2.40) and (2.42), the following four equations are obtained

$$S_{12}^{(11)} = S_{12}^{(21)} \quad , \quad S_{12}^{(12)} = S_{12}^{(22)}$$

$$h_1\phi_2^{(11)} + h_2\phi_2^{(12)} + 2R_t S_{12}^{(11)} = \frac{\partial w_i}{\partial x_2} \tag{2.78}$$

$$h_1\phi_2^{(12)} + h_2\phi_2^{(22)} = \frac{\partial w_i}{\partial x_2}$$

where h_β is normalized as shown in (2.65a). Using (2.63), (2.64) and (2.64), these equations become

$$\begin{bmatrix} h_1^* & 0 & D_2 & 0 \\ 0 & h_1 & 0 & D_2 \\ G_{12}^{(f)} & 0 & -G^{(m)} & 0 \\ 0 & 1 & 0 & -1 \end{bmatrix} \begin{Bmatrix} \sigma_1^{(11)} \\ \phi_1^{(12)} \\ \phi_1^{(21)} \\ \phi_1^{(22)} \end{Bmatrix} = \begin{Bmatrix} w_{1,2} - 2R_t G_{12}^{(f)} w_{2,1} \\ w_{1,2} \\ (G^{(m)} - G_{12}^{(f)}) w_{2,1} - G^{(m)} 2L_{12}^{(21)} \\ 2L_{12}^{(12)} - 2L_{12}^{(22)} \end{Bmatrix} \tag{2.79}$$

where

$$h_1^* = h_1 + 2R_t G_{12}^{(f)}$$

$$(\cdot)_{,i} = \frac{\partial}{\partial x_i}$$

Inverting the coefficient matrix, the local displacements $\phi_2^{(\beta\gamma)}$ are

$$\begin{Bmatrix} \phi_2^{(11)} \\ \phi_2^{(12)} \\ \phi_2^{(21)} \\ \phi_2^{(21)} \end{Bmatrix} = \begin{bmatrix} G^{(m)}/\Delta_{12} & 0 & h_2/\Delta_{12} & 0 \\ 0 & 1 & 0 & h_2 \\ G_{12}^{(f)}/\Delta_{12} & 0 & -h_1^*/\Delta_{12} & 0 \\ 0 & 1 & 0 & -h_2 \end{bmatrix} \begin{Bmatrix} w_{1,2} - 2R_t G_{12}^{(f)} w_{2,1} \\ w_{1,2} \\ (G^{(m)} - G_{12}^{(f)}) w_{2,1} - G^{(m)} 2L_{12}^{(21)} \\ 2L_{12}^{(12)} - 2L_{12}^{(22)} \end{Bmatrix} \tag{2.80}$$

where

$$\Delta_{12} = h_1 G^{(m)} + h_2 G_{12}^{(f)} + 2R_t G^{(m)} G_{12}^{(f)}$$

The average subcell stresses $S_{12}^{(\beta\gamma)}$ and average stress $\bar{\sigma}_{12}$ can now be evaluated, noting the terms $w_{1,2}$ and $w_{2,1}$ combine to form a $2\varepsilon_{12} = w_{1,2} + w_{2,1}$. The required constitutive relations are summarized as follows:

$$\begin{Bmatrix} S_{12}^{(11)} \\ S_{12}^{(12)} \\ S_{12}^{(21)} \\ S_{12}^{(22)} \\ \bar{\sigma}_{12} \end{Bmatrix} = \begin{bmatrix} \frac{G^{(m)} G_{12}^{(f)}}{\Delta_{12}} & 0 & \frac{h_2 G^{(m)} G_{12}^{(f)}}{\Delta_{12}} & 0 \\ G^{(m)} & h_1 G^{(m)} & 0 & h_2 G^{(m)} \\ \frac{G^{(m)} G_{12}^{(f)}}{\Delta_{12}} & 0 & \frac{h_2 G^{(m)} G_{12}^{(f)}}{\Delta_{12}} & 0 \\ G^{(m)} & h_1 G^{(m)} & 0 & h_2 G^{(m)} \\ G_{12}^{*} & V_{12} G^{(m)} & \frac{V_{21} G^{(m)} G_{12}^{(f)}}{\Delta_{12}} & V_{22} G^{(m)} \end{bmatrix} \begin{Bmatrix} 2\bar{\varepsilon}_{12} \\ -2L_{12}^{(12)} \\ -2L_{12}^{(21)} \\ -2L_{12}^{(22)} \end{Bmatrix} \tag{2.81}$$

where

$$G_{12}^{*} = \frac{G^{(m)}}{\Delta_{12}} [G_{12}^{(f)}(V_{11} + V_{21} + V_{22}) + G^{(m)} V_{12} + 2\ell_2 R_t G^{(m)} G_{12}^{(f)}]$$

and the terms Δ_{12} and $V_{\beta\gamma}$ are defined in (2.80) and (2.27), respectively.

The longitudinal shear response in the 13 direction is obtained by considering (2.23), (2.41) and (2.43) with i = 3. These equations are solved in a similar fashion, like the shear response in the 12 direction. For completeness, these results will only be stated.

$$\begin{Bmatrix} S_{13}^{(11)} \\ S_{13}^{(12)} \\ S_{13}^{(21)} \\ S_{13}^{(22)} \\ \bar{\sigma}_{13} \end{Bmatrix} = \begin{bmatrix} \frac{G^{(m)}G_{13}^{(f)}}{\Delta_{13}} & \frac{\ell_2 G^{(m)}G_{13}^{(m)}}{\Delta_{13}} & 0 & 0 \\ G & \frac{\ell_2 G^{(m)}G_{13}^{(f)}}{\Delta_{13}} & 0 & 0 \\ G & 0 & \ell_1 G^{(m)} & \ell_2 G^{(m)} \\ \frac{G^{(m)}G_{13}^{(f)}}{\Delta_{13}} & 0 & \ell_1 G^{(m)} & \ell_2 G^{(m)} \\ G_{13}^{*} & \frac{V_{12}G^{(m)}G_{13}^{(f)}}{\Delta_{13}} & V_{21}G^{(m)} & V_{22}G^{(m)} \end{bmatrix} \begin{Bmatrix} 2\varepsilon_{13} \\ -2L_{13}^{(12)} \\ -2L_{13}^{(21)} \\ -2L_{13}^{(22)} \end{Bmatrix} \tag{2.82}$$

where

$$G_{13}^{*} = \frac{G^{(m)}}{\Delta_{13}} \left[G_{13}^{(f)}(V_{11} + V_{12} + V_{22}) + G^{(m)}V_{21} + 2h_2 R_t G^{(m)}G_{13}^{(f)}\right]$$

$$\Delta_{13} = \ell_1 G^{(m)} + \ell_2 G_{13}^{(f)} + 2R_t G^{(m)}G_{13}^{(f)}$$

2.3.3 Transverse Shear

The transverse shear response is evaluated by considering $\bar{\sigma}_{23} \neq 0$ and all other stress components $\sigma_{ij} = 0$. From the traction continuity relations (2.32) and (2.33), we obtain

$$S_{23}^{(1\gamma)} = S_{23}^{(2\gamma)} \tag{2.83}$$

$$S_{23}^{(\beta 1)} = S_{23}^{(\beta 2)} \tag{2.84}$$

Careful examination of these equations along with (2.30), we can conclude that

$$\bar{\sigma}_{23} = S_{23}^{(11)} = S_{23}^{(12)} = S_{23}^{(21)} = S_{23}^{(22)} \tag{2.85}$$

An expression for the average strain $\bar{\varepsilon}_{23}$ in terms of the subcell strains $E_{23}^{(\beta\gamma)}$ is also necessary. This can be developed by considering (2.40) with i = 3, multiplied by ℓ_1 when $\gamma = 1$ and ℓ_2 when $\gamma = 2$ and (2.41) with i = 2, multiplied by h_1 when $\beta = 1$ and h_2 when $\beta = 2$. The four resulting equations are added together to yield

$$\frac{\partial w_2}{\partial x_3} + \frac{\partial w_3}{\partial x_2} = \sum_{\beta,\gamma=1}^{2} V_{\beta\gamma}[\phi_3^{(\beta\gamma)}) + \psi_2^{(\beta\gamma)}] + 2(\ell_1 + h_1)R_t\, S_{23}^{(11)} \qquad (2.86)$$

Using (2.46f) and (2.52), we obtain the required expression for the average strain

$$2\bar{\varepsilon}_{23} = \sum_{\beta,\gamma=1}^{2} V_{\beta\gamma} 2E_{23}^{(\beta\gamma)} + 2(\ell_1 + h_1)R_t\, S_{23}^{(11)} \qquad (2.87)$$

The effective response of the composite is obtained by introducing (2.63), (2.69) and (2.80) into (2.82). Solving for $\bar{\sigma}_{23}$ we have

$$\bar{\sigma}_{23} = 2G_{23}^{*}[\bar{\varepsilon}_{23} - V_{12}L_{23}^{(12)} - V_{21}L_{23}^{(21)} - V_{22}L_{23}^{(22)}] \qquad (2.88)$$

where

$$G_{23}^{*} = \frac{G^{(m)}G_{23}^{(f)}}{V_{11}G + (V_{12} + V_{21} + V_{22})G_{23}^{(m)} + 2(h_1 + \ell_1)R_tG^{(m)}G_{23}^{(f)}}$$

Since the transverse shear stress is uniform in the fiber and matrix (2.85), the above expression for $\bar{\sigma}_{23}$ is a Reuss bound or an upper bound solution [1].

2.3.4 Transversely Isotropic Averaging

In the preceeding sections, the effective constitutive relations were established for a continuously reinforced composite. The solution of the effective behavior was facilitated by utilizing the uncoupling of the shear and normal material response. These effects are now combined

to give

$$\bar{\underset{\sim}{\sigma}} = \underset{\sim}{C}^{*}\bar{\underset{\sim}{\varepsilon}} - \sum_{\substack{\beta,\gamma=1 \\ \beta+\gamma\neq 2}}^{2} \underset{\sim}{C}^{*(\beta\gamma)}\, \underset{\sim}{L}^{(\beta\gamma)} - \Delta T\, \underset{\sim}{C}^{*(T)} \tag{2.89}$$

where the effective elastic modulus matrix is

$$\underset{\sim}{C}^{*} = \begin{bmatrix} \underset{\sim}{C}^{*}_{N} & & & \text{zero} \\ & G^{*}_{12} & & \\ & & G^{*}_{13} & \\ \text{zero} & & & G^{*}_{23} \end{bmatrix}$$

The matrices $\underset{\sim}{C}^{*(\beta\gamma)}$ are formed in a similar fashion from (2.68), (2.81), (2.82) and (2.88), and the vector $\underset{\sim}{C}^{*(T)}$ is defined as

$$\underset{\sim}{C}^{*(T)} = \{\underset{\sim}{C}^{*(T)}_{N}, 0, 0, 0\}$$

By factoring the matrix $\underset{\sim}{C}^{*}$ from all of the terms, the average plastic strains $\bar{\underset{\sim}{\varepsilon}}^{P}$ and average thermal strains $\bar{\varepsilon}^{T}$ are easily identified by the relation

$$\bar{\underset{\sim}{\sigma}} = \underset{\sim}{C}^{*}(\bar{\underset{\sim}{\varepsilon}} - \bar{\underset{\sim}{\varepsilon}}^{P} - \bar{\underset{\sim}{\varepsilon}}^{T}) \tag{2.90}$$

where

$$\bar{\underset{\sim}{\varepsilon}}^{P} = (C^{*})^{-1} \sum_{\beta,\gamma=1}^{2} \underset{\sim}{C}^{*(\beta\gamma)}\, \underset{\sim}{L}^{(\beta\gamma)} \tag{2.91}$$

$$\bar{\underset{\sim}{\varepsilon}}^{T} = \Delta T(\underset{\sim}{C}^{*})^{-1}\underset{\sim}{C}^{*(T)} \tag{2.92}$$

In general, the Aboudi micromechanics theory, due to the rectangular fiber array, produces orthotropic elastic constants characterized by a total of nine independent constants. Usually in applying the Aboudi

theory, the fibers are assumed to be square ($h_1 = \ell_1$) and equally spaced ($h_2 = \ell_2$). The resulting square symmetry reduces the total number of independent elastic constants to six (C^*_{11}, $C^*_{22} = C^*_{33}$, $C^*_{12} = C^*_{13}$, C^*_{23}, $C^*_{44} = C^*_{55}$ and C^*_{66}). If transversely isotropic elastic constants are desired instead, Aboudi [48] has developed an averaging method which can be utilized. This method will be referred to as transversely isotropic averaging (TIA).

The procedure is developed by considering the elastic modulus matrix $\underset{\sim}{C}^*$ rotated an arbitrary angle ξ about the fiber axis (the x_1-axis). The rotated modulus matrix $\underset{\sim}{C}^{*\prime}(\xi)$ is determined using standard tensor transformations. The transversely isotropic modulus matrix $\overline{\underset{\sim}{C}}^*$ is obtained by averaging $\underset{\sim}{C}^{*\prime}(\xi)$ over all possible orientations such that

$$\overline{\underset{\sim}{C}}^* = \frac{1}{\pi}\int_0^{\pi} \underset{\sim}{C}^{*\prime}(\xi)\, d\xi \tag{2.93}$$

Performing the indicated integration, the nonzero elements in the symmetric matrix $\underset{\sim}{C}$ are given by

$$\begin{aligned}
\overline{C}^*_{11} &= C^*_{11} \\
\overline{C}^*_{12} &= \overline{C}^*_{13} = \tfrac{1}{2}(C^*_{12} + C^*_{13}) \\
\overline{C}^*_{22} &= \overline{C}^*_{33} = \tfrac{3}{8}(C^*_{22} + C^*_{33}) + \frac{C^*_{23}}{4} + \frac{C^*_{66}}{6} \\
\overline{C}^*_{23} &= \tfrac{1}{8}(C^*_{22} + C^*_{33}) + \frac{3C^*_{23}}{4} - \frac{C^*_{66}}{6} \\
\overline{C}^*_{44} &= \overline{C}^*_{55} = \tfrac{1}{2}(C^*_{44} + C^*_{55}) \\
\overline{C}^*_{66} &= \tfrac{1}{2}(\overline{C}^*_{22} - \overline{C}^*_{23})
\end{aligned} \tag{2.94}$$

These equations comprise the five independent constants characteristic of a transversely isotropic material.

The transversely isotropic elastic modulus matrix $\underset{\sim}{C}$ is incorporated into the effective constitutive relations by replacing $\underset{\sim}{C}^*$ by $\overline{\underset{\sim}{C}}^*$ in (2.90), while retaining the expressions (2.91) and (2.92) without modification for the average plastic and thermal strains. It should be noted that by replacing $\underset{\sim}{C}^*$ with $\overline{\underset{\sim}{C}}^*$, the subcell stresses $S_{ij}^{(\beta\gamma)}$ are no longer related to the average stresses $\overline{\sigma}_{ij}$ through (2.30). Although this method introduces a certain degree of approximation, Pindera and his coworkers [79] have employed TIA to obtain excellent response predictions for a boron/aluminum composite.

2.3.5 Plane Stress

The previously developed constitutive relations are modified to incorporate the assumption of plane stress in the x_1-x_2 plane. Due to the anisotropy of the composite, this assumption only alters the normal stress-strain equations. For the state of plane stress $\overline{\sigma}_{33} = 0$, the reduced constitutive equations for the normal stresses are expressed as

$$\underset{\sim}{\sigma}_R = \hat{\underset{\sim\sim}{C}}\underset{\sim}{e}_R \tag{2.95}$$

and

$$\underset{\sim}{S}_N = \hat{\underset{\sim\sim}{D}}\underset{\sim}{e}_R \tag{2.96}$$

where the vectors $\overline{\underset{\sim}{\sigma}}_R$ and $\underset{\sim}{e}_R$ are the same as $\overline{\underset{\sim}{\sigma}}_N$ and $\underset{\sim}{e}$ with $\overline{\varepsilon}_{33}$ eliminated. The components of the reduced stiffness matrices $\hat{\underset{\sim}{C}}$ and $\hat{\underset{\sim}{D}}$ are defined as

$$\hat{c}_{ij} = \begin{cases} \bar{c}_{ij} = \dfrac{\bar{c}_{i3}\bar{c}_{3j}}{\bar{c}_{33}} & \begin{matrix} i = 1,2 \\ j = 1,2 \end{matrix} \\ \bar{c}_{i(j+1)} = \dfrac{\bar{c}_{i3}\bar{c}_{3(j+1)}}{\bar{c}_{33}} & \begin{matrix} i = 1,2 \\ j = 3,4,5,\ldots,12 \end{matrix} \end{cases} \tag{2.97}$$

and

$$\hat{d}_{ij} = \begin{cases} \bar{d}_{ij} - \dfrac{\bar{d}_{i3}\bar{c}_{3j}}{\bar{c}_{33}} & \begin{matrix} i = 1,2,3,\ldots,12 \\ j = 1,2 \end{matrix} \\ \bar{d}_{i(j+1)} - \dfrac{\bar{d}_{i3}\bar{c}_{3(j+1)}}{\bar{c}_{33}} & \begin{matrix} i = 1,2,3,\ldots,12 \\ j = 3,4,5,\ldots,12 \end{matrix} \end{cases} \tag{2.98}$$

where $\bar{c}_{ij}$ and $\bar{d}_{ij}$ are elements of the $\underset{\sim}{\bar{C}}$ and $\underset{\sim}{\bar{D}}$ matrices defined in (2.77) and (2.75), respectively. The matrices $\underset{\sim}{\hat{C}}$ and $\underset{\sim}{\hat{D}}$ are partitioned similarly to $\underset{\sim}{\bar{C}}$ and $\underset{\sim}{\bar{D}}$ to obtain

$$\underset{\sim}{\hat{C}} = \left[\underset{\sim}{\hat{C}}^{*}_{N} \,\middle|\, \underset{\sim}{\hat{C}}^{*}_{N}(12) \,\middle|\, \underset{\sim}{\hat{C}}^{*}_{N}(21) \,\middle|\, \underset{\sim}{\hat{C}}^{*}_{N}(22) \,\middle|\, \underset{\sim}{\hat{C}}^{*}(T)\right] \tag{2.99}$$

$$\underset{\sim}{\hat{D}} = \left[\underset{\sim}{\hat{D}}^{*}_{N} \,\middle|\, \underset{\sim}{\hat{D}}^{*}_{N}(12) \,\middle|\, \underset{\sim}{\hat{D}}^{*}_{N}(21) \,\middle|\, \underset{\sim}{\hat{D}}^{*}_{N}(22) \,\middle|\, \underset{\sim}{\hat{D}}^{*}(T)\right] \tag{2.100}$$

Combining the normal and shear equations, the plane stress constitutive relations are

$$\underset{\sim}{\sigma}' = \underset{\sim}{Q}\underset{\sim}{\varepsilon}' - \underset{\sim}{\sigma}'_{P} - \underset{\sim}{\sigma}'_{T} \tag{2.101}$$

where

$$\underset{\sim}{\sigma}' = \{\bar{\sigma}_{11}, \bar{\sigma}_{22}, \bar{\sigma}_{12}, \bar{\sigma}_{13}, \bar{\sigma}_{23}\}^{T}$$

$$\underset{\sim}{\varepsilon}' = \{\bar{\varepsilon}_{11}, \bar{\varepsilon}_{22}, 2\bar{\varepsilon}_{12}, 2\bar{\varepsilon}_{13}, 2\bar{\varepsilon}_{23}\}^{T}$$

$$\underset{\sim}{\sigma}'_{P} = \{\sigma^{P}_{11}, \sigma^{P}_{22}, \sigma^{P}_{12}, \sigma^{P}_{13}, \sigma^{P}_{23}\}^{T}$$

$$\underset{\sim}{\sigma}'_T = \{\sigma_{11}^T, \sigma_{22}^T, 0, 0, 0\}^T$$

and $\underset{\sim}{Q}$ is the reduced stiffness matrix. Notationally, the prime (') in (2.52) is introduced to indicate either reduced stress or reduced strain vectors with respect to the x_1, x_2, x_3 coordinate system.

Using (2.52), (2.81), (2.82) and (2.88) we find

$$\underset{\sim}{Q} = \begin{bmatrix} \hat{c}_{11} & \hat{c}_{12} & 0 & 0 & 0 \\ \hat{c}_{21} & \hat{c}_{22} & 0 & 0 & 0 \\ 0 & 0 & G_{12}^* & 0 & 0 \\ 0 & 0 & 0 & G_{13}^* & 0 \\ 0 & 0 & 0 & 0 & G_{23}^* \end{bmatrix} \tag{2.102}$$

The upper (2 x 2) sub-matrix of $\underset{\sim}{Q}$ should be identified as $\hat{\underset{\sim}{C}}_N^*$ from (2.99).

The vector $\underset{\sim}{\sigma}'_P$ characterizes the inelastic response of the composite. This vector will be referred to as the plastic stress vector which is defined as

$$\underset{\sim}{\sigma}'_P = \sum_{\substack{\beta,\gamma=1 \\ \beta+\gamma\neq 2}}^{2} \underset{\sim}{Q}^{(\beta\gamma)} \underset{\sim}{L}^{(\beta\gamma)} \tag{2.103}$$

where $\underset{\sim}{L}^{(\beta\gamma)}$ is given in (2.54) and $\underset{\sim}{Q}^{(\beta\gamma)}$ is established in a manner similar to $\underset{\sim}{Q}$. For example,

$$\underset{\sim}{Q}^{(12)} = \begin{bmatrix} \hat{C}_{13} & \hat{C}_{14} & \hat{C}_{15} & 0 & 0 & 0 \\ \hat{C}_{23} & \hat{C}_{24} & \hat{C}_{25} & 0 & 0 & 0 \\ 0 & 0 & 0 & V_{12}G^{(m)} & 0 & 0 \\ 0 & 0 & 0 & 0 & \dfrac{V_{12}G^{(m)}G_{13}^{(f)}}{\Delta_{13}} & 0 \\ 0 & 0 & 0 & 0 & 0 & V_{12}G_{23}^{*} \end{bmatrix} \tag{2.104}$$

where the normal response is given by the upper (2 x 3) sub-matrix which is $\hat{\underset{\sim}{C}}_N^{*(12)}$ in (2.99) and the shear terms are identified as coefficients of $-2L_{ij}^{(12)}$ from (2.81), (2.82) and (2.88).

Similarly the vector $\underset{\sim}{\sigma}_T^{\prime}$ is introduced to account for stresses resulting from thermal expansion. The thermal stress vector is defined as

$$\underset{\sim}{\sigma}_T^{\prime} = \Delta T \, \underset{\sim}{Q}^{(T)} = \Delta T \begin{Bmatrix} \hat{\underset{\sim}{C}}^{*(T)} \\ 0 \\ 0 \\ 0 \end{Bmatrix} \tag{2.105}$$

2.3.6 Transformation of Constitutive Relations

Transformed constitutive relations are required in order to develop the lamination theory in the next chapter. Due to the added complexity of using a micromechanics theory and the incorporation of inelastic effects, the transformation of the stress-strain relations will be addressed in some detail.

Consider the lamina constitutive relations established in the previous section which define the stress-strain behavior with respect to the x_1, x_2, x_3 coordinate system. We shall introduce a second coordinate system x, y, z which is rotated relative to the x_1, x_2, x_3 system by an angle θ as shown in Fig. 2.4. The x_1, x_2, x_3 and x, y, z coordinate systems will be called the material and structural coordinate systems, respectively. For a given rotation θ, we have the following relation:

$$\begin{Bmatrix} \bar{\sigma}_{11} \\ \bar{\sigma}_{22} \\ \bar{\sigma}_{12} \\ \bar{\sigma}_{13} \\ \bar{\sigma}_{23} \end{Bmatrix} = \begin{bmatrix} m^2 & n^2 & 2mn & 0 & 0 \\ n^2 & m^2 & -2mn & 0 & 0 \\ -mn & mn & (m^2 - n^2) & 0 & 0 \\ 0 & 0 & 0 & m & n \\ 0 & 0 & 0 & -n & m \end{bmatrix} \begin{Bmatrix} \sigma_{xx} \\ \sigma_{yy} \\ \sigma_{xy} \\ \sigma_{xz} \\ \sigma_{yz} \end{Bmatrix} \qquad (2.106a)$$

or in matrix notation

$$\underset{\sim}{\sigma}' = \underset{\sim\sigma}{T} \underset{\sim}{\sigma} \qquad (2.106b)$$

where

$$m = \cos \theta$$

$$n = \sin \theta$$

Similarly, the strains are related through

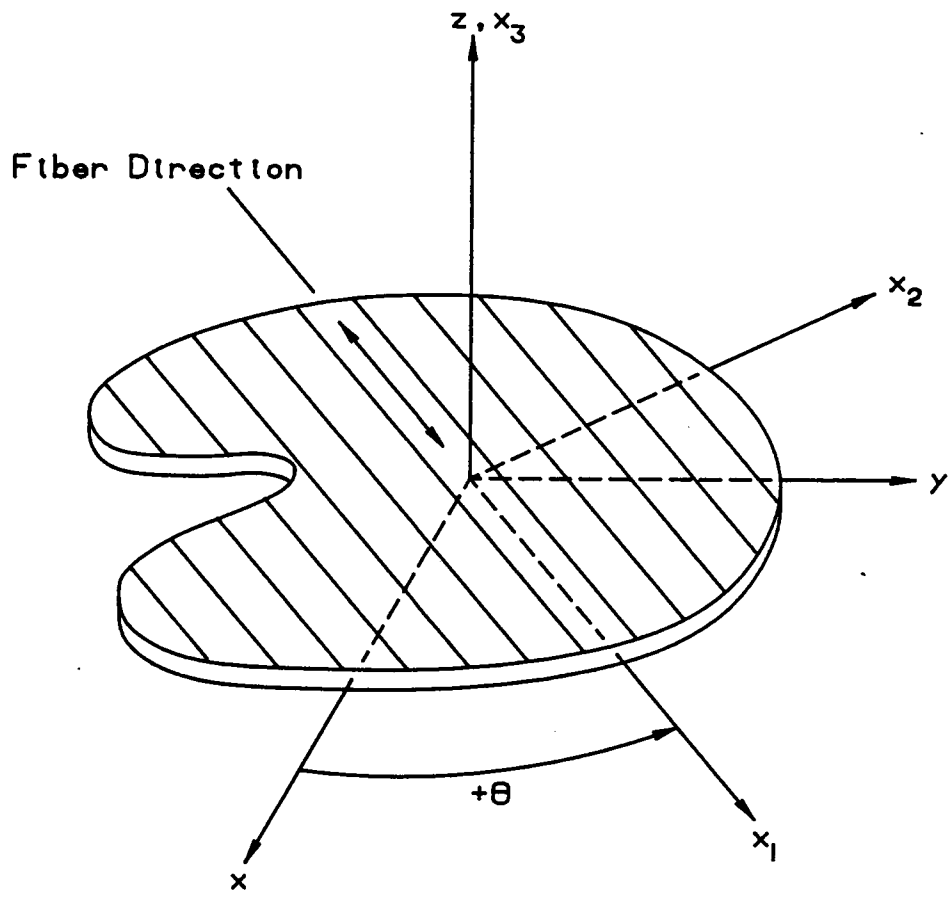

x_1, x_2, x_3 - Material Coordinate System

x, y, z - Structural Coordinate System

Figure 2.4. Typical Lamina

$$\begin{Bmatrix} \bar{\varepsilon}_{11} \\ \bar{\varepsilon}_{22} \\ 2\bar{\varepsilon}_{12} \\ 2\bar{\varepsilon}_{13} \\ 2\bar{\varepsilon}_{23} \end{Bmatrix} = \begin{bmatrix} m^2 & n^2 & mn & 0 & 0 \\ n^2 & m^2 & -mn & 0 & 0 \\ -2mn & 2mn & (m^2 - n^2) & 0 & 0 \\ 0 & 0 & 0 & m & n \\ 0 & 0 & 0 & -n & m \end{bmatrix} \begin{Bmatrix} \varepsilon_{xx} \\ \varepsilon_{yy} \\ 2\varepsilon_{xy} \\ 2\varepsilon_{xz} \\ 2\varepsilon_{yz} \end{Bmatrix} \quad (2.107a)$$

or

$$\underset{\sim}{\varepsilon}' = \underset{\sim\varepsilon}{T} \underset{\sim}{\varepsilon} \quad (2.107b)$$

Using (2.101), (2.106) and (2.107), the stress-strain relations relative to the structural coordinate system are given by

$$\underset{\sim}{\sigma} = \underset{\sim}{\bar{Q}} \underset{\sim}{\varepsilon} - \underset{\sim}{\sigma}_P - \underset{\sim}{\sigma}_T \quad (2.108)$$

where

$$\underset{\sim}{\bar{Q}} = \underset{\sim\sigma}{T}^{-1} \underset{\sim}{Q} \underset{\sim\varepsilon}{T}$$

$$\underset{\sim}{\sigma}_P = \underset{\sim\sigma}{T}^{-1} \underset{\sim}{\sigma}'_P = \underset{\sim\sigma}{T}^{-1} \sum_{\substack{\beta,\gamma=1 \\ \beta+\gamma\neq 2}}^{2} \underset{\sim}{Q}^{(\beta\gamma)} \underset{\sim}{L}^{(\beta\gamma)}$$

$$\underset{\sim}{\sigma}_T = \underset{\sim\sigma}{T}^{-1} \underset{\sim}{\sigma}'_T = \Delta T \, (\underset{\sim\sigma}{T})^{-1} \underset{\sim}{Q}^{(T)}$$

3. LAMINATED PLATE THEORY

3.1 Introduction

The nonlinear constitutive relations developed in the previous chapter are incorporated into a refined plate theory which will be termed a first-order shear deformation theory [84]. This distinction is used to identify the order of the displacement expansion used through the thickness of the plate. The theory presented here is an extension of theories originally proposed by Hildebrand, Reissner, and Thomas [80] and Mindlin [81]. The fundamental assumptions of the first-order shear deformation theory are:

1. The displacements of the midsurface are small compared to the thickness of the plate.
2. Straight lines normal to the midsurface before deformation remain straight and inextensible but not necessarily normal to the midsurface after deformation.
3. Stresses normal to the midsurface are negligible irrespective of the loading.

3.2 Kinematics

A cartesian coordinate system (x, y, z), which we shall call the structural coordinate system is used, see Fig. 3.1. The structural coordinate system is oriented so that the x-y plane coincides with the midsurface of the plate. According to assumption 2 above, the displacement field can be assumed in the following form

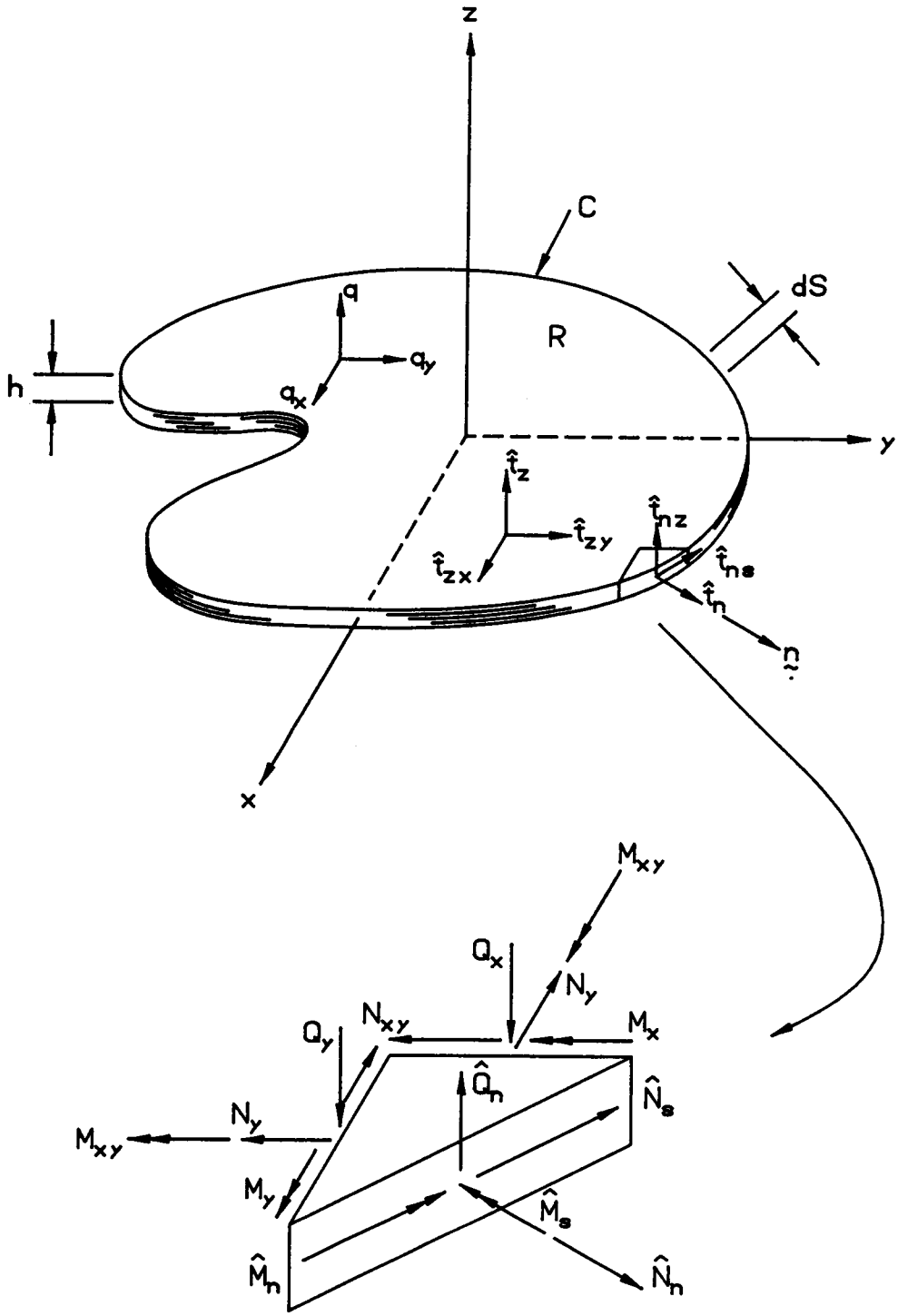

Figure 3.1. Typical Laminated Plate

$$u_x(x,y,z,t) = u(x,y,t) + z\psi_x(x,y,t)$$

$$u_y(x,y,z,t) = v(x,y,t) + z\psi_y(x,y,t) \tag{3.1}$$

$$u_z(x,y,z,t) = w(x,y,t)$$

where the functions u, v and w are the displacements at the midsurface $z = 0$ and the functions ψ_x and ψ_y characterize the rotations of normals to the midsurface in the x and y direction, respectively. We should note that the classical Love-Kirchhoff theory is obtained by setting

$$\psi_x = -\frac{\partial w}{\partial x}$$

$$\psi_y = -\frac{\partial w}{\partial y} \tag{3.2}$$

We can express the infinitesimal strains ε_{mn} associated with the displacement field (3.1) as

$$\varepsilon_{mn} = \varepsilon_{mn(0)} + z\varepsilon_{mn(1)}, \text{ for } m,n = x,y,z \tag{3.3}$$

where

$$\varepsilon_{xx(0)} = \frac{\partial u}{\partial x}, \qquad \varepsilon_{xx(1)} = \frac{\partial \psi_x}{\partial x}$$

$$\varepsilon_{yy(0)} = \frac{\partial v}{\partial y}, \qquad \varepsilon_{yy(1)} = \frac{\partial \psi_y}{\partial y}$$

$$2\varepsilon_{yy(0)} = \frac{\partial u}{\partial y} + \frac{\partial v}{\partial x}, \qquad 2\varepsilon_{xy(1)} = \frac{\partial \psi_x}{\partial y} + \frac{\partial \psi_y}{\partial x}$$

$$2\varepsilon_{xz(0)} = \psi_x + \frac{\partial w}{\partial x}, \qquad \varepsilon_{xz(1)} = 0$$

$$2\varepsilon_{yz(0)} = \psi_y + \frac{\partial w}{\partial y}, \qquad \varepsilon_{yz(1)} = 0$$

$$\varepsilon_{zz} = \varepsilon_{zz(0)} = \varepsilon_{zz(1)} = 0$$

Separating the strains into inplane and transverse shear components, we obtain

$$\begin{Bmatrix} \underset{\sim}{\varepsilon}_I \\ \underset{\sim}{\varepsilon}_S \end{Bmatrix} = \begin{Bmatrix} \underset{\sim}{\varepsilon}_o \\ \underset{\sim}{\varepsilon}_S \end{Bmatrix} + z \begin{Bmatrix} \underset{\sim}{\kappa} \\ \underset{\sim}{0} \end{Bmatrix} \tag{3.4}$$

where

$$\underset{\sim}{\varepsilon}_I = \{\varepsilon_{xx}, \varepsilon_{yy}, 2\varepsilon_{xy}\}^T$$

$$\underset{\sim}{\varepsilon}_o = \{\varepsilon_{xx(0)}, \varepsilon_{yy(0)}, 2\varepsilon_{xy(0)}\}^T$$

$$\underset{\sim}{\kappa} = \{\varepsilon_{xx(1)}, \varepsilon_{yy(1)}, 2\varepsilon_{xy(1)}\}^T$$

$$\underset{\sim}{\varepsilon}_S = \{2\varepsilon_{xz}, 2\varepsilon_{yz}\}^T$$

and $\underset{\sim}{0}$ is the zero vector.

3.3 Laminated Plate Constitutive Relations

By assumption 3, the laminate is in an approximate state of plane stress. For the m^{th} lamina which is oriented by an angle θ relative to the structural system, the stress-strain relations are given by (2.108). After partitioning these equations into inplane and transverse stress components, we obtain

$$\underset{\sim}{\sigma}_I = \overline{\underset{\sim}{Q}}_I^{(m)} (\underset{\sim}{\varepsilon}_o + z\underset{\sim}{\kappa}) - \underset{\sim}{\sigma}_{IP}^{(m)} - \underset{\sim}{\sigma}_{IT}^{(m)} \tag{3.5a}$$

and

$$\underset{\sim}{\sigma}_S = \overline{\underset{\sim}{Q}}_S^{(m)} \underset{\sim}{\varepsilon}_S - \sigma_{SP}^{(m)} \tag{3.5b}$$

where

$$\underset{\sim}{\sigma}_I^{(m)} = \{\sigma_{xx}, \sigma_{yy}, \sigma_{xy}\}_{(m)}^T$$

$$\underset{\sim}{\sigma}_{IP}^{(m)} = \{\sigma_{xx}^{P}, \sigma_{yy}^{P}, \sigma_{xy}^{P}\}_{(m)}^{T}$$

$$\underset{\sim}{\sigma}_{IT}^{(m)} = \{\sigma_{xx}^{T}, \sigma_{yy}^{T}, \sigma_{xy}^{T}\}_{(m)}^{T}$$

$$\underset{\sim}{\sigma}_{S}^{(m)} = \{\sigma_{xz}, \sigma_{yz}\}_{(m)}^{T}$$

$$\underset{\sim}{\sigma}_{SP}^{(m)} = \{\sigma_{xz}^{P}, \sigma_{yz}^{P}\}_{(m)}^{T}$$

$\overline{\underset{\sim}{Q}}_I$ and $\overline{\underset{\sim}{Q}}_S$ are defined through the relation

$$\overline{\underset{\sim}{Q}} = \begin{matrix} \overline{\underset{\sim}{Q}}_I & \underset{\sim}{\theta} \\ \underset{\sim}{\theta} & \overline{\underset{\sim}{Q}}_S \end{matrix}$$

where $\underset{\sim}{\theta}$ is the zero matrix.

To develop the required constitutive relations, we now introduce the following stress resultants:

$$\begin{bmatrix} \underset{\sim}{N} & \underset{\sim}{N}^{P} & \underset{\sim}{N}^{T} \\ \underset{\sim}{M} & \underset{\sim}{M}^{P} & \underset{\sim}{M}^{T} \end{bmatrix} = \int_{-\frac{h}{2}}^{+\frac{h}{2}} \begin{Bmatrix} 1 \\ Z \end{Bmatrix} \left[\underset{\sim}{\sigma}_{I}^{(m)} \;\; \underset{\sim}{\sigma}_{IP}^{(m)} \;\; \underset{\sim}{\sigma}_{IT}^{(m)}\right] dz \qquad (3.6a)$$

$$(\underset{\sim}{Q}, \underset{\sim}{Q}^{P}) = \int_{-\frac{h}{2}}^{+\frac{h}{2}} (\underset{\sim}{\sigma}_{S}^{(m)}, \underset{\sim}{\sigma}_{SP}^{(m)}) dz \qquad (3.6b)$$

where

$$\underset{\sim}{N} = \{N_x, N_y, N_{xy}\}^{T}$$

$$\underset{\sim}{N}^{P} = \{N_x^{P}, N_y^{P}, N_{xy}^{P}\}^{T}$$

$$\underset{\sim}{N}^{T} = \{N_x^{T}, N_y^{T}, N_{xy}^{T}\}^{T}$$

$$\underset{\sim}{M} = \{M_x, M_y, M_{xy}\}^{T}$$

$$\underset{\sim}{M}^P = \{M_x^P, M_y^P, M_{xy}^P\}^T$$

$$\underset{\sim}{M}^T = \{M_x^T, M_y^T, M_{xy}^T\}^T$$

$$\underset{\sim}{Q} = \{Q_x, Q_y\}^T$$

$$\underset{\sim}{Q}^P = \{Q_x^P, Q_y^P\}^T$$

By introducing (3.5a) into the expressions for $\underset{\sim}{N}$ and $\underset{\sim}{M}$ from (3.6a) the in-plane constitutive equations are now established as

$$\begin{Bmatrix} \underset{\sim}{N} \\ \underset{\sim}{M} \end{Bmatrix} = \begin{bmatrix} \underset{\sim}{A} & \underset{\sim}{B} \\ \underset{\sim}{B} & \underset{\sim}{D} \end{bmatrix} \begin{Bmatrix} \underset{\sim}{\varepsilon}_o \\ \underset{\sim}{\kappa} \end{Bmatrix} - \begin{Bmatrix} \underset{\sim}{N}^P \\ \underset{\sim}{M}^P \end{Bmatrix} - \begin{Bmatrix} \underset{\sim}{N}^T \\ \underset{\sim}{M}^T \end{Bmatrix} \qquad (3.7a)$$

where

$$(\underset{\sim}{A}, \underset{\sim}{B}, \underset{\sim}{D}) = \int_{-h/2}^{+h/2} \overline{\underset{\sim}{Q}}_I (1, z, z^2) dz$$

Similarly the transverse shear constitutive relation are obtained

$$\underset{\sim}{Q} = k(\underset{\sim}{A}^S \underset{\sim}{\varepsilon}_S - \underset{\sim}{Q}^P) \qquad (3.7b)$$

where

$$\underset{\sim}{A}^S = \int_{-h/2}^{+h/2} \overline{\underset{\sim}{Q}}_S dz$$

and k has been added as a shear correction coefficient. Unless stated otherwise the value k = 5/6 will be used. For further discussion of the shear correction coefficient the text by Whitney [82] is suggested.

Equations (3.7a) and (3.7b) form the constitutive relations for the inelastic thermomechanical behavior for a laminated plate. Often these relations are referred to as lamination theory, for example see Jones [83]. For the case of classical plate theory, (3.7b) will vanish leaving only (3.7a).

The evaluation of the constitutive relations (3.7) is complicated due to the inclusion of the plastic stress resultants $\underset{\sim}{N}^P$, $\underset{\sim}{M}^P$ and $\underset{\sim}{Q}^P$. These stress resultants are based on the integration through the thickness of the plate of the plastic stresses $\underset{\sim}{\sigma}_{IP}^{(m)}$ and $\underset{\sim}{\sigma}_{SP}^{(m)}$. The plastic stresses are functions of the subcell plastic strains $L_{ij}^{(\beta\gamma)}$. These strains are evaluated by integrating the plastic flow rule (2.56) in addition to the plastic work expression (2.61). The integration of these equations form a typical initial value problem. Due to the lack of simple analytical expressions for the plastic stresses, numerical integration is used for both the temporal integration of the plastic subcell strains and the spatial integration of the plastic stress resultants. This process will require introducing a set of integration points through the thickness of the plate for computing the stress resultants. At each integration point, an explicit time integration scheme is employed such that the plastic subcell strains are computed at $t + \Delta t$, using the current information available at time t.

Given $\underset{\sim}{N}(t)$, $\underset{\sim}{M}(t)$, $\underset{\sim}{Q}(t)$ and $\Delta T(t)$, the computations required for a typical time step t are summarized as:

1. Evaluate the stress resultants $\underset{\sim}{N}$, $\underset{\sim}{M}$ and $\underset{\sim}{Q}$
2. Evaluate the thermal stress resultants $\underset{\sim}{N}^T$ and $\underset{\sim}{M}^T$
3. Integrate the plastic stress resultants $\underset{\sim}{N}^P$, $\underset{\sim}{M}^P$ and $\underset{\sim}{Q}^P$

4. Solve (3.7) for $\underset{\sim}{\varepsilon}_0$, $\underset{\sim}{\kappa}$ and $\underset{\sim}{\varepsilon}_S$
5. Compute as required for output:
   a) Lamina stresses from (3.5)
   b) Fiber/matrix stresses from (2.96), (2.81), (2.82), (2.85) and (2.88)
6. For each integration point in the laminate:
   a) Evaluate $\dot{L}_{ij}^{(\beta\gamma)}$ and $\dot{W}_p^{(\beta\gamma)}$
   b) Integrate $L_{ij}^{(\beta\gamma)}$ and $W_p^{(\beta\gamma)}$ forward to $t + \Delta t$
7. Increment time counter
8. If $t < t_{end}$
   Then go to step 1
   Else stop

For the first time step, the process is begun with the initial conditions $L_{ij}^{(\beta\gamma)}(0) = 0$ and $W_p^{(\beta\gamma)}(0) = 0$. The specific details of integrating the stress resultants and the plastic subcell strains will be addressed in subsequent sections.

3.4 Equilibrium Equations

The equilibrium equations are developed utilizing the principle of virtual work. First, consider a general body with volume V which has a bounding surface S. The body is in a state of equilibrium subjected to prescribed displacements $\hat{u}_i$ on surface S_1 and prescribed tractions $\hat{t}_i$ on S_2. The surfaces S_1 and S_2 combine to form S without overlapping. The principle of virtual work states that when a body is perturbed from an equilibrium position by a kinematically admissible virtual displacement δu_i, the resulting virtual work is zero

$$\int_V \sigma_{ij}\delta\varepsilon_{ij}dV - \int_{S_2} \hat{t}_i\delta u_i dS = 0 \qquad (3.8)$$

where the first integral is the virtual work of the internal forces and the second integral is the virtual work due to external forces on S_2. The virtual work due to external forces on S_1 is zero since δu_i must vanish on S_1 for a kinematically admissible virtual displacement field.

In order to apply the principle of virtual work to the first-order shear deformation plate theory, consider a plate in the x-y plane of uniform thickness h, see Fig. 3.1. The middle surface of the plate at z = 0 is bounded by the curve C. The area interior to the curve C will be denoted by R. The internal virtual work of the plate is expressed as

$$\int_v \sigma_{ij}\delta\varepsilon_{ij}dV = \int_{-h/2}^{+h/2} \int_R (\sigma_{xx}\delta\varepsilon_{xx} + \sigma_{yy}\delta\varepsilon_{yy} + 2\sigma_{xy}\delta\varepsilon_{xy}$$

$$+ 2\sigma_{xz}\delta\varepsilon_{xz} + 2\sigma_{yz}\delta\varepsilon_{yz})dxdydz \qquad (3.9)$$

In order to evaluate the external virtual work, we need to consider tractions which are applied to the upper and lower surfaces of the plate ($z = \pm h/2$) as well as the perimeter C of the plate. The tractions on the upper and lower surfaces of the plate are $\hat{t}_z$, $\hat{t}_{zx}$ and $\hat{t}_{zy}$, see Fig. (3.1). Considering only the normal traction $\hat{t}_z$, the transverse load q(x,y) is defined as

$$q = \hat{t}_z\big|_{+h/2} - \hat{t}_z\big|_{-h/2} \qquad (3.10)$$

On the edge of the plate, tractions are denoted t_n, t_{ns} and t_{nz} where n and s refer to the normal and tangential directions, respectively. By integrating the tractions across the thickness of the plate, the follow-

ing resultants are obtained

$$(\hat{N}_n, \hat{N}_s, \hat{Q}_n) = \int_{-h/2}^{+h/2} (\hat{t}_n, \hat{t}_{ns}, \hat{t}_{nz}) dz \tag{3.11}$$

$$(\hat{N}_n, \hat{M}_s) = \int_{-h/2}^{+h/2} (\hat{t}_n, \hat{t}_{ns}) z dz$$

The external virtual work for the plate can now be expressed as

$$\begin{aligned} \int_{S_2} \hat{t}_i \delta u_i \, dS = & \int_R q \, \delta w \, dx dy + \int_{C_1} \hat{N}_n \delta u_n \, dS \\ & + \int_{C_2} \hat{N}_s \delta u_s \, dS + \int_{C_3} \hat{M}_n \delta \psi_n \, dS \\ & + \int_{C_4} \hat{M}_s \delta \psi_s \, dS + \int_{C_5} \hat{Q}_n \delta w \, dS \end{aligned} \tag{3.12}$$

where

$$\begin{bmatrix} u_n & \psi_n \\ u_s & \psi_s \end{bmatrix} = \begin{bmatrix} n_x & n_y \\ -n_y & n_x \end{bmatrix} \begin{bmatrix} u & \psi_x \\ v & \psi_y \end{bmatrix} \tag{3.13}$$

and the portions of the plate boundary C on which the stress resultants $\hat{N}_n$, $\hat{N}_s$, $\hat{M}_n$, $\hat{M}_s$ and $\hat{Q}_n$ are specified are indicated by C_1 through C_5, respectively.

Combining (3.9) and (3.12) and using (3.3) and (3.6), the weak form of the equilibrium equations are obtained

$$\begin{aligned} \int_R \{ & (N_x \frac{\partial}{\partial x} + N_{xy} \frac{\partial}{\partial y}) \delta u + (N_{xy} \frac{\partial}{\partial x} + N_y \frac{\partial}{\partial y}) \delta v \\ & + (Q_x \frac{\partial}{\partial x} + Q_y \frac{\partial}{\partial y} - q) \delta w + (M_x \frac{\partial}{\partial x} + M_{xy} \frac{\partial}{\partial y} + Q_x) \delta \psi_x \end{aligned} \tag{3.14}$$

$$+ (M_{xy}\frac{\partial}{\partial x} + M_y\frac{\partial}{\partial y} + Q_y)\delta\psi_y\}dxdy + \int_{C_1}\hat{N}_n\delta u_n dS + \int_{C_2}\hat{N}_s\delta u_s dS$$

$$+ \int_{C_3}\hat{M}_n\delta\psi_n dS + \int_{C_4}\hat{M}_s\delta\psi_s dS + \int_{C_5}\hat{Q}_s\delta w\, dS = 0$$

Using integration by parts where needed to isolate δu, δv, δw, $\delta\psi_x$ and $\delta\psi_y$, the Euler equations can be identified to form the equilibrium equations. These may be found in [84] along with the natural and essential boundary conditions. For the purpose of developing the required finite element model, the weak form of the equilibrium equations (3.14) are sufficient.

3.5 Finite Element Model

Due to the inelastic material response, exact analytical solutions are not possible even for the simplest problems. In order to obtain an approximate numerical solution, the finite element method is selected due to its superior ability to model complex geometries. In the finite element method the domain R of the plate is divided into simpler subdomains R^e which are called elements. The field quantities are approximated within the element as a finite linear combination of functions with undetermined parameters. Utilizing a variational statement or weak form of the governing equations, an approximate solution is obtained by locating the stationary point of the functional in terms of the previously undetermined parameters.

For the plate problem previously introduced, the displacement field within a typical element is expressed as

$$u(x,y,t) = \sum_{i=1}^{r} \phi_i(x,y)\, u_i^e(t)$$

$$v(x,y,t) = \sum_{i=1}^{r} \phi_i(x,y)\, v_i^e(t)$$

$$w(x,y,t) = \sum_{i=1}^{r} \phi_i(x,y)\, w_i^e(t) \qquad (3.15)$$

$$\psi_x(x,y,t) = \sum_{i=1}^{r} \phi_i(x,y)\, \psi_{xi}^e(t)$$

$$\psi_y(x,y,t) = \sum_{i=1}^{r} \phi_i(x,y)\, \psi_{yi}^e(t)$$

where ϕ_i are Lagrange interpolating polynomials (typically called shape functions), u_i^e, v_i^e, w_i^e, ψ_{xi}^e and ψ_{yi}^e are the nodal values of (u, v, w, ψ_x, ψ_y) at the i^{th} node of the element and r is the total number of nodes in the element. In (3.15), the nodal displacements take on the role of undetermined parameters in the displacement expansion.

The required weak form of the equilibrium equations (3.14) were previously derived using the principle of virtual work. The element level system of equations is obtained by considering (3.14) for a typical element. By introducing (3.15) and (3.3) into this equation and requiring the variations of the displacements to be arbitrary, the following system of equations is obtained

$$[K^e]\ \{\Delta^e\} = \{\hat{F}^e\} + \{F_p^e\} + \{F_T^e\} \qquad (3.16)$$

where $[K^e]$ is the linear stiffness matrix of the element, $\{\Delta^e\}$ is the nodal displacement vector, and $\{\hat{F}^e\}$, $\{F_p^e\}$, $\{F_T^e\}$ are the nodal force vectors due to the applied loads, plastic strains and thermal strains,

respectively. Refer to Appendix A for the explicit form of these equations. In order to model the complete domain, the equations from each element are assembled into a global system of equations. By introducing the assembly operator A, the global system is

$$[K]\{\Delta\} = \{\hat{F}\} + \{F_p\} + \{F_T\} \tag{3.17}$$

and

$$[K] = \mathop{A}_{e=1}^{N} [K^e]$$

$$\{\hat{F}\} = \mathop{A}_{e=1}^{N} \{\hat{F}^e\}$$

$$\{F_p\} = \mathop{A}_{e=1}^{N} \{F_p^e\}$$

$$\{F_T\} = \mathop{A}_{e=1}^{N} \{F_T^e\}$$

where $\{\Delta\}$ is the global displacement vector and $[K]$, $\{\hat{F}\}$, $\{F_p\}$, $\{F_T\}$ are the global counterparts from (3.16).

This formulation is typically called an initial strain formulation [85]. The advantage of this formulation is its simplicity. Since the standard linear stiffness matrix is used, only a single factorization is required. An explicit time integration scheme is employed to evaluate the plastic strains. The nodal force vectors are then formed and the displacements $\{\Delta\}$ are evaluated simply by resolution.

The computations required for a typical time step t are summarized as:

1. Form $\{\hat{F}\}$, $\{F_p\}$ and $\{F_T\}$
2. Solve (3.17) for the nodal displacements $\{\Delta\}$
3. Compute element stresses as required for output
4. For each integration point within each element
   a) Evaluate $\dot{L}_{ij}^{(\beta\gamma)}$ and $\dot{W}_p^{(\beta\gamma)}$
   b) Integrate $L_{ij}^{(\beta\gamma)}$ and $W_p^{(\beta\gamma)}$ forward to $t + \Delta t$
5. Increment time counter
6. If $t < t_{end}$

   Then go to step 1

   Else stop

For the initial time step, the initial conditions $L_{ij}^{(\beta\gamma)}(0) = 0$ and $W_p^{(\beta\gamma)}(0) = 0$ are used.

3.6 Numerical Integration of Plastic Stress Resultants

Techniques for numerical integration (sometimes called quadrature) are often expressed as a weighted sum

$$\int_{-1}^{+1} f(\xi)\, d\xi \approx \sum_{n=1}^{N} H_n\, f(\xi_n) \tag{3.18}$$

where H_n are weighting coefficients and ξ_n are the base points of the particular formula. In [86] Stroud and Secrest, provide a comprehensive tabulation of several methods such as Gauss-Legendre, Lobatto and several other integration rules.

In order to numerically integrate the plastic stress resultants using a quadrature method of the form defined by (3.18), the required integration must be expressed over the interval [-1, +1]. Since the stress distribution through the thickness of the laminate is typically

discontinuous between two adjacent plies, the integration will be subdivided at each ply interface. Examining the plastic bending moment $\underset{\sim}{M}^P$ from (3.6), the required integration is subdivided as follows

$$\underset{\sim}{M}^P = \sum_{m=1}^{M} \int_{z_{m-1}}^{z_m} z\, \underset{\sim}{\sigma}_{IP}(z)\, dz \tag{3.19}$$

where M is the total number of plies and z_m, z_{m-1} are the coordinates of the upper and lower surfaces of the m^{th} ply, respectively.

The integration limits of (3.19) are transformed by utilizing the following relation

$$z = z_{m-1} + \frac{h_m}{2}(1 + \xi) \quad , \quad -1 \le \xi \le +1 \tag{3.20}$$

where $h_m = z_m - z_{m-1}$. Introducing (3.20) into (3.19) we obtain

$$\underset{\sim}{M}^P = \sum_{m=1}^{M} \frac{h_m}{2} \int_{-1}^{+1} [z_{m-1} + \frac{h_m}{2}(1 + \xi)]\underset{\sim}{\sigma}_{IP}(\xi)\, d\xi \tag{3.21}$$

From (3.18), the above expression becomes

$$\underset{\sim}{M}^P = \sum_{m=1}^{M} \sum_{n=1}^{N_m} \frac{h_m}{2} H_n [z_{m-1} + \frac{h_m}{2}(1 + \xi_n)]\underset{\sim}{\sigma}_{IP}(\xi_n) \tag{3.22a}$$

where N_m is the total number of base points used in the m^{th} ply. Similarly the other plastic stress resultants are obtained

$$\underset{\sim}{N}^P = \sum_{m=1}^{M} \sum_{n=1}^{N_m} \frac{h_m}{2} H_n\, \underset{\sim}{\sigma}_{IP}(\xi_n) \tag{3.22b}$$

$$\underset{\sim}{Q}^P = \sum_{m=1}^{M} \sum_{n=1}^{N_m} \frac{h_m}{2} H_n\, \underset{\sim}{\sigma}_{SP}(\xi_n) \tag{3.22c}$$

The parameters N_m are introduced to allow different order integration rules for the different plies. This can be used to bias the integration order toward the outer surfaces of the laminate where the plastic

strains are the largest. The selection of the integration method will be discussed next.

Numerical integration methods can be classified by examining the placement of the base points within the integration interval. Newton-Cotes quadrature uses equally spaced base points. Usually these are selected to include the end points of the integration interval. For N = 2 and N = 3, the Newton-Cotes formulas give the familar trapezoidal and Simpson's integration rules, respectively. With regards to accuracy using N base points, Newton-Cotes quadrature will exactly integrate a polynomial of order N - 1.

Gauss-Legendre quadrature uses optimally placed base points to allow the exact integration of a 2N + 1 order polynomial using only N base points. The optimal placement of the base points results in the unequal spacing of these within the integration interval. This quadrature rule for the case N = 1 is typically called the midpoint rule due to the central location of the single base point. Gauss-Legendre quadrature is computationally more efficient than Newton-Cotes quadrature since it can integrate exactly a given polynomial with considerably few base points.

For some applications, it is advantageous to have base points located at the end points of the integration interval. Labatto quadrature uses this idea by placing base points at the integration end points while the remaining base points are placed optimally within the integration interval. For N = 2 and N = 3, Labatto and Newton-Cotes integration rules are identical. Since the base points within the interior of the integration interval are optimally located, as the number of base

points increases, the accuracy of Labatto quadrature improves from that of Newton-Cotes quadrature toward the accuracy of Gauss-Legendre quadrature.

Cormeau [87] examined the relative performance of several quadrature rules for the integration of inelastic strains through the thickness of a degenerate solid element. His experiences are summarized below.

- Repeated use of the midpoint rule was found to underestimate the inelastic displacements.
- Repeated use of the trapezoidal rule was found to overestimate the inelastic displacements.
- Gauss-Legendre quadrature was found to converge the fastest, however, the convergence was not uniform.
- Labatto integration was observed to behave similarly to Gauss-Legendre quadrature when N was greater than 3 or 4, however, the convergence was not as fast.

In view of Cormeau's observations, Gauss-Legendre integration will be used in this study to evaluate the plastic stress resultants.

3.7 Integration of the Plastic Strains

The integration of the plastic strains is the single most important aspect in the solution procedure. The selected integration scheme governs the overall solution accuracy, numerical stability and the computational effort required for both the laminated plate constitutive relations and the finite element model. For this reason, two integration strategies are considered; the Euler method and a predictor-correc-

tor method. Both of these methods incorporate some type of local error estimation to adjust the integration step size.

The Euler method is the simpler of the two methods and will be examined in some detail. For now, consider a single ordinary differential equation

$$\frac{dy}{dt} = F(y,t) \quad , \quad t \geq 0 \tag{3.23}$$

with the initial condition $y(0) = y_0$.

We desire an integration scheme in which $y_{n+1} = y(t_{n+1})$ is evaluated based on information at $y_n = y(t_n)$. Consider the Taylor series expansion of (3.23)

$$y_{n+1} = y_n + F_n \Delta t + \frac{1}{2} \frac{dF_n}{dt} \Delta t^2 + \ldots \tag{3.24}$$

where $\Delta t = t_{n+1} - t_n$. Euler's method is obtained by retaining only the linear terms of the Taylor series

$$y_{n+1} = y_n + F_n \Delta t \tag{3.25}$$

In order for Euler's method to provide an accurate estimate for y_{n+1}, the remaining higher order terms in the Taylor series must be relatively negligible. With this goal in mind, the quadratic term $\frac{dF_n}{dt} \Delta t^2$ from the series is used to develop an expression for selecting a suitable step size.

Banthia and Mukherjee [88] suggested using the quadratic term in the Taylor series normalized by the local rate of y as a measure of the local truncation error

$$e^* = \frac{\left|\frac{dF_n}{dt}\right| \Delta t^2}{\text{Max } (|F_n|, |F_{n-1}|)} \tag{3.26}$$

The higher order derivative is eliminated by introducing a backward difference approximation

$$\frac{dF_n}{dt} \approx \frac{F_n - F_{n-1}}{\Delta t} \tag{3.27}$$

This allows the local truncation error to be expressed as

$$e^* = \frac{|F_n - F_{n-1}|\Delta t}{\text{Max } (|F_n|, |F_{n-1}|)} \tag{3.28}$$

By prescribing an upper bound on the error e^*_{max}, the time step is then expressed as

$$\Delta t = \frac{e^*_{max} \text{ Max}(|F_n|, |F_{n-1}|)}{|F_n - F_{n-1}|} \tag{3.29}$$

Banthia and Mukeherjee, based on their experience with stiff inelastic constitutive equations, related the error e^*_{max} to $\dot{\varepsilon}^P_{max}$ which is the maximum inelastic strain rate in the body at $t = t_n$

$$e^*_{max} = \frac{e}{|\dot{\varepsilon}^P_{max}|} \tag{3.30}$$

where e is a positive constant established by experimentation.

The Euler method is generalized to a system of equations by simply replacing y and F in (3.25) by their vector counterparts $\underset{\sim}{y}$ and $\underset{\sim}{F}$. In computing the time step Δt, a suitable vector norm of the local truncation error e^* is used. In this study a 1-norm is used which is simply the sum of the absolute value of the elements of the vector.

One final aspect of the time step selection method used for Euler's method is required. During elastic loading of the structure Δt can become very large by (3.29) and (3.30) since $\dot{\varepsilon}^{p}_{max}$ is small or even zero. In order to prevent the integration from proceeding past sudden changes in the response, the time step is constrained such that

$$\Delta t \leq \Delta t_{max} \tag{3.31}$$

where Δt_{max} is an upper limit imposed on the time step which is established by experience.

The second integration scheme is an Adams predictor-corrector method developed by Shampine and Gordon [89]. This method is implemented in a software package available from Sandia Laboratories [90]. The program incorporates a variable-step/variable-order Adams method with a set of sophisticated error measures.

These two integration methods are selected since they range from very simple to extremely complex. In the next chapter, we shall examine the relative performance of these integration schemes and assess their suitability for integrating the Bodner-Partom plasticity theory.

4. APPLICATIONS

4.1 Introduction

This chapter contains results for several sample problems which are analyzed using the Aboudi micromechanics theory. The first few examples address the computational aspects of the analysis, specifically the temporal integration of the plastic strains and the spatial integration of the plastic moments. The accuracy of the finite element model is investigated by examining a classical problem, the bending of an elastic-perfectly plastic beam. Results are presented for metal-matrix components subjected to several loading conditions. Comparisons with experimental results are given wherever possible.

4.2 Temporal Integration

The integration of the plastic strains is carried out using Euler's method and a predictor-corrector method. The relative performance of the two integration methods is examined with regards to their accuracy and computational effort.

For this purpose, the uniaxial loading of a $[\pm 45]_S$ boron/aluminum laminate is examined. The constituent material properties obtained by Pindera and Lin [91] are used (see Table 4.1). A uniform normal stress σ is applied such that $N_x = h\sigma$ and all other stress resultants are zero. For this loading, the stress distribution is constant in the xy-plane so that only the constitutive relations are required for evaluation. Due to the kinematic assumptions, the plastic stress resultants are computed exactly using a one point Gaussian quadrature rule. The

Table 4.1.

Boron/Aluminum Constituent Properties at Room Temperature From Reference [91].

Boron Properties

$E = 58.0$ msi

$\nu = 0.2$

Aluminum Properties (6061)

$E = 10.5$ msi

$\nu = 0.33$

$D_o = 10^4 \text{ sec}^{-1}$

$z_o = 14.5$ ksi

$z_1 = 27.6$ ksi

$m = 70$

$n = 10$

Composite Properties

Fiber Volume Fraction, $V_f = 0.46$

laminate is loaded at a rate of $\dot{\sigma}$ = 0.25 ksi/sec to a maximum load of 25 ksi.

Results of the integration are presented in Table 4.2. Typical stress-strain curves obtained by each method are given in Figures 4.1 and 4.2. For the Euler method, integration control is specified by two parameters e and Δt_{max}, the local truncation error and maximum time step, respectively. The predictor-corrector method requires specifying relative and absolute local error tolerances. These parameters are set equal and are denoted by e in the table.

The number of function evaluations in the table refers to the number of times the plastic strain rates are calculated. These are included as a measure of computational effort. For the Euler method this is the number of time steps required to integrate the function. For the predictor-corrector method each time step requires two function evaluations, one for the predictor phase and one for the corrector phase. Information from the predictor and corrector phases of the time step is then used to assess the local error. If the error is within an acceptable limit, the step is accepted and the integration continues. If the error is not within an acceptable limit, the last step is rejected, a new time step size is selected and the step is attempted again until an acceptable error is obtained.

Examining the number of function evaluations required to integrate the laminate response to σ = 25 ksi, the Euler method requires approximately half as many function evaluations as the predictor-corrector method. The performance of the Euler method can be attributed to two factors. The first is that the Euler method uses the maximum plastic

Table 4.2.

Temporal Integration of a $[\pm 45]_s$ Boron/Aluminum Laminate

Integration Type	Error Parameter e	Δt_{max} (sec)	Number of Function Evaluations	Strain(%) at σ = 25 ksi	Percent Error*
E	1.E-1	0.5	---	unstable	---
E	1.E-2	0.5	838	1.38793	9.997
E	1.E-3	0.5	2064	1.26500	0.254
E	1.E-4	0.5	2383	1.26218	0.031
E	1.E-5	0.5	3254	1.26187	0.006
E	1.E-6	0.5	4452	1.26186	0.006
E	1.E-7	0.5	10916	1.26186	0.006
E	1.E-1	0.1	---	unstable	---
E	1.E-2	0.1	1571	1.38780	9.987
E	1.E-3	0.1	2514	1.26521	0.271
E	1.E-4	0.1	3363	1.26197	0.014
E	1.E-5	0.1	3722	1.26186	0.006
E	1.E-6	0.1	4807	1.26186	0.006
E	1.E-7	0.1	11393	1.26186	0.006
P-C	1.E-1	---	---	unstable	---
P-C	1.E-2	---	4759	1.30116	3.120
P-C	1.E-3	---	5923	1.27917	1.377
P-C	1.E-4	---	6955	1.26573	0.312
P-C	1.E-5	---	7651	1.26188	0.007
P-C	1.E-6	---	7796	1.26179	0.000
P-C	1.E-7	---	7909	1.26179	0.000

E = Euler's Method
P-C = Predictor-Corrector Method
* Percent Error from 1.26179% Strain

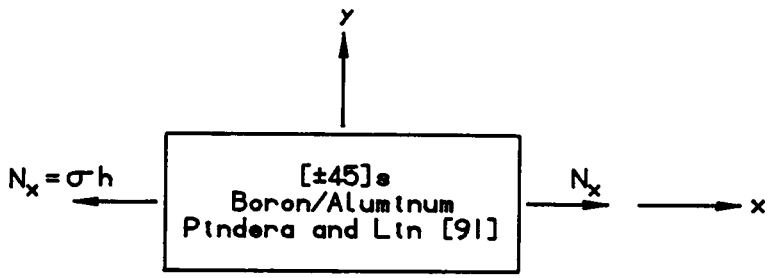

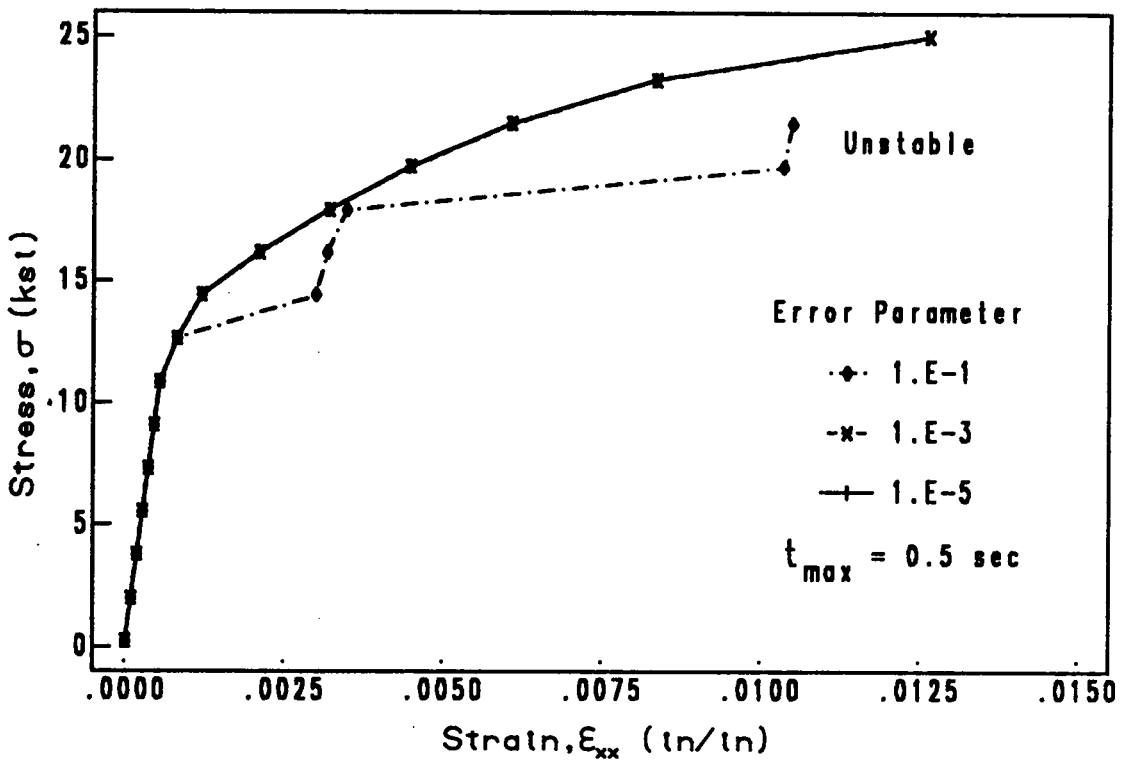

Figure 4.1. Effect of Error Parameter on the Integration Accuracy Using Euler's Method

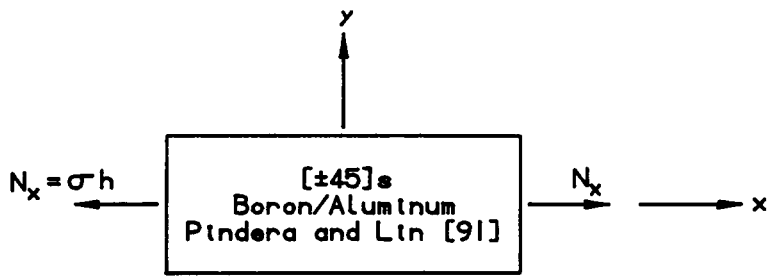

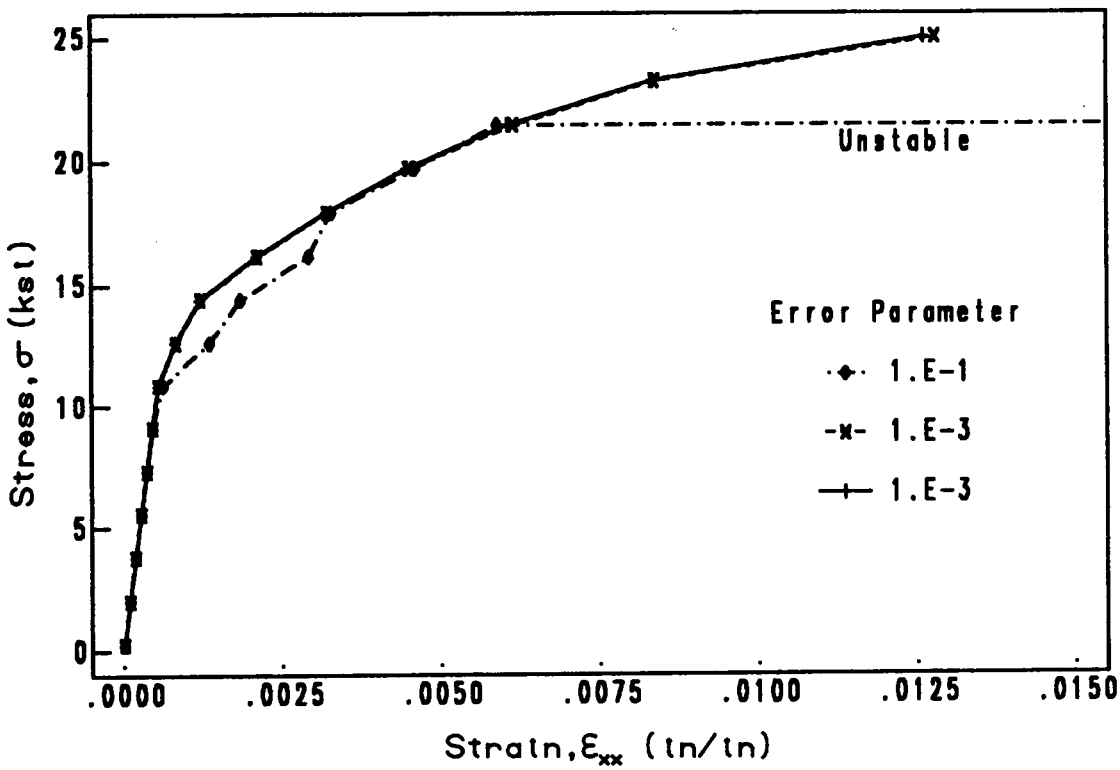

Figure 4.2. Effect of Error Parameter on the Integration Accuracy Using a Predictor/Corrector Method

strain rate $\dot{\varepsilon}^{p}_{max}$ as an indication of the numerical stiffness of the system of equations. This seems to be an excellent device for controlling the integration error. The predictor-corrector method, which is designed for more general applications, uses other more conservative error bounds. The second factor which assists the Euler method is that the error analysis is performed prior to taking the integration step. This allows the Euler method to always make progress without the possibility of repeating steps due to unacceptable step sizes, as in the case of the predictor-corrector method.

The strain computed at the load $\sigma = 25$ ksi is used to evaluate the relative accuracy of the two methods. Both methods display monotonic convergence to slightly different values. The predictor-corrector method is probably more accurate due to its conservative error measures. For the Euler method, results for two different values of Δt_{max} are provided in Table 4.2. The smaller Δt_{max}, resulted in only a slight improvement in accuracy but only for the smaller values of the error parameter. The overall increase in the number of function evaluations required for the smaller value of Δt_{max} is not warranted considering the small gain in accuracy.

Comparing the two integration methods in Table 4.2, the Euler method is in general superior to the predictor-corrector method based on relative accuracy and computational effort. From an implementation point of view, the Euler method is again better than the predictor-corrector method since it requires much less computer storage. The Euler method can, however, be more difficult to use since it requires two control parameters e and Δt_{max}. Experience indicates that

conclusions based on the simple problem presented in this section are also valid for much larger problems.

Unless stated otherwise, the temporal integration of the plastic strains will be performed using Euler's method with e = 1.E-3 and Δt_{max} = 0.5 sec.

4.3 Integration of Plastic Moments

The use of Gauss-Legendre quadrature is addressed by considering two sample problems. Due to the kinematic assumptions incorporated in the laminated plate constitutive relations, a laminate subjected to in-plane extension will have a uniform stress distribution for each ply. This results in the exact integration of the plastic stress resultants using only a one point integration rule within each ply. For a laminate subjected to bending, the stress distribution within a single ply, in general, will be nonlinear as a result of inelastic deformation. In this case, a higher-order integration rule is required to evaluate the plastic stress resultants.

To evaluate the behavior of Gauss-Legendre quadrature, we shall examine the bending response of two laminates. Both laminates are boron/aluminum and loaded in pure bending at a rate of $0.25/E^f h^2/$ sec. The boron/aluminum material properties used are listed in Table 4.1. The temporal integration is performed using the predictor-corrector method with the error tolerance of 1.E-5.

The first laminate considered is a $[90]_T$ which is flexed transverse to the fiber direction. The moment-curvature response of the laminate is shown in Fig. 4.3. The plastic stress resultants are integrated

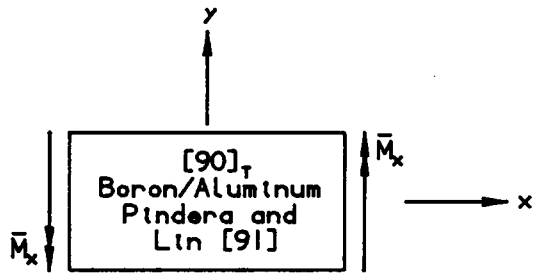

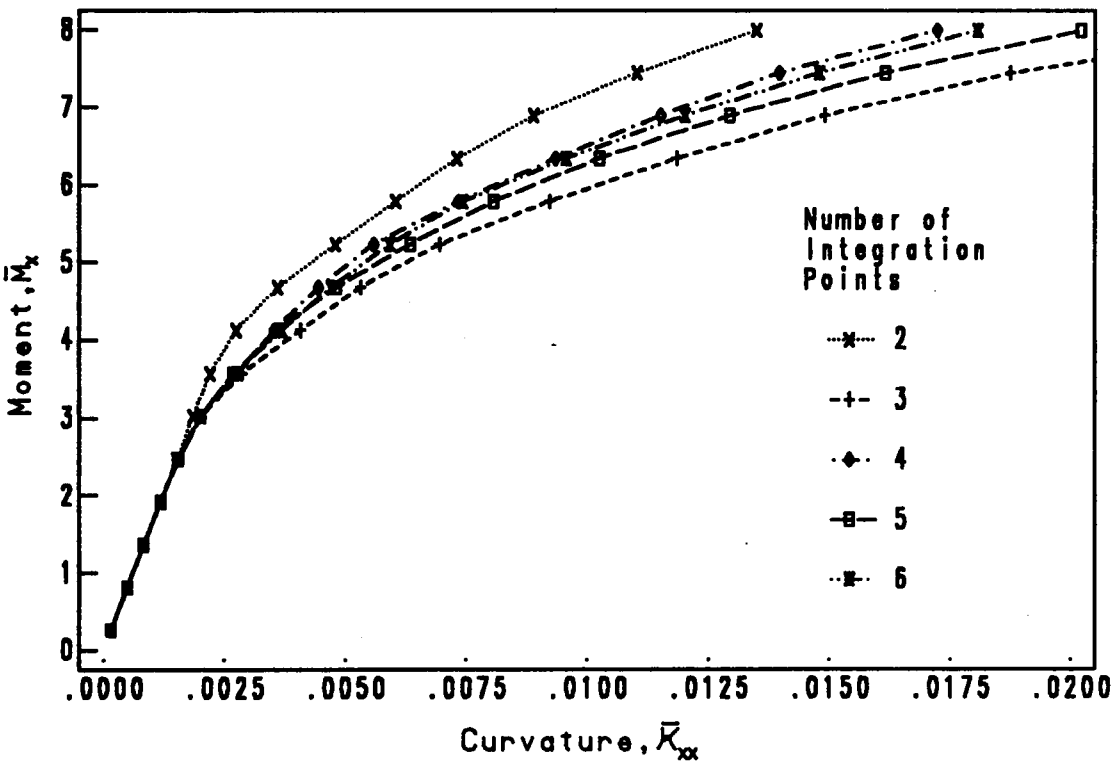

Figure 4.3. Bending Response of a $[90]_T$ Boron/Aluminum Laminate Using Simple Quadrature Rules

using two through six integration points through the total thickness of the laminate. The figure shows considerable difference between the five curves and a lack of monotonic convergence. This behavior is what Cormeau [87] described as nonuniform convergence.

In order to investigate this behavior in more detail we shall examine the curvatures at a nondimensional moment of $\bar{M}_x = 8.0/E^f h^2$ calculated using several integration rules. For this purpose we shall introduce a composite Gauss-Legendre quadrature rule.

In a composite Gauss-Legendre quadrature rule, the given integration interval is subdivided into r equally spaced subintervals in which s integration points are used. Notationally, this will be denoted by (r x s). For a single lamina such as the $[90]_T$, each subinterval will have a thickness of h/r and a total number of integration points of r·s.

Results for several composite quadrature rules are presented in Table 4.3. To aid in the visualization of the convergence of the various quadrature rules, the curvature is plotted against the total number of integration points in Fig. 4.4. In this figure, the integration rules are grouped together based on the order of the quadrature rule within each subinterval. An "exact" value is listed accurate to five significant digits in the table and is indicated in the figure. This value is determined using several integration rules using up to 140 integration points. Even with the use of high-order integration rules, the results continue to oscillate but these are confined to the sixth and larger significant digits.

The reason for the oscillatory behavior exhibited by the Gauss-Legendre quadrature can be traced back to the plastic stresses which are

Table 4.3.

Bending Response of a $[90]_T$ Boron/Aluminum Laminate Using Several Quadrature Rules

Quadrature Rule, (r x s)	Number of Integration Points, r·s	Curvature, $\kappa_x h$ at $\bar{M}_x = 8.0/E^f h^2$	Percent Error
(2 x 1)	2	0.7191E-2	-61.578
(3 x 1)	3	1.0889E-2	41.820
(4 x 1)	4	1.2375E-2	-33.880
(5 x 1)	5	1.4159E-2	-24.348
(6 x 1)	6	1.4895E-2	-20.416
(7 x 1)	7	1.5829E-2	-15.429
(8 x 1)	8	1.6192E-2	-13.486
(9 x 1)	9	1.6816E-2	-10.152
(1 x 2)	2	1.3494E-2	-27.901
(2 x 2)	4	1.8805E-2	0.476
(3 x 2)	6	1.8304E-2	-2.201
(4 x 2)	8	1.8756E-2	0.214
(1 x 3)	3	2.4505E-2	30.931
(2 x 3)	6	1.8797E-2	0.433
(3 x 3)	9	1.8940E-2	0.951
(4 x 3)	12	1.8708E-2	-0.043
(1 x 4)	4	1.7227E-2	-7.956
(2 x 4)	8	1.8691E-2	-0.134
(3 x 4)	12	1.8603E-2	-0.604
(4 x 4)	16	1.8757E-2	0.219
(1 x 5)	5	2.0206E-2	7.961
(2 x 5)	10	1.8739E-2	0.123
(3 x 5)	15	1.8809E-2	0.497
(4 x 5)	20	1.8692E-2	-0.128
(1 x 6)	6	1.8080E-2	-3.398
(2 x 6)	12	1.8767E-2	0.272
(3 x 6)	18	1.8686E-2	-0.160
(4 x 6)	24	1.8716E-2	0.000
EXACT	140	1.8716E-2	---

(r x s) = r equally spaced subintervals through the thickness of the laminate with s integration points per subinterval.

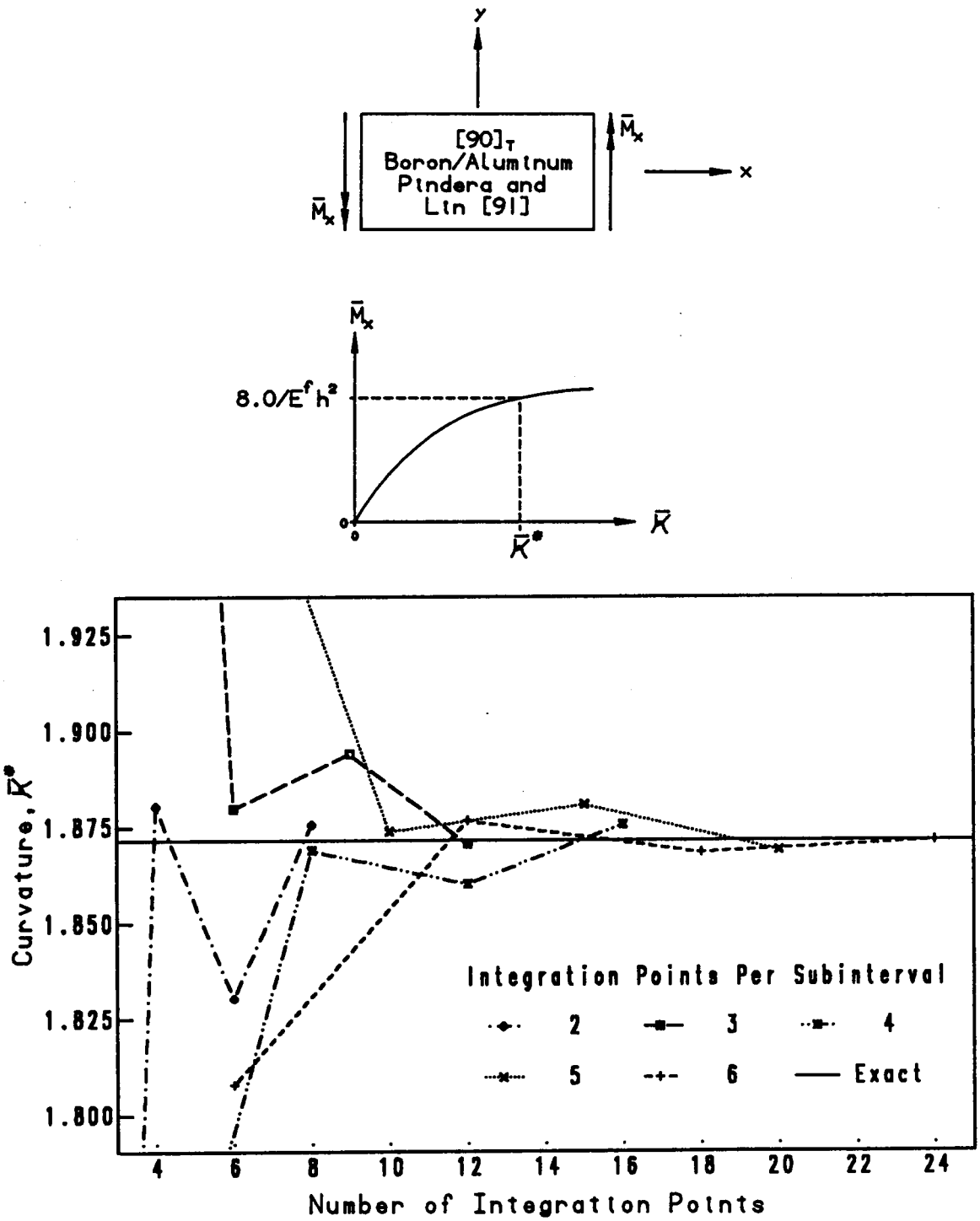

Figure 4.4. Curvature as a Function of Quadrature Rule

integrated to form the plastic stress resultants. The Gauss-Legendre quadrature rule is termed an interpolatory quadrature formula, since the integrand is approximated by an interpolating polynomial. In order for a function to be approximated well by a polynomial, however, the function must have a suitable number of continuous derivatives. For the plastic stresses a problem exists at the point of transition from the elastic to plastic regions. At this point, the plastic stresses have only a C^0 or C^1 continuity. The lack of continuous higher-order derivatives results in a poor representation of the plastic stresses by an interpolating polynomial. As a result, integration of the plastic stresses by Gauss-Legendre quadrature exhibits an oscillatory or nonuniform convergence, as shown in Fig. 4.4.

Since the composite Gauss-Legendre quadrature does not converge in a "nice" uniform manner, the selection of the "best" quadrature rule is now considerably more difficult. In selecting the quadrature rule we are once again faced with two competing issues, accuracy and computational efficiency. The computational effort required to analyze a particular laminate is directly related to the number of integration points used to evaluate the plastic stress resultants. This requires the selection of a quadrature rule which is the most accurate while using the least number of integration points.

Consider the problem of selecting the best integration rule which uses only four integration points. For equally spaced subintervals, we have the following possibilities: (4 x 1), (2 x 2) and (1 x 4). From Table 4.3, the (2 x 2) quadrature rule is found to be most accurate.

Unfortunately, due to the nonuniform convergence, these results might not have been directly obvious.

Examining all the quadrature rules listed in Table 4.3, we find the better quadrature rules are: (2 x 2), (2 x 3) and (2 x 4). Using these quadrature rules, the moment-curvature response for the $[90]_T$ laminate is shown in Fig. 4.5. These three quadrature rules are virtually indistinguishable from each other. The only exception is a minor deviation from the others made by the (2 x 2) quadrature rule.

The previous example was selected since it clearly demonstrates the care needed in selecting a suitable integration rule for bending analysis. The next example is the bending of a $[\pm 45]_S$ laminate, which is more representative of what might be encountered in an actual application. The bending response of the laminate is presented in Figure 4.6. Results are shown for one to six integration points per ply. For this laminate, the response curves computed using two to six integration points appear virtually identical. To examine the convergence, the curvatures calculated at the nondimensional moment $\bar{M}_x = 6.0/E^f h^2$ are provided in Table 4.4. The tabulated values of curvature demonstrate nonuniform convergence, however, the rate of convergence in this case is at a significantly higher rate than in the previous example. The curvature computed using five and six integration points per ply agree, indicating convergence. Using the converged value the percent error is computed. The table shows very accurate results using only two integration points per ply with only -0.10% error.

The examples presented in this section are intended to illustrate the problem of nonuniform convergence exhibited by Gauss-Legendre

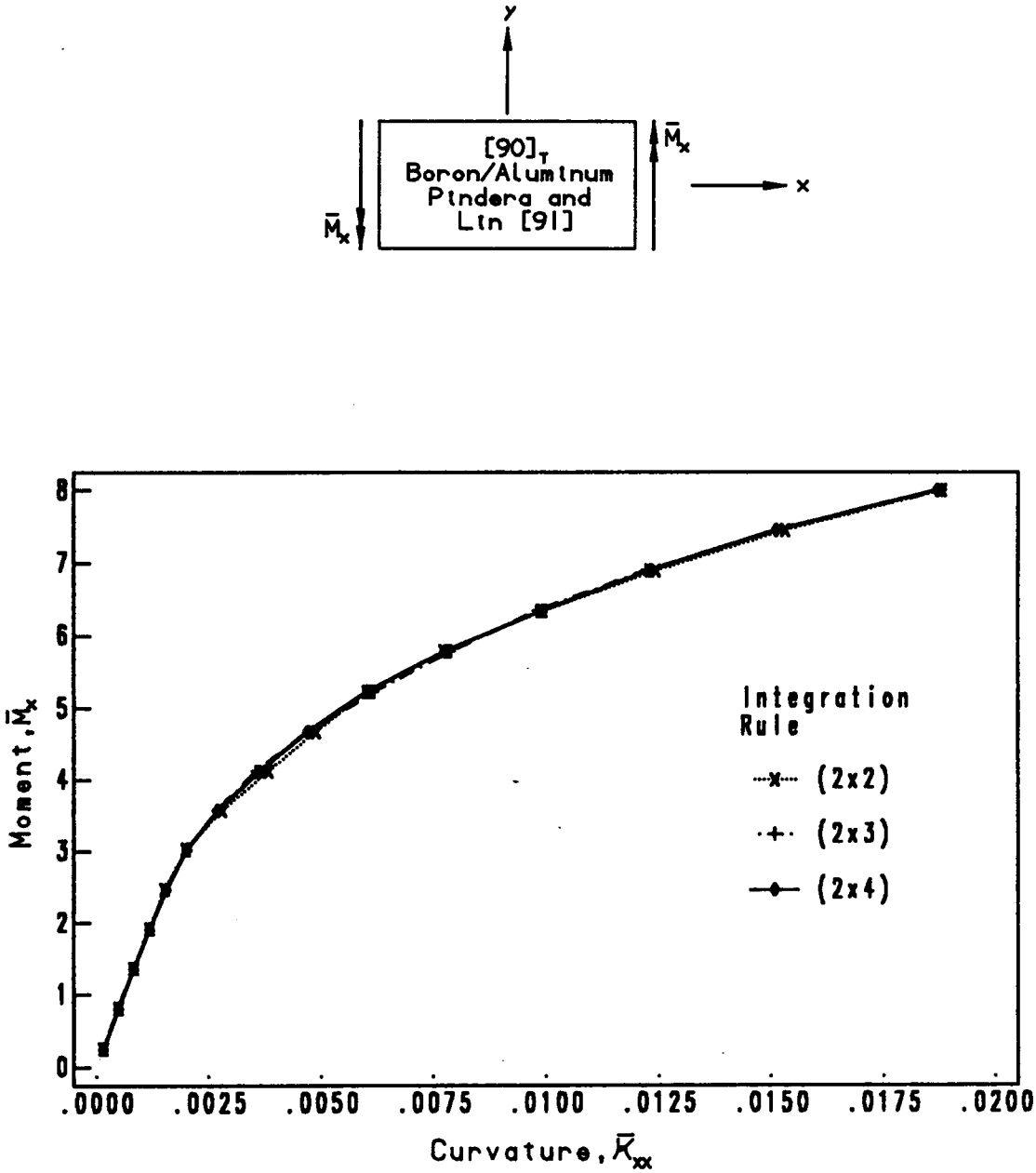

Figure 4.5. Bending Response of a $[90]_T$ Boron/Aluminum Laminate Using Improved Quadrature Rules

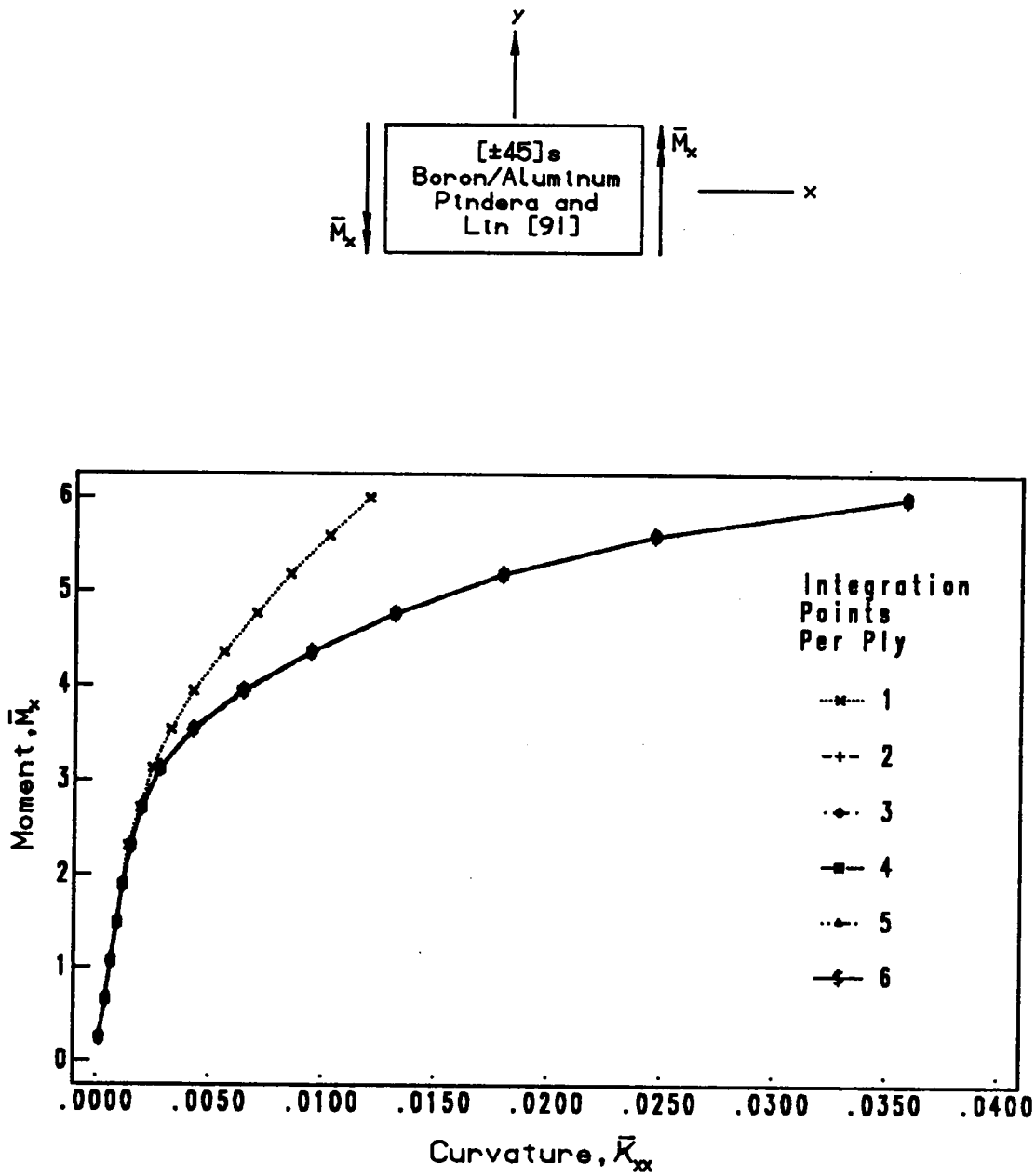

Figure 4.6. Bending Response of a [±45]s Boron/Aluminum Laminate

Table 4.4.

Bending Response of a $[\pm 45]_S$ Boron/Aluminum Laminate Using Several Quadrature Rules

Integration Points Per Ply	Number of Integration Points	Curvature, $K_x h$ at $\bar{M} = 6.0/E^f h^2$	Percent Error
1	4	1.2038E-2	-66.45
2	8	3.5846E-2	- 0.10
3	12	3.5811E-2	- 0.20
4	16	3.5898E-2	0.04
5	20	3.5883E-2	0.00
6	24	3.5883E-2	0.00

quadrature when computing plastic stress resultants. The lack of uniform convergence requires the analyst to exercise some degree of care in selecting an appropriate quadrature rule. Despite this undesirable aspect, Gauss-Legendre quadrature does provide considerable savings in terms of computational effort due to the few integration points typically required to obtain accuracy suitable for most engineering applications.

4.4 Flexure of an Elastic-Perfectly Plastic Beam

The analysis of a simply supported elastic-perfectly plastic beam subjected to a uniformly distributed transverse load is presented. This problem is selected to test the capabilities of the proposed finite element model. Although the selected problem is not a metal matrix composite, it does test many of the important aspects of the finite element model and an exact solution exists for comparison.

The geometric configuration and material properties for the simply supported beam are shown in Figure 4.7. The required elastic-perfectly plastic material behavior is obtained by setting $z_0 = z_1$ in the Bodner-Partom plasticity theory, refer to equation (2.62). This eliminates all the strain hardening and the need for the work hardening parameter m. Using a zero fiber volume fraction in the micromechanics model and the material properties from Fig. 4.7, the uniaxial response is predicted as shown in Fig. 4.8. The figure shows initial yielding slightly before the yield stress (Y = 40 ksi) and a negligibly small amount of strain hardening. This deviation is thought to be due to the selected independent-dependent variables used to compute the material response.

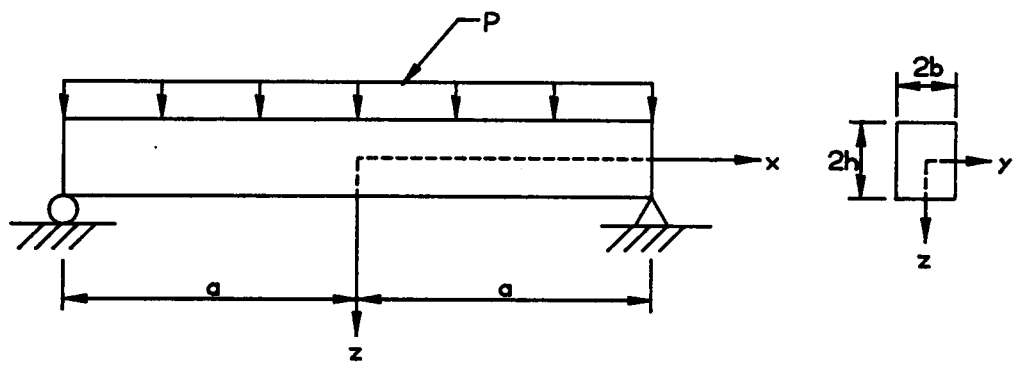

CONFIGURATION

$a = 50.0$ in
$b = 0.5$ in
$h = 0.5$ in

MATERIAL PROPERTIES

$E = 10.0$ msi
$\nu = 0.30$
$Y = 40.0$ ksi

BODNER-PARTOM PARAMETERS

$D_0 = 10^4\ sec^{-1}$
$n = 10.0$
$z_0 = 46.6$ ksi
$z_1 = 46.6$ ksi

Figure 4.7. Simply Supported Beam

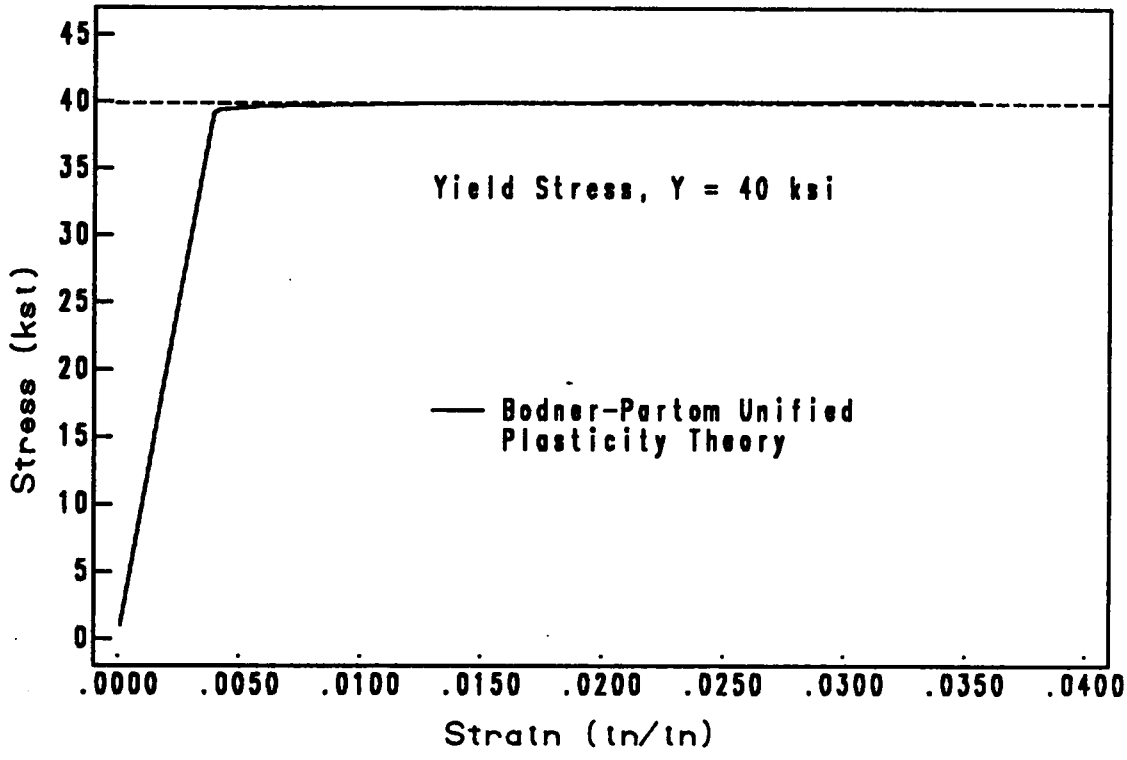

Figure 4.8. Elastic-Perfectly Plastic Material Response Predicted by Bodner-Partom Theory

In Fig. 4.8, the applied stress is the independent variable and the resulting strain is the dependent variable. This selection results in multiple values of the strain when the applied stress reaches the yield stress. A better choice would be to use the strain as the independent variable, so the stress is always a single valued function in terms of the applied strain.

For evaluation of the plastic stress resultants, several quadrature rules are examined. A (2 x 3) quadrature was determined superior to other quadrature rules which used six or fewer integration points. The moment-curvature response is presented in Fig. 4.9 by considering a typical cross section of the beam. The exact solution shown in the figure is easily obtained from the elementary theory of beams. The agreement between the numerically integrated results and the exact response are good in an average sense. The "kinks" in the numerical predictions are due to the sudden yielding of the material. The number of integration points required to smooth out this behavior is significantly larger than the six used in the figure and would not be practical for use in the finite element solution.

The simply supported beam is analyzed using five 9-node quadrilateral elements (see Fig. 4.10). Due to symmetry only half of the beam is modeled. The elements in the mesh are biased toward the region of maximum moment where the inelastic deformations are concentrated. The element stiffness matrices are evaluated using selective integration in the xy-plane. A 3 x 3 Gauss rule is used for all terms in the stiffness matrices with the exception of those associated with the transverse shear strain energy where a 2 x 2 Gauss rule is used. The nodal forces

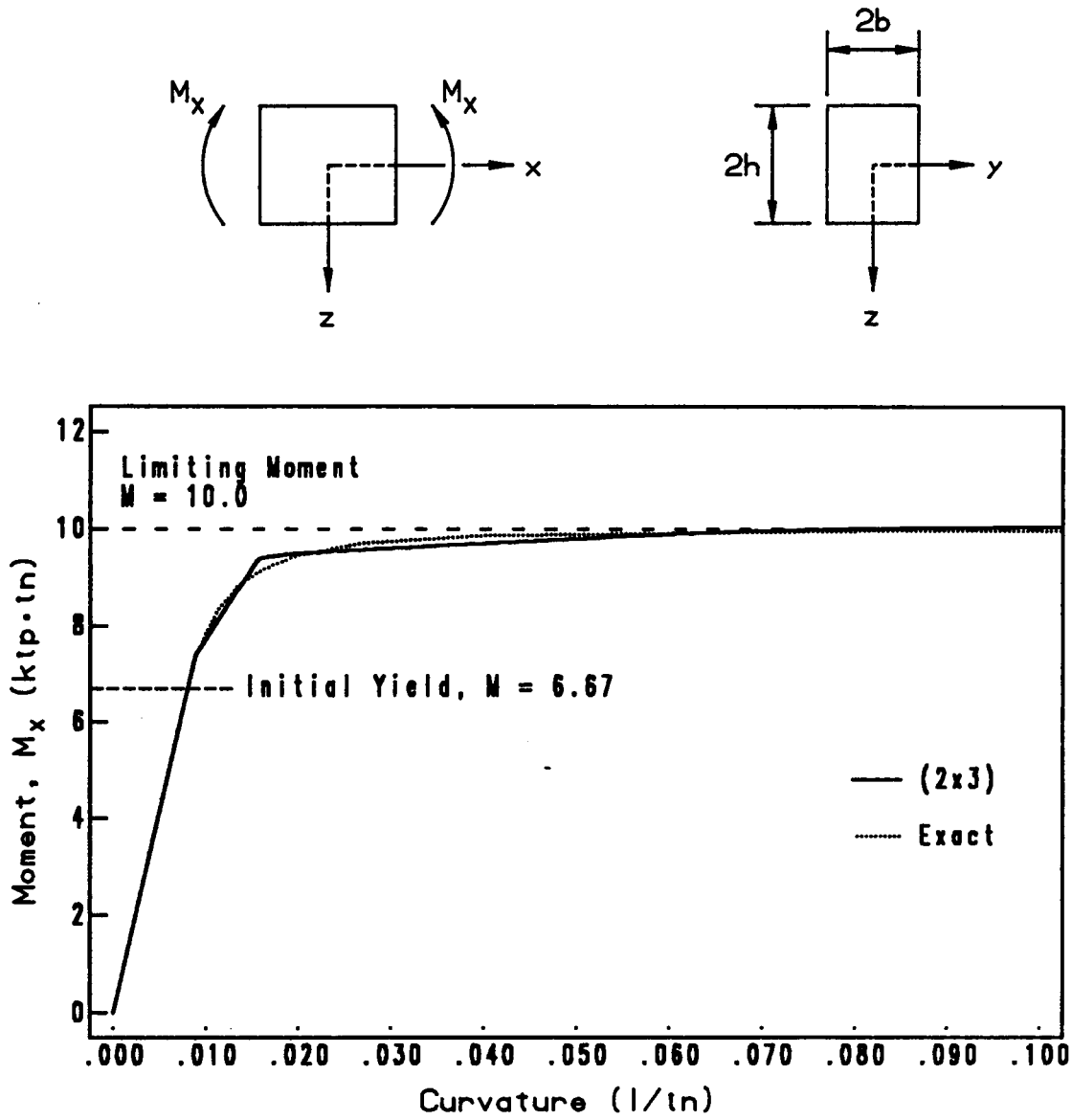

Figure 4.9. Elastic-Perfectly Plastic Bending Response

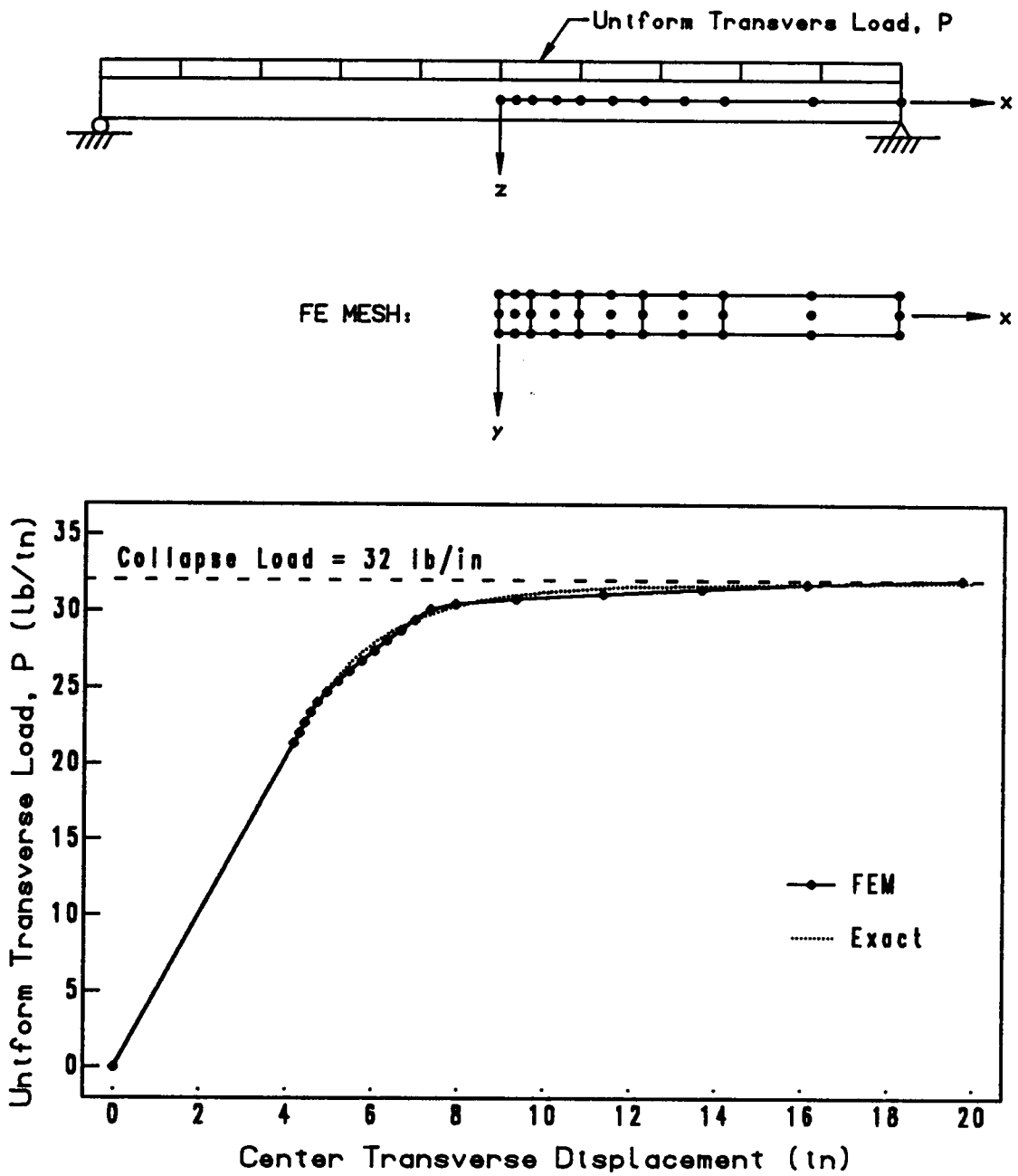

Figure 4.10. Center Displacement of a Simply Supported Elastic-Perfectly Plastic Beam

due to the plastic deformations are evaluated using a 2 x 2 Gauss rule in the xy-plane of the element and a (2 x 3) Gauss rule for the plastic stress resultants.

The load-displacement behavior for the simply supported beam is shown in Fig. 4.10. In the figure, the center displacement from the finite element model is compared to the exact solution of Prager and Hodge [92]. The finite element solution follows the exact solution very closely. The observed discrepancies are due to the quadrature rule used to evaluate the plastic stress resultants. The results presented for the simply supported beam are very good considering the computational difficulty associated with the elastic-perfectly plastic material behavior. This behavior is very difficult to model due to the sudden yielding exhibited by the material.

4.5. Analysis of Notched Test Coupons

Experimental test data for boron/aluminum notched test coupons reported by Shukow [93] is used to evaluate the accuracy of the proposed finite element model. First the necessary material properties are established. The characterization of the Aboudi micromechanics model is performed in a two phase operation.

The first phase in characterizing the micromechanics model consists of determining the linear elastic material properties. Using available published data for the constituent material properties as a guide, the constituent properties are "backed-out" in order to fit the test data. The constituent material properties determined in this process are presented in Table 4.5. The effective lamina and laminate properties

Table 4.5.

Constituent Material Properties for Boron/Aluminum at Room Temperature

Boron Properties

$E = 58.0$ msi

$\nu = 0.2$

$\alpha_L = 3.5\ \mu$ in/in/°F

$\alpha_T = 4.6\ \mu$ in/in/°F

Aluminum Properties

$E = 8.69$ msi

$\nu = 0.25$

$\alpha = 11.7\ \mu$ in/in/°F

$D_o = 10^4$ sec^{-1}

$m = 60$

$n = 10$

$z_o = 14.0$ ksi

$z_1 = 26.0$ ksi

Composite Properties

Fiber Volume Fraction, $V_f = 0.44$

Effective Processing Temperature, $\Delta T_p = -250$°F

predicted by the micromechanics theory are compared to the experimental results in Tables 4.6 and 4.7, respectively. In general good agreement is observed.

The second phase of the characterization consists of determining the required plasticity parameters and an effective processing temperature. An effective processing temperature is introduced in order to provide an approximation to the residual stresses known to exist as a result of the fabrication process. The effective processing temperature ΔT_p is defined as the temperature change required to approximate the residual stress state when using room temperature material properties. The experimental data from the axial response of a $[\pm 45]_{2s}$ laminate is used to evaluate the plasticity parameters and the effective processing temperature. This particular laminate is well suited for this task due to the degree of nonlinear behavior which it exhibits. Again, the required parameters are "backed-out" in order to fit the test data and are also included in Table 4.5. The results of this characterization is shown in Fig. 4.11.

We shall now examine the validity of the model parameters by predicting the behavior of a $[0/\pm 45/90]_s$ laminate, see Fig. 4.12. The response is essentially bilinear, showing distinct initial and secondary moduli. As seen in the figure, the micromechanics model overestimates the initial yield point of the laminate and underestimates the secondary modulus. Overall the agreement between the micromechanics model and the experimental data is good, with a maximum discrepancy of only 2 ksi.

With the characterization completed we shall examine the behavior of a notched test coupon for two laminates $[\pm 45]_{2s}$ and $[0/\pm 45/90]_s$. The

Table 4.6.

Unidirectional Lamina Mechanical Properties

SOURCE	E_{11} (msi)	E_{22} (msi)	G_{12} (msi)	ν_{12}
Experimental	30.59	19.20	6.50	0.218
Micromechanics	30.39	16.03	6.51	0.229

Table 4.7.

Laminate Mechanical Properties

Laminate	E_x(msi) Experimental	E_x(msi) Micromechanical	ν_{xy} Experimental	ν_{xy} Micromechanical
$[\pm 45]_{2s}$	17.36	17.67	0.373	0.358
$[0/\pm 45/90]_s$	21.25	20.70	0.267	0.249
$[0_2/\pm 45]_s$	24.36	24.16	0.304	0.299

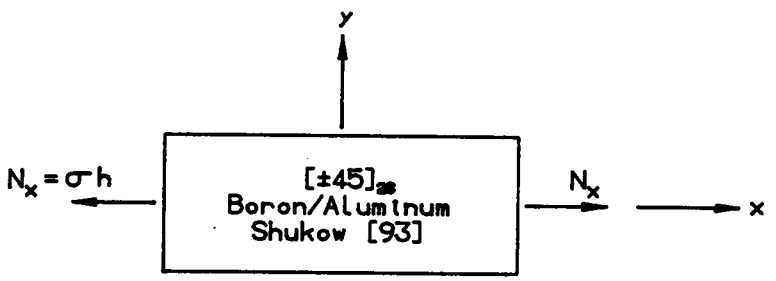

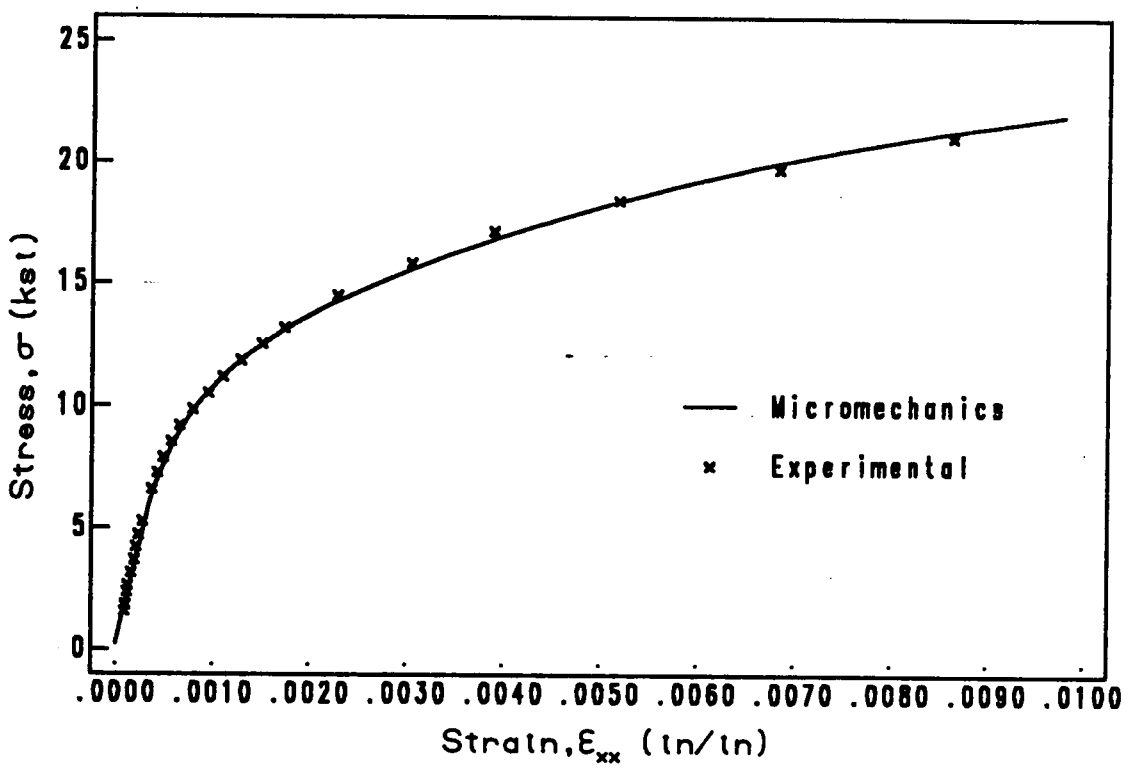

Figure 4.11. Extensional Response of a $[\pm 45]_{2s}$ Boron/Aluminum Laminate

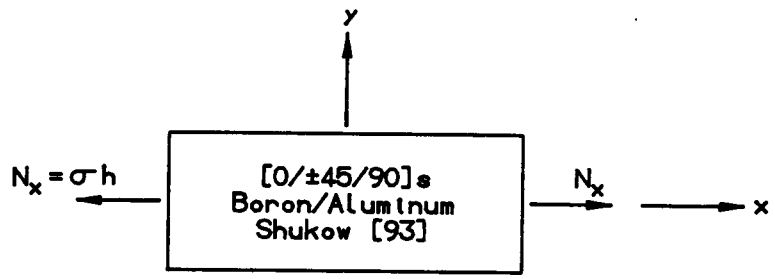

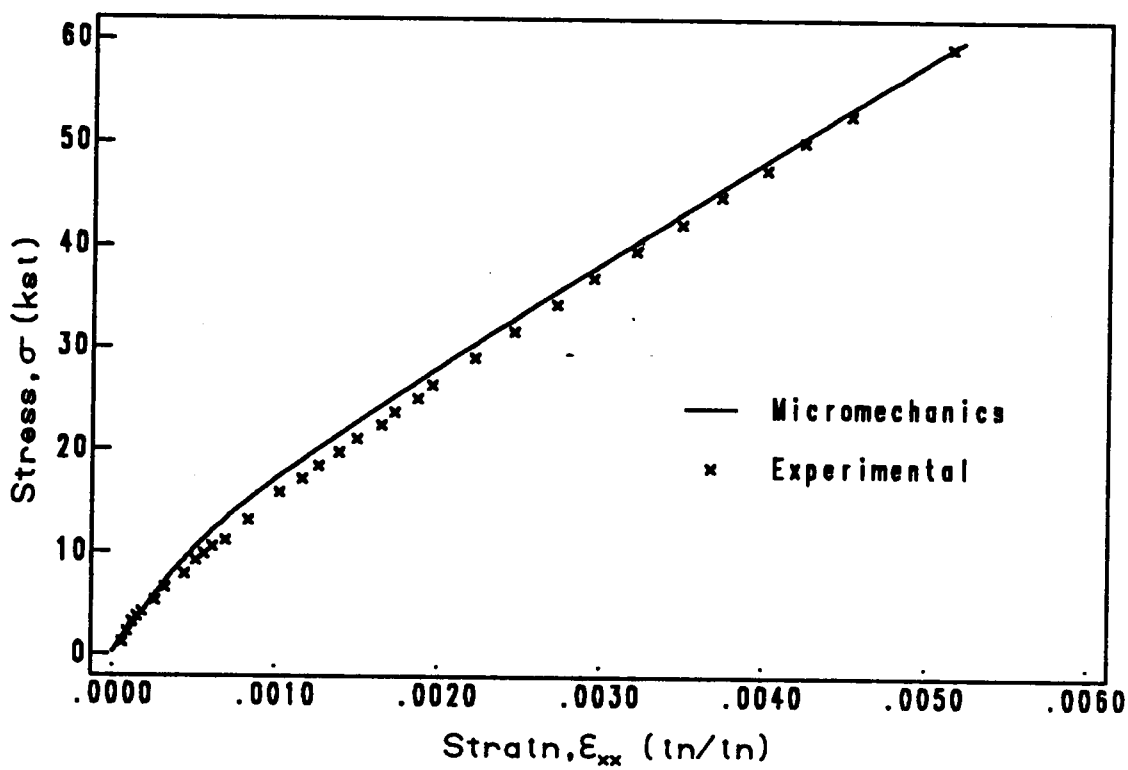

Figure 4.12. Predicted Response of a Quasi-Isotropic Boron/Aluminum Laminate

test coupon geometry and strain gage locations are shown in Fig. 4.13. Utilizing the symmetry of the test coupon and the selected laminates, one quarter of the test coupon is modeled using 8 node quadrilateral elements. The specifics of the finite element mesh are provided in Fig. 4.14. The element stiffness matrices are evaluated using selective integration. The nodal forces due to inelastic strains are evaluated using reduced integration, a 2 x 2 Gauss rule in the xy-plane. The plastic stress resultants are evaluated using a one point Gauss rule per ply in the z-direction.

The axial strain ε_{xx} at the edge of the hole and at the far field strain gages as a function of the applied load is shown in Figs. 4.15 and 4.16 for the $[\pm 45]_{2S}$ and $[0/\pm 45/90]_{S}$ laminates, respectively. The experimental data presented in these figures is taken from Shukow [93]. For the $[\pm 45]_{2S}$ laminate, the finite element solution for the far field strain is in excellent agreement with the experimental data. The predicted results for the strain at the edge of the hole closely agrees with the experimentally measured strain up to a value of 0.6%. At this point, the finite element solution begins to under predict the axial strain for a given applied load. The probable reason for the observed discrepancy is the presence of 3-dimensional effects at the free-edge of the hole which are not included in the current analyses. Additionally, some of the discrepancy could be attirubted to geometrically nonlinear effects especially for the larger strains or possibly delaminations.

For the quasi-isotropic laminate, $[0/\pm 45/90]_{S}$, the finite element predictions are in excellent agreement with the experimental data. At the far field strain gage the results are very similar to those of the

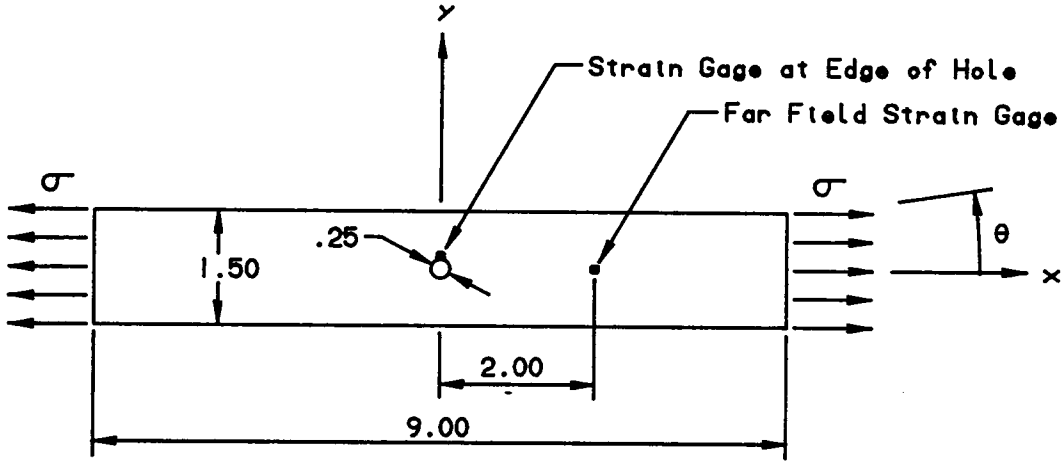

All dimensions are in inches.

Figure 4.13. Geometry of Notched Test Coupon

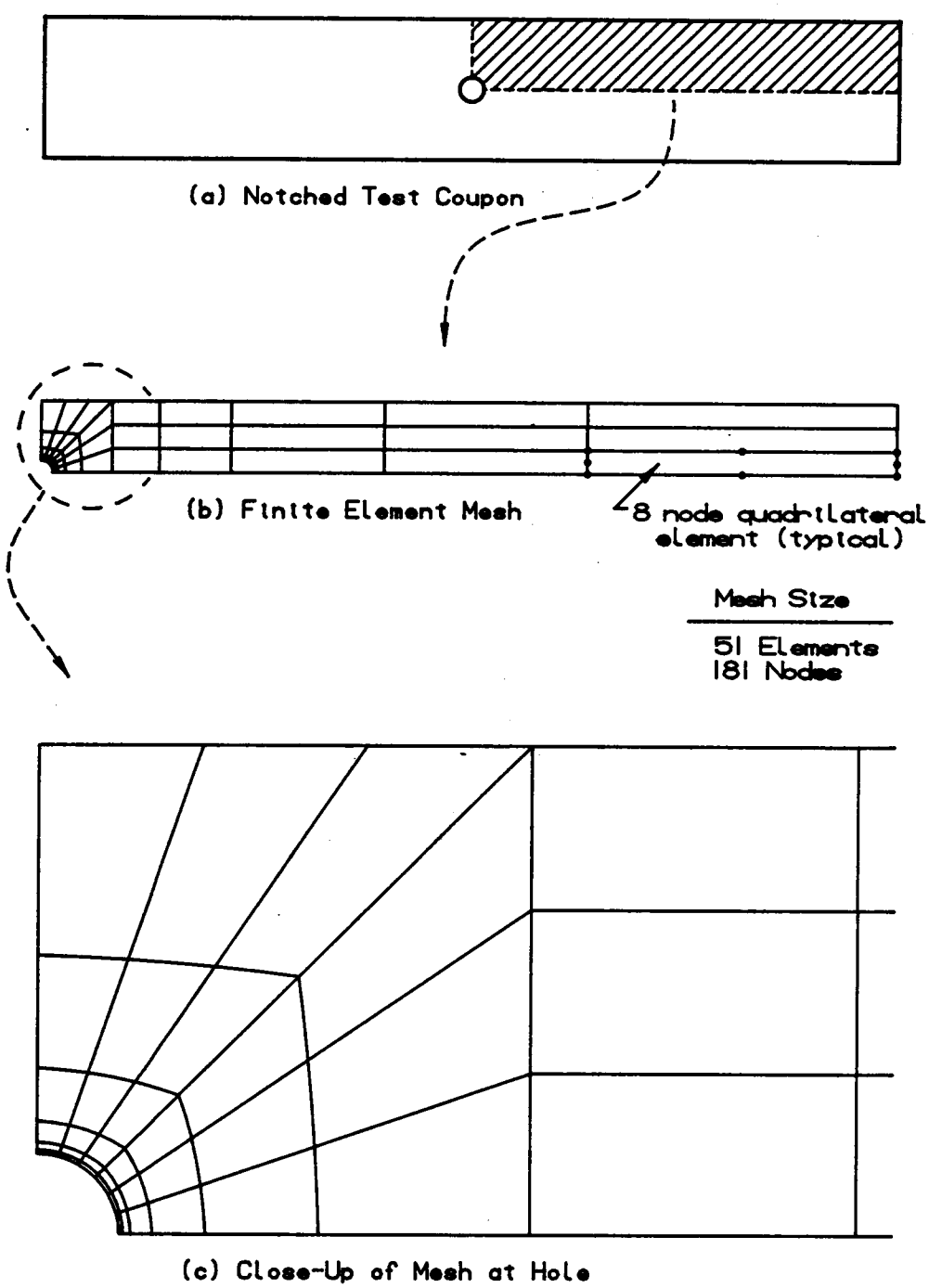

Figure 4.14. Finite Element Mesh of Notched Test Coupon

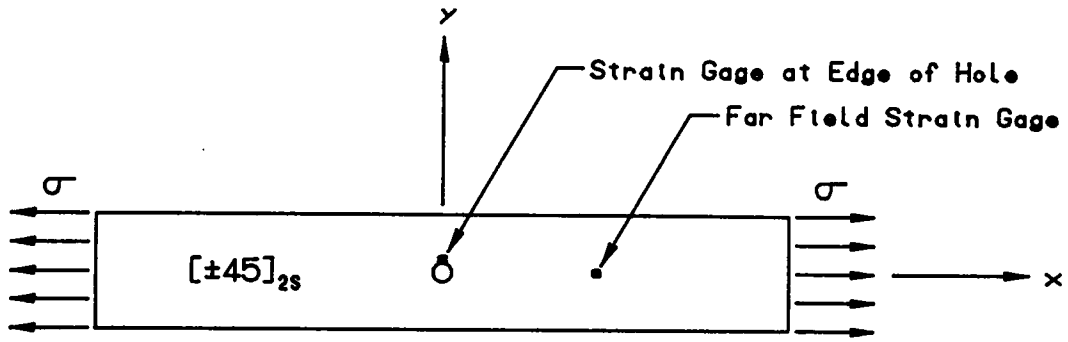

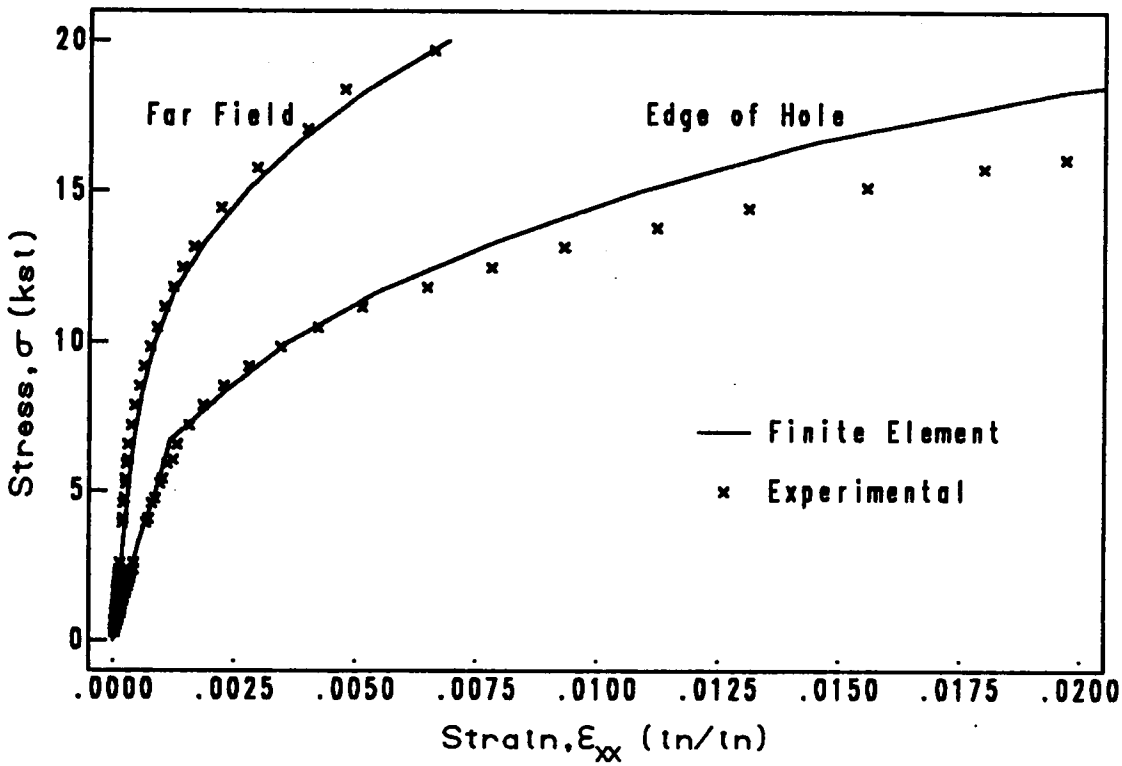

Figure 4.15. Axial Response of a Notched $[\pm 45]_{2s}$ Boron/Aluminum Laminate

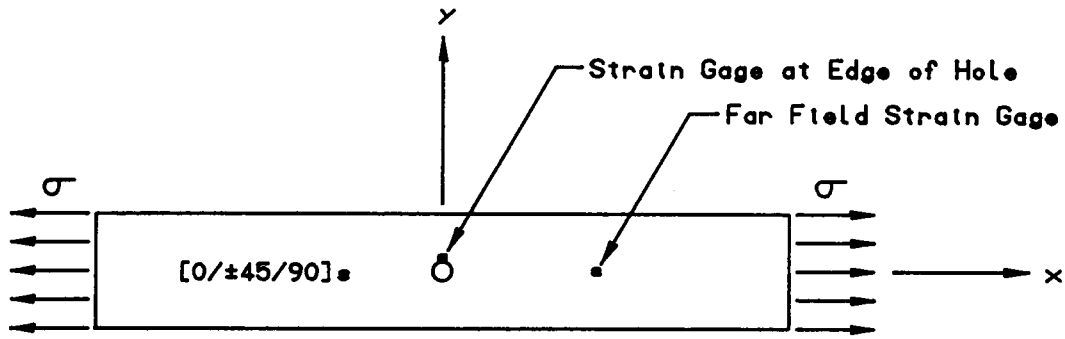

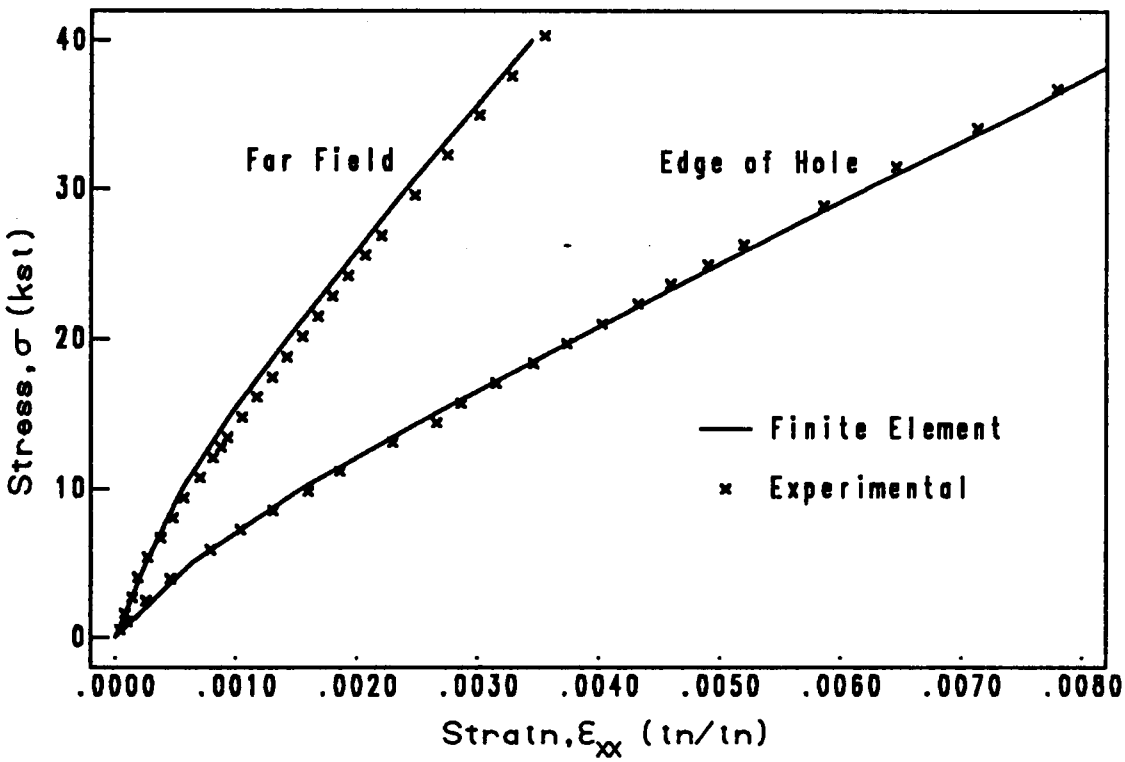

Figure 4.16. Axial Response of a Notched Quasi-Isotropic Boron/Aluminum Laminate

unnotched test coupon shown in Fig. 4.12. The axial strain computed at the edge of the hole follows the experimental data very well all the way to the failure of the coupon at about 40 ksi.

Next we shall examine the extent of the plastic deformation and the stress distribution in the $[\pm 45]_{2s}$ laminate. Instead of examining the individual plastic strain components, we shall introduce a scalar parameter which will indicate the relative intensity of the plastic deformation. For this purpose the equivalent uniaxial plastic strain ε^* is introduced

$$\varepsilon^* = \frac{3}{2} \bar{\varepsilon}^P_{ij} \bar{\varepsilon}^P_{ij} \tag{4.1}$$

The evolution of the plastic zones in the two plies of the $[\pm 45]_{2s}$ laminate are shown in Figs. 4.17 and 4.18. Examination of these figures indicates the evolution of the plastic zones in the +45° and the -45° plies are virtually identical. The plastic zone begins at the side of notch and develops along a diagonal band which is aligned very closely to the lines $\theta = \pm 45°$.

The in-plane stress distribution for both plies is presented in Figs. 4.19 through 4.24. These contour plots show stress components computed with respect to the lamina material coordinate system which is aligned with lamina fiber orientation. In Fig. 4.19, the normal stress in the fiber direction σ_{11} in the +45° ply, contains two distinct tensile and compressive zones which are oriented along the plastic zone described previously. The transition region from tensile stress to compressive stress produces a region of high shear stresses which can be observed in the contour plot of σ_{12} shown in Fig. 4.23.

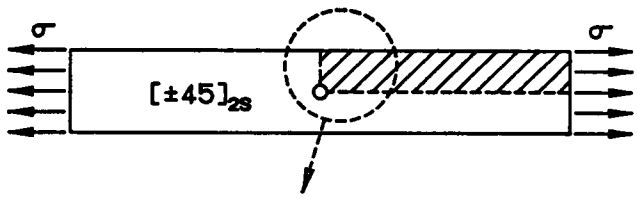

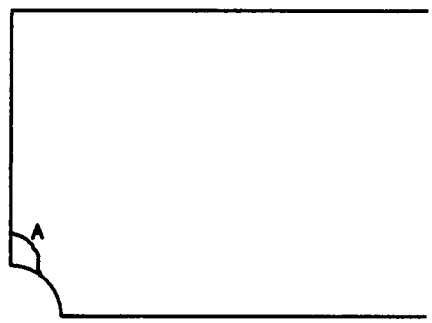

(a) Load = 5.0 ksi

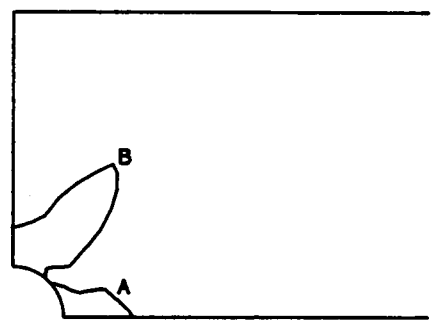

(b) Load = 10.0 ksi

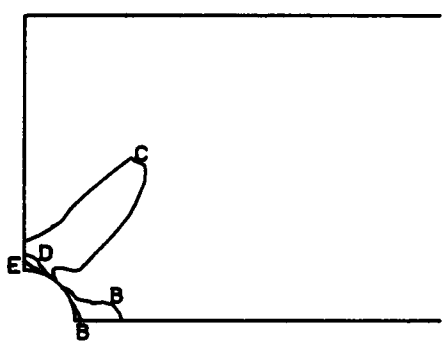

(c) Load = 15.0 ksi

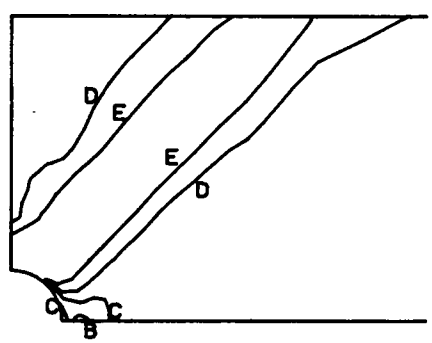

(d) Load = 20.0 ksi

Label	Strain (in/in)
A	0.5E-3
B	1.0E-3
C	4.0E-3
D	7.0E-3
E	10.0D-3

Figure 4.17. Equivalent Uniaxial Plastic Strain in the +45° Plies of a $[\pm 45]_{2s}$ Laminate

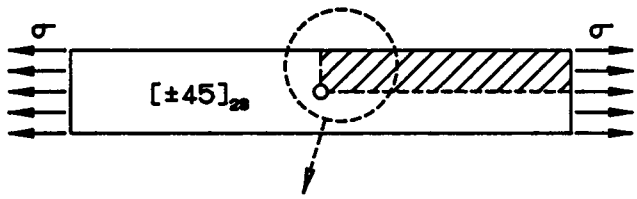

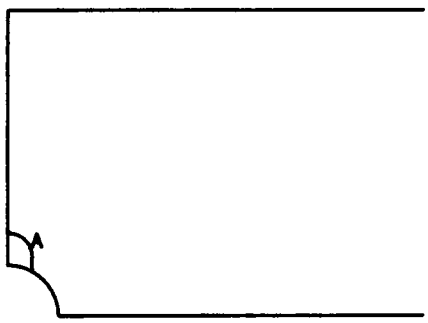

(a) Load = 5.0 ksi

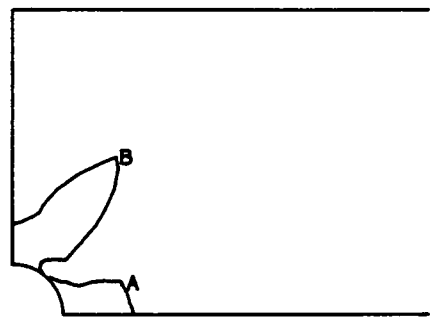

(b) Load = 10.0 ksi

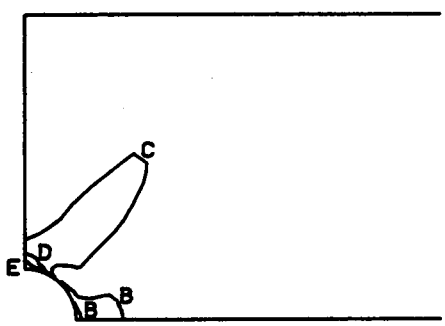

(c) Load = 15.0 ksi

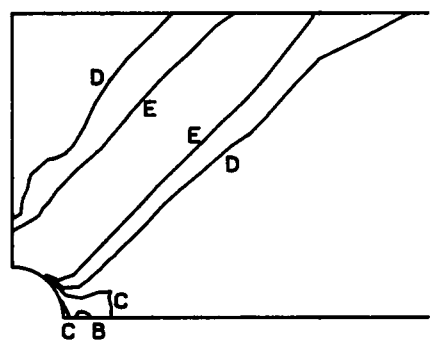

(d) Load = 20.0 ksi

Label	Strain (in/in)
A	0.5E-3
B	1.0E-3
C	4.0E-3
D	7.0E-3
E	10.0E-3

Figure 4.18. Equivalent Uniaxial Plastic Strain in the -45° Plies of a $[\pm 45]_{2s}$ Laminate

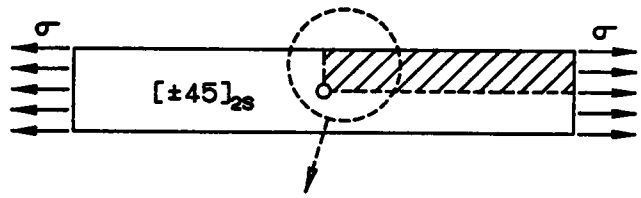

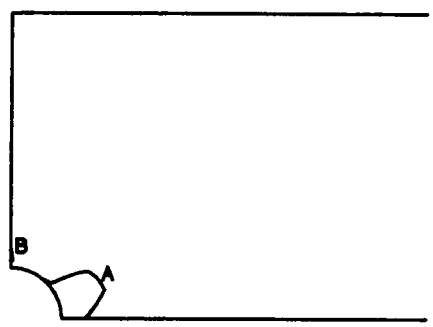

(a) Load = 5.0 ksi

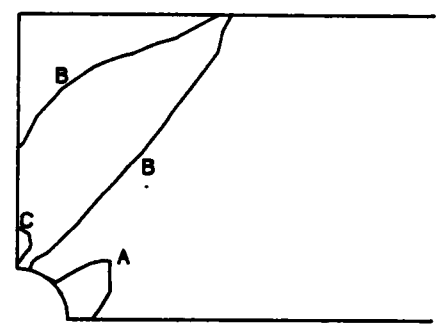

(b) Load = 10.0 ksi

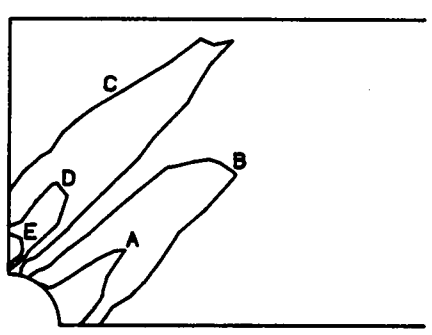

(c) Load = 15.0 ksi

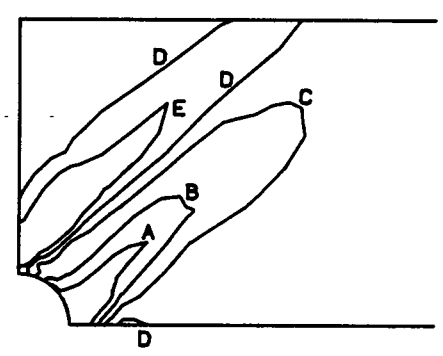

(d) Load = 20.0 ksi

Label	Stress (ksi)
A	-8.0
B	0.0
C	8.0
D	16.0
E	24.0

Figure 4.19. Normal Stress σ_{11} in the +45° Plies of a $[\pm 45]_{2s}$ Laminate

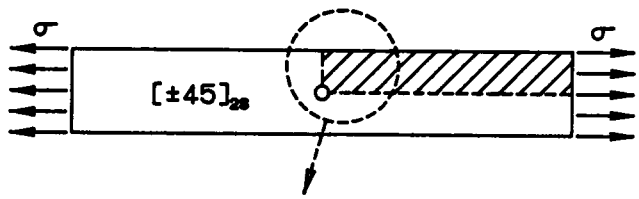

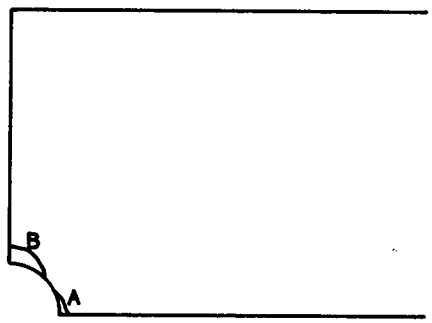

(a) Load = 5.0 ksi

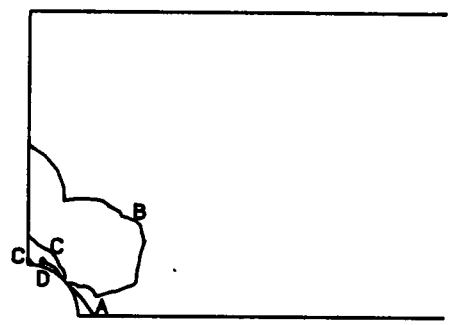

(b) Load = 10.0 ksi

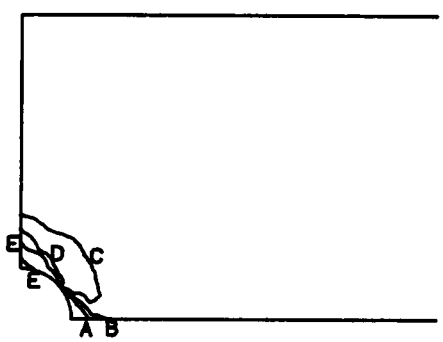

(c) Load = 15.0 ksi

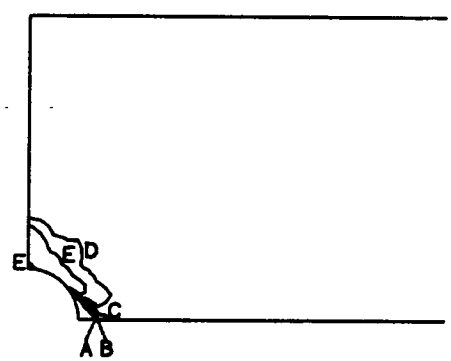

(d) Load = 20.0 ksi

Label	Stress (ksi)
A	-10.0
B	0.0
C	10.0
D	20.0
E	30.0

Figure 4.20. Normal Stress σ_{11} in the -45° Plies of a $[\pm 45]_{2s}$ Laminate

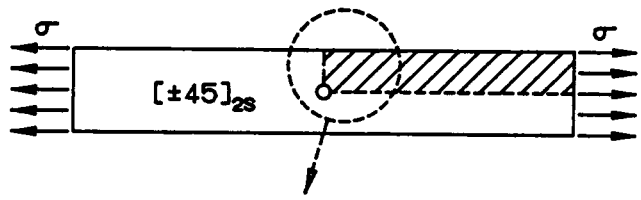

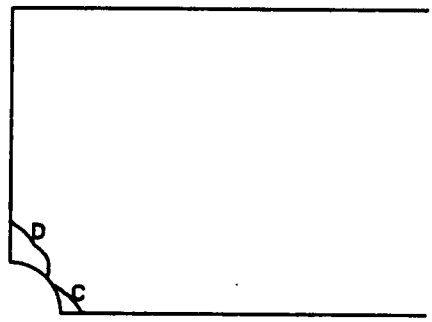

(a) Load = 5.0 ksi

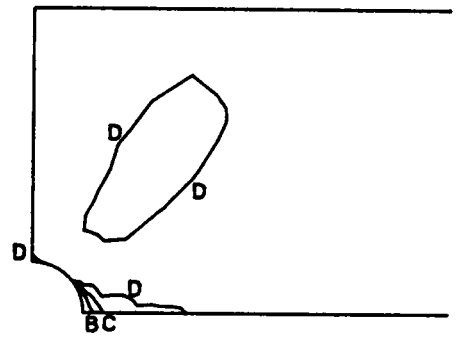

(b) Load = 10.0 ksi

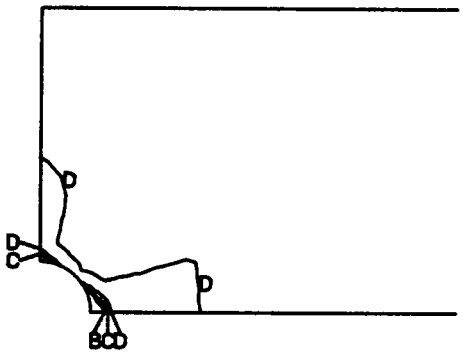

(c) Load = 15.0 ksi

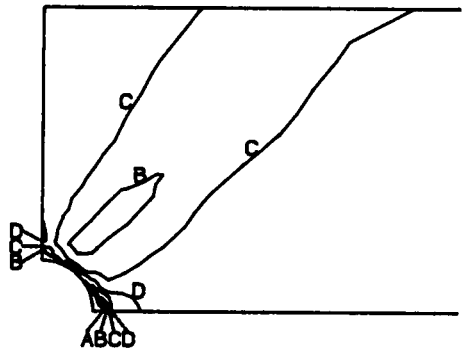

(d) Load = 20.0 ksi

Label	Stress (ksi)
A	2.0
B	5.0
C	8.0
D	11.0

Figure 4.21. Normal Stress σ_{22} in the +45° Plies of a $[\pm 45]_{2s}$ Laminate

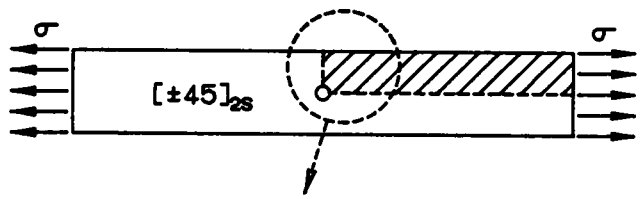

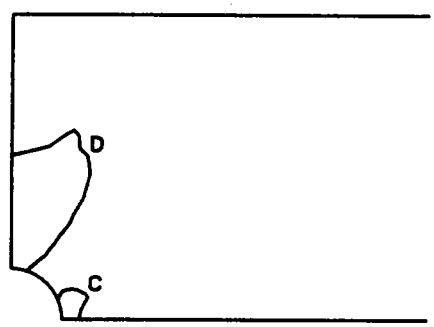

(a) Load = 5.0 kst

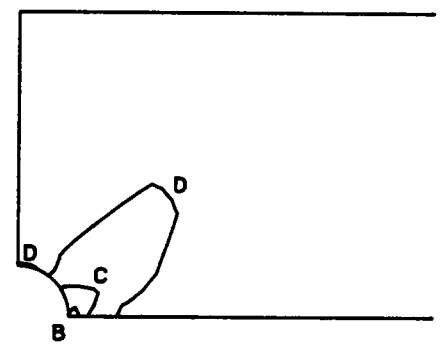

(b) Load = 10.0 kst

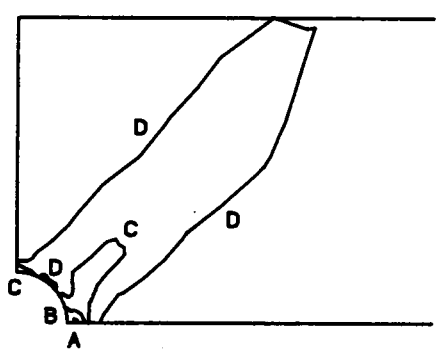

(c) Load = 15.0 kst

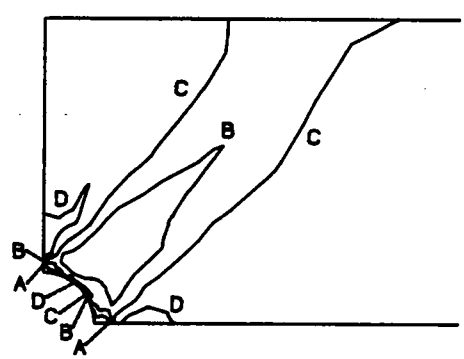

(d) Load = 20.0 kst

Label	Stress (kst)
A	2.5
B	5.0
C	7.5
D	10.0

Figure 4.22. Shear Stress σ_{22} in the -45° Plies of a $[\pm 45]_{2s}$ Laminate

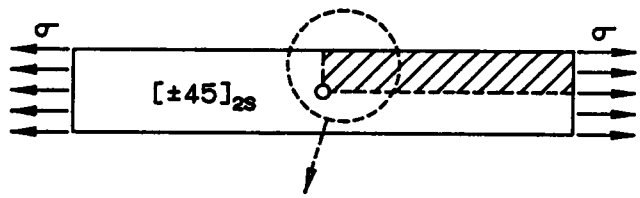

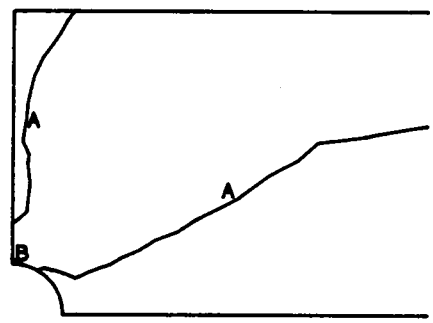

(a) Load = 5.0 kst

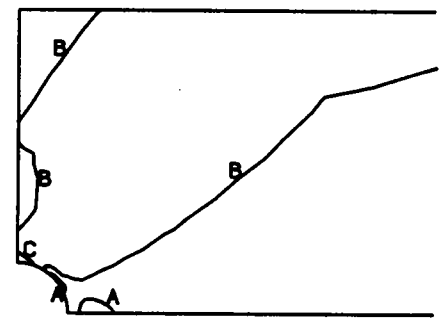

(b) Load = 10.0 kst

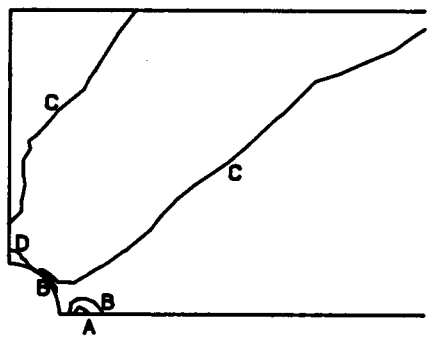

(c) Load = 15.0 kst

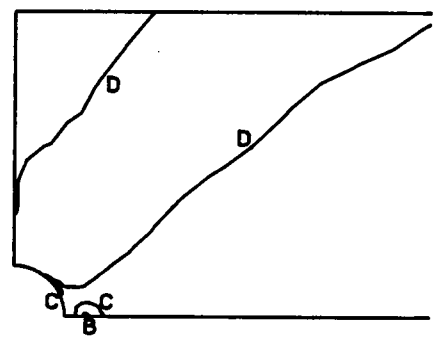

(d) Load = 20.0 kst

Label	Stress (kst)
A	-2.5
B	-5.0
C	-7.5
D	-10.0

Figure 4.23. Shear Stress σ_{12} in the +45° Plies of a $[\pm 45]_{2s}$ Laminate

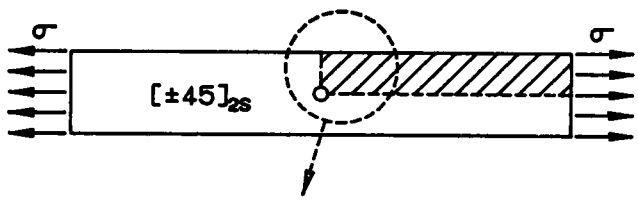

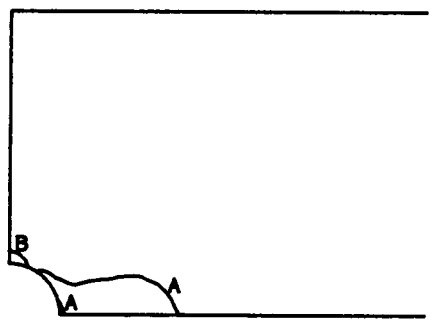

(a) Load = 5.0 ksi

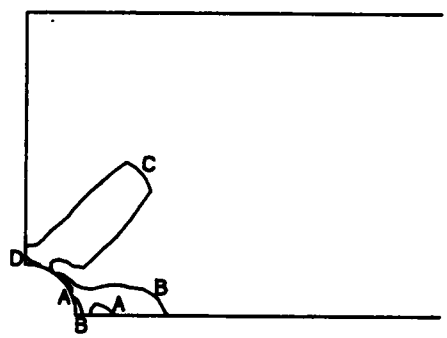

(b) Load = 10.0 ksi

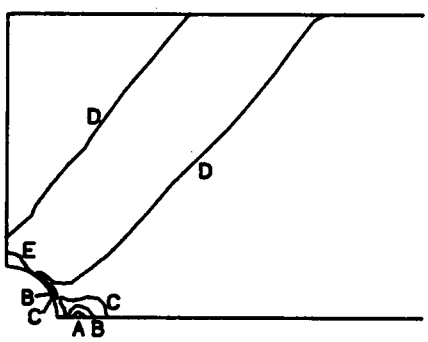

(c) Load = 15.0 ksi

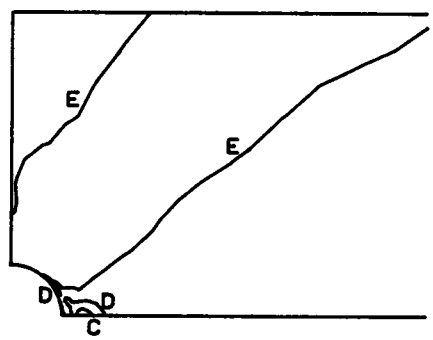

(d) Load = 20.0 ksi

Label	Stress (ksi)
A	2.0
B	4.0
C	6.0
D	8.0
E	10.0

Figure 4.24. Shear Stress σ_{12} in the -45° Plies of a $[\pm 45]_{2s}$ Laminate

The fibers in the -45° plies are oriented in the quadrant which was analyzed so that they reinforce the hole and restrict its elongation. This reinforcement results in large tensile stresses normal to the fibers which are oriented diagonally across the edge of the hole as shown in Fig. 4.20. Regarding the stress distributions of the normal stress transverse to the fibers σ_{22}, see Figs. 4.21 and 4.22. In both plies, a stress redistribution is observed in which the stresses in the plastic zone actually decrease as the applied load increases. The shear stress σ_{12} in the two plies is characterized by a region of high stress which coincides with the zone of significant plastic strains, see Figs. 4.23 and 4.24.

To examine the stress state at the edge of the hole the circumferential stresses $\sigma_{\theta\theta}$ as a function of applied load are presented in Fig. 4.25. The circumferential stresses are measured with respect to a polar coordinate system r, θ with its origin at the center of the hole. The circumferential stresses presented in the figure have been normalized with respect to the applied load σ so that the relative redistribution of the stresses is readily apparent. The stress distribution in the -45° plies is simply a mirror image of the 45° plies. Figures for both plies are included for completeness and to allow easy comparisons between the two fiber orientations.

Examining the circumferential stress distribution in the +45° plies, most noticeable in the figures is the increasing relative stress in the vicinity of θ = -45°. The increasing relative stress at this location is indicative of the stress redistribution from the -45° plies which has yielded transverse to the fiber direction. This effect is

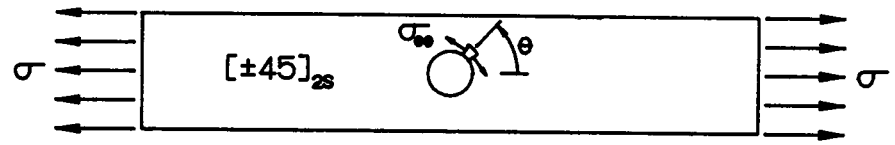

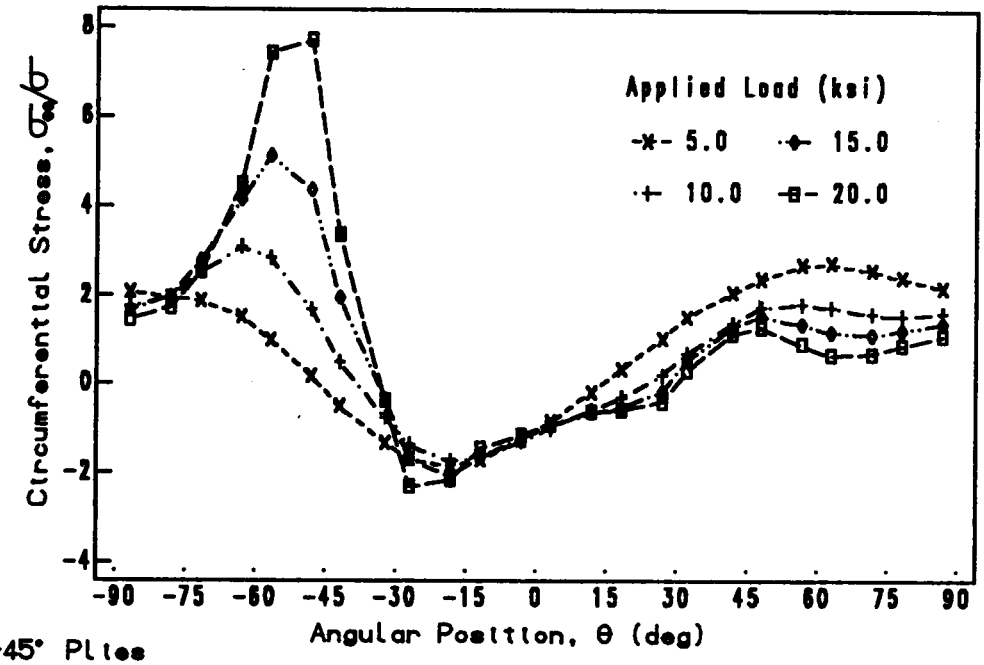

(a) +45° Plies

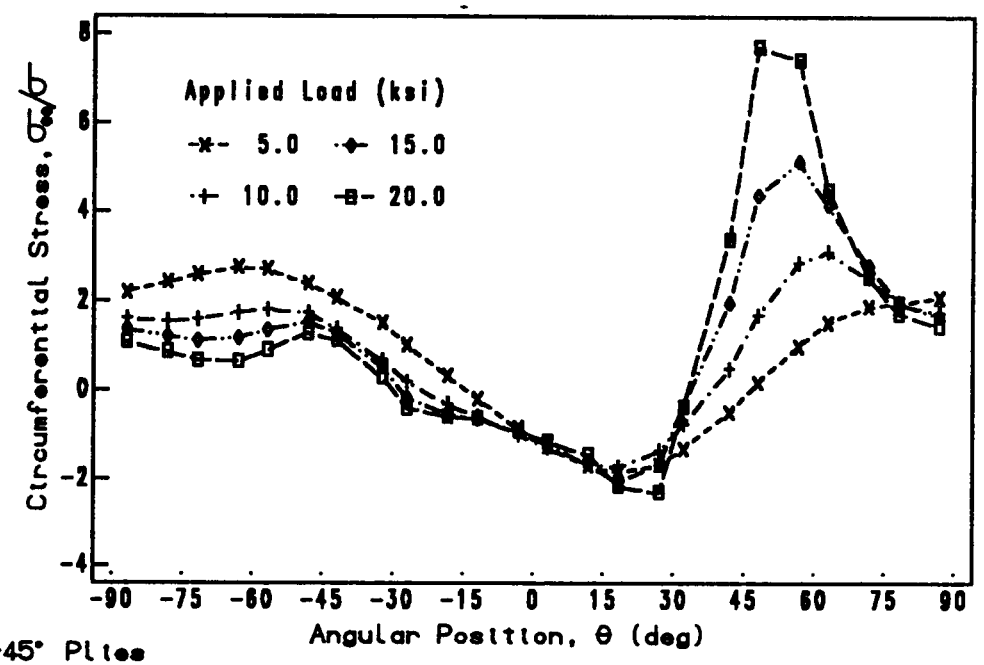

(b) -45° Plies

Figure 4.25. Circumferential Stresses at Edge of Hole in $[\pm 45]_{2s}$ Boron/Aluminum Laminate

observed by noting the decrease in the relative circumferential stress in the -45° plies at $\theta = -45°$. As a result, the +45° plies must carry an additional portion of the load in the stiff fiber direction.

Next, we shall examine the plastic zones and in-plane stress distributions for the previously analyzed $[0/\pm45/90]_s$ lamiante. In Figure 4.26, the plastic zones for the separate lamina are shown at a load of 40 ksi. Again, the scalar parameter equivalent uniaxial plastic strain ε^* is used to indicate the magnitude of the plastic deformation. Regarding the overall size of the plastic regions, the 0° plies have a plastic region which is considerably smaller than the other laminae. All laminae with the exception of the 0° plies exhibit plastic zones which emanate from the notch along the lines $\theta = \pm 45°$.

The in-plane stress distributions at the applied load of $\sigma = 40$ ksi are presented in Figs. 4.27 through 4.32. For the σ_{11} stress component, distinct stress concentrations are observed in both the 0° and -45° plies. In these plies, the σ_{11} stress component is well over 150 ksi, which results in a stress concentration factor in excess of 3.8 given the applied load of 40 ksi.

Regarding the normal stress σ_{22} transverse to the fiber orientation in the +45° plies, a region of high stress is located at the edge of the hole (see Fig. 4.29). Due to the yielding in the highly stressed region and the softening associated with the plastic deformation, the stress has been locally redistributed into the adjacent plies. The stress redistribution is a definite contributing factor for the σ_{11} stress concentration in the -45° plies which was previously discussed. A similar stress redistribution from the 90° plies to the 0° plies is

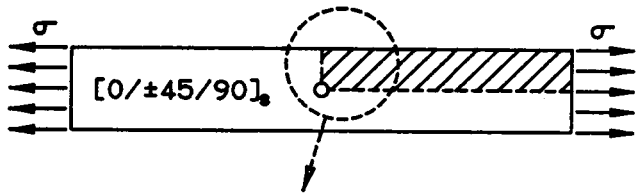

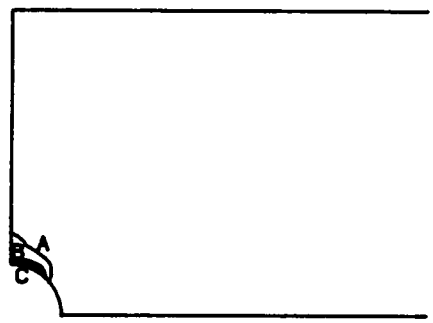

a) 0° Plies

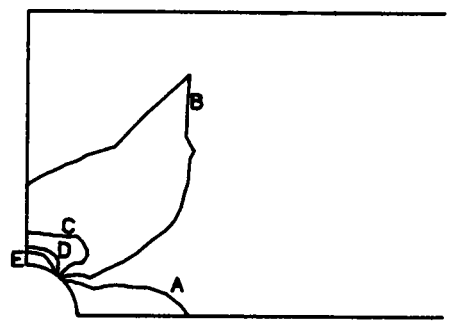

(b) +45° Plies

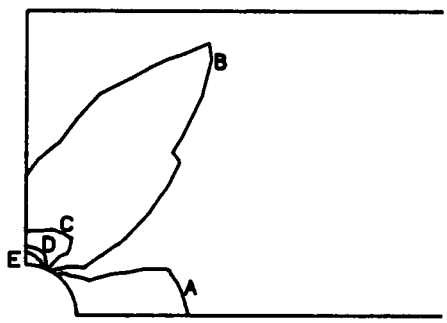

(c) -45° Plies

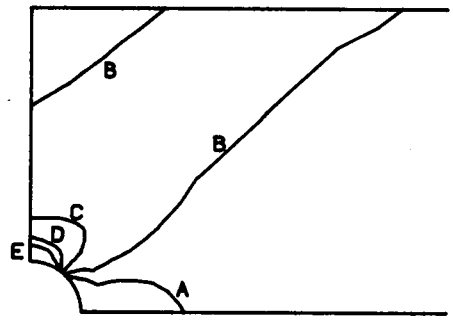

(d) 90° Plies

Label	Strain (in/in)
A	2.0E-3
B	3.0E-3
C	4.0E-3
D	5.0E-3
E	6.0E-3

Figure 4.26. Equivalent Uniaxial Plastic Strain in a Notched Quasi-Isotropic Laminate at a Load of 40.0 ksi

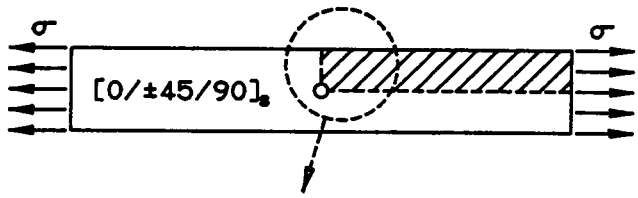

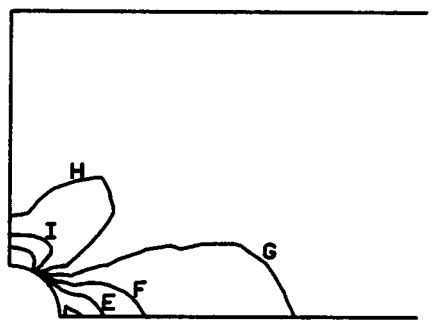

(a) 0° Plies

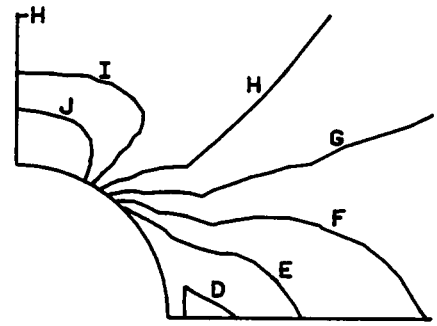

(b) Close-Up of 0° Plies at Hole

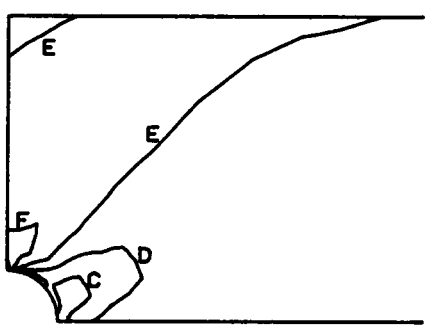

(c) +45° Plies

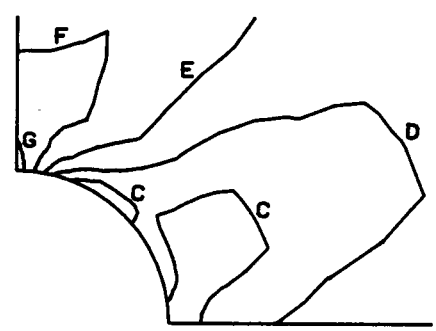

(d) Close-Up of +45° Plies at Hole

Label	Stress (ksi)
A	-75.0
B	-50.0
C	-25.0
D	0.0
E	25.0
F	50.0
G	75.0
H	100.0
I	125.0
J	150.0

Figure 4.27. Normal Stress σ_{11} in the 0° and +45° Plies of a Quasi-Istropic Boron/Aluminum Laminate at a Load of 40.0 ksi

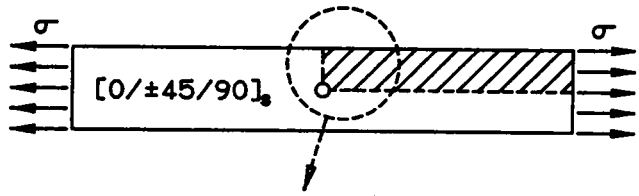

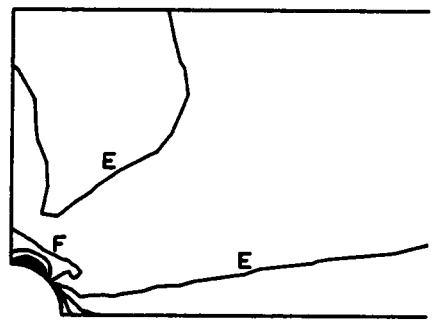

(a) -45° Plies

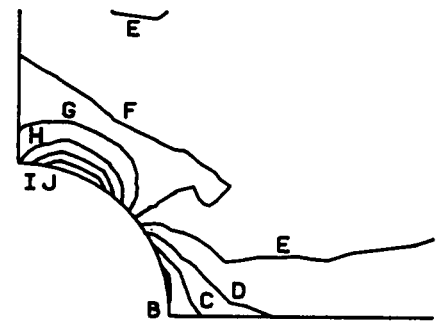

(b) Close-Up of -45° Plies at Hole

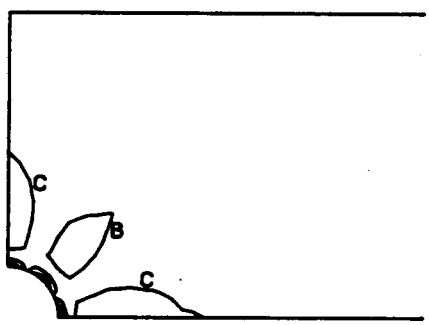

(c) 90° Plies

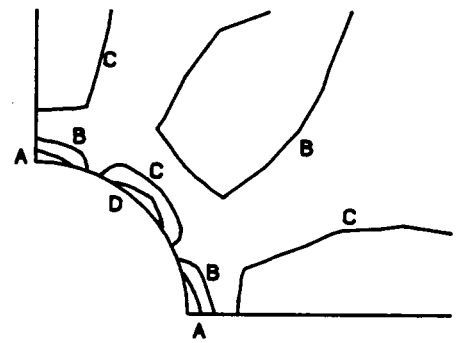

(d) Close-Up of 90° Plies at Hole

Label	Stress (ksi)
A	-75.0
B	-50.0
C	-25.0
D	0.0
E	25.0
F	50.0
G	75.0
H	100.0
I	125.0
J	150.0

Figure 4.28. Normal Stress σ_{11} in the -45° and 90° Plies of a Quasi-Istropic Boron/Aluminum Laminate at a Load of 40.0 ksi

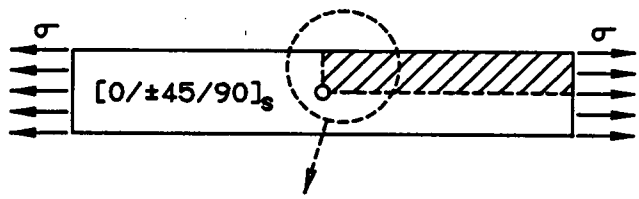

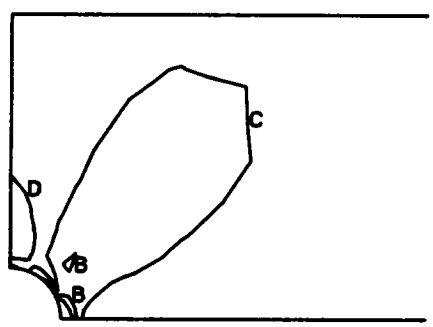

(a) 0° Plies

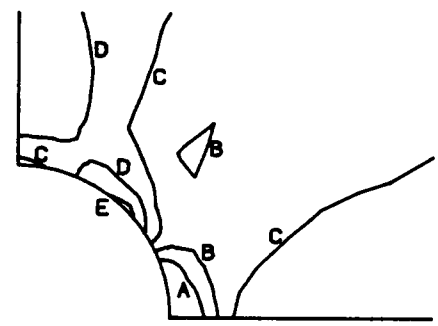

(b) Close-Up of 0° Plies at Hole

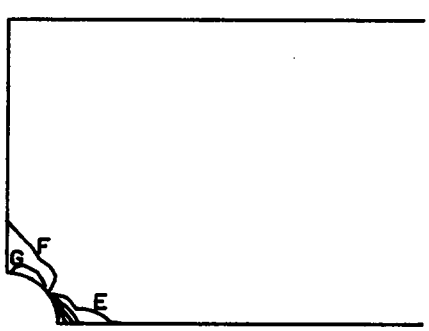

(c) +45° Plies

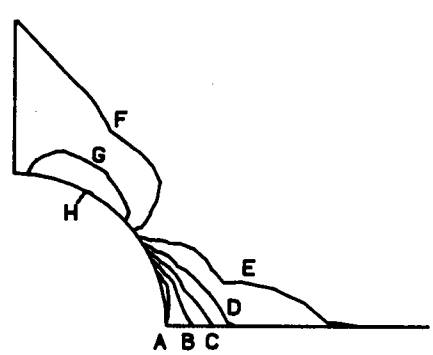

(d) Close-Up of +45° Plies at Hole

Label	Stress (ksi)
A	-5.0
B	0.0
C	5.0
D	10.0
E	15.0
F	20.0
G	25.0
H	30.0

Figure 4.29. Normal Stress σ_{22} in the 0° and +45° Plies of a Quasi-Istropic Boron/Aluminum Laminate at a Load of 40.0 ksi

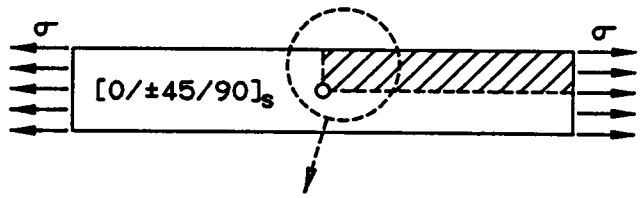

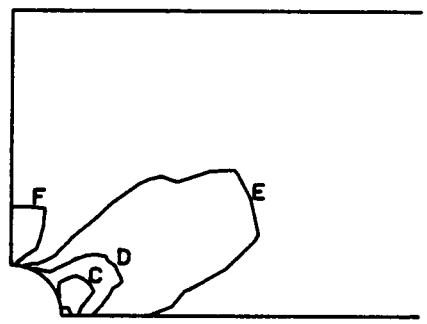

(a) -45° Plies

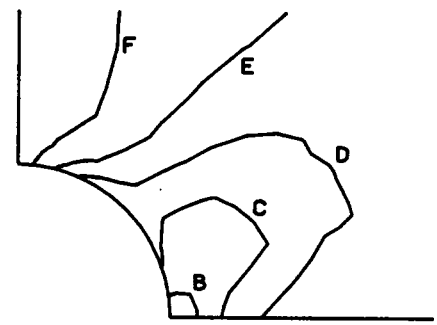

(b) Close-Up of -45° Plies at Hole

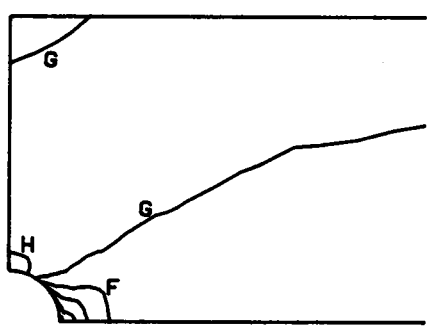

(c) 90° Plies

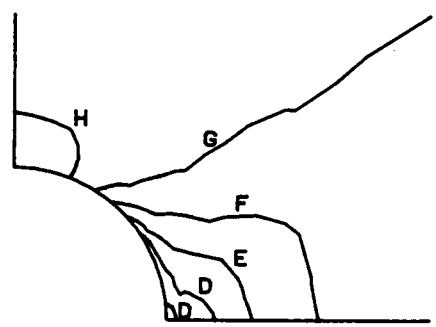

(d) Close-Up of 90° Plies at Hole

Label	Stress (ksi)
A	-5.0
B	0.0
C	5.0
D	10.0
E	15.0
F	20.0
G	25.0
H	30.0

Figure 4.30. Normal Stress σ_{22} in the -45° and 90° Plies of a Quasi-Istropic Boron/Aluminum Laminate at a Load of 40.0 ksi

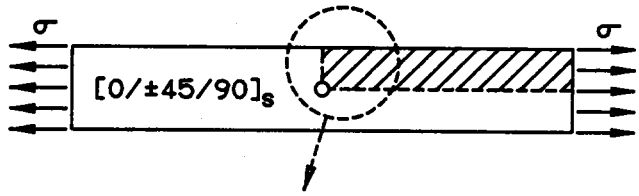

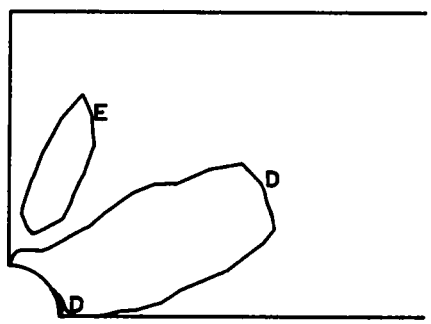

(a) 0° Plies

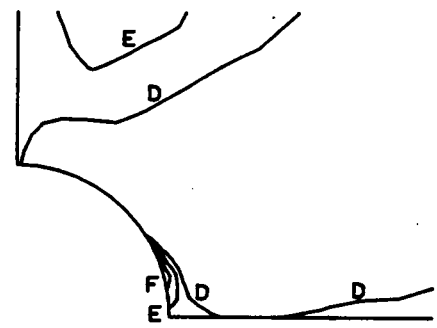

(b) Close-Up of 0° Plies at Hole

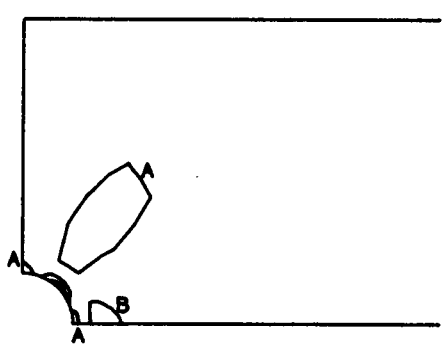

(c) +45° Plies

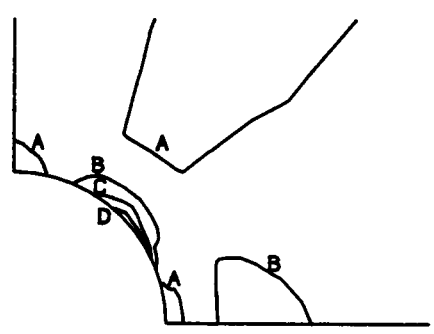

(d) Close-Up of +45° Plies at Hole

Label	Stress (ksi)
A	-7.0
B	-5.0
C	-3.0
D	-1.0
E	1.0
F	3.0

Figure 4.31. Shear Stress σ_{12} in the 0° and +45° Plies of a Quasi-Istropic Boron/Aluminum Laminate at a Load of 40.0 ksi

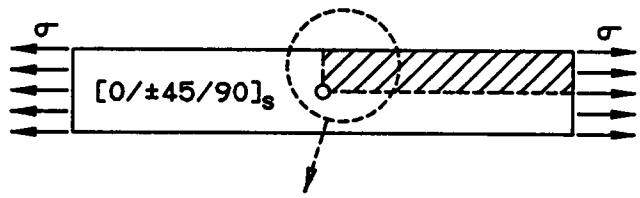

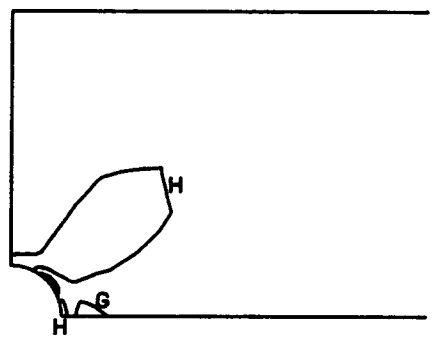

(a) -45° Plies

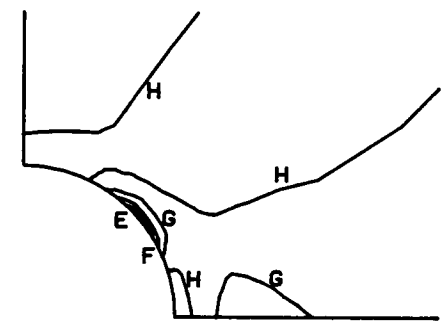

(b) Close-Up of -45° Plies at Hole

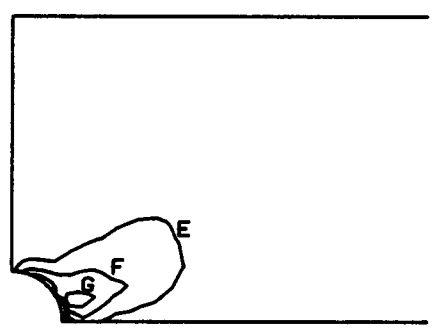

(c) 90° Plies

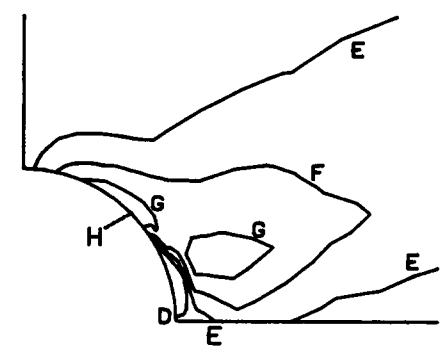

(d) Close-Up of 90° Plies at Hole

Label	Stress (ksi)
D	-1.0
E	1.0
F	3.0
G	5.0
H	7.0

Figure 4.32. Shear Stress σ_{12} in the -45° and 90° Plies of a Quasi-Istropic Boron/Aluminum Laminate at a Load of 40.0 ksi

present. This redistribution in the 90° plies occurs at the zone of large σ_{22} stress, see Fig. 4.30, which is also the location of the σ_{11} concentrations in the 0° plies.

The magnitude of the shear stress σ_{12} is generally less than 10 ksi for all the laminae, see Figs. 4.31 and 4.32. The reason for the small shear stress is the stiff 0° plies which carry a significant portion of the load in the laminate without introducing large shear stresses in the softer off-axis plies.

The circumferential stress at the edge of the hole for the quasi-isotropic laminate is shown in Figs. 4.33 and 4.34. These figures present clear evidence of the stress redistribution. The load transfer between the 90° plies and the 0° plies at $\theta = \pm 90°$, results in a decrease in the normalized circumferential stress in the 90° plies from 2.2 to 0.9 while the 0° plies increase from 4.5 to 7.0. Similar behavior is also noted in the +45° and -45° plies at $\theta = \pm 60°$.

4.6 Bending of Square and Circular Plates

Analysis of square and circular plates subjected to a uniformly distributed transverse load is presented in this section. The plates which are considered consist of a single boron/aluminum orthotropic layer (i.e. a $[0]_T$ laminate). The material properties used for this analysis are from Table 4.5. Two plate configurations are considered: (1) a 10.0" square plate 0.1" thick and (2) a 10.0" diameter circular plate 0.1" thick. The dimensions used are selected so the effect of transverse shear deformation is negligible. A summary of the plate

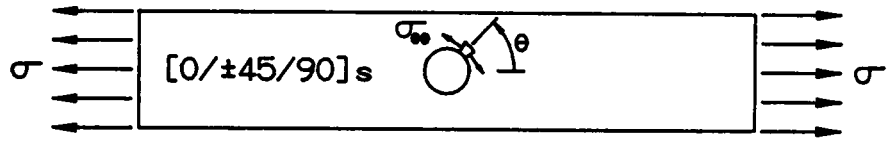

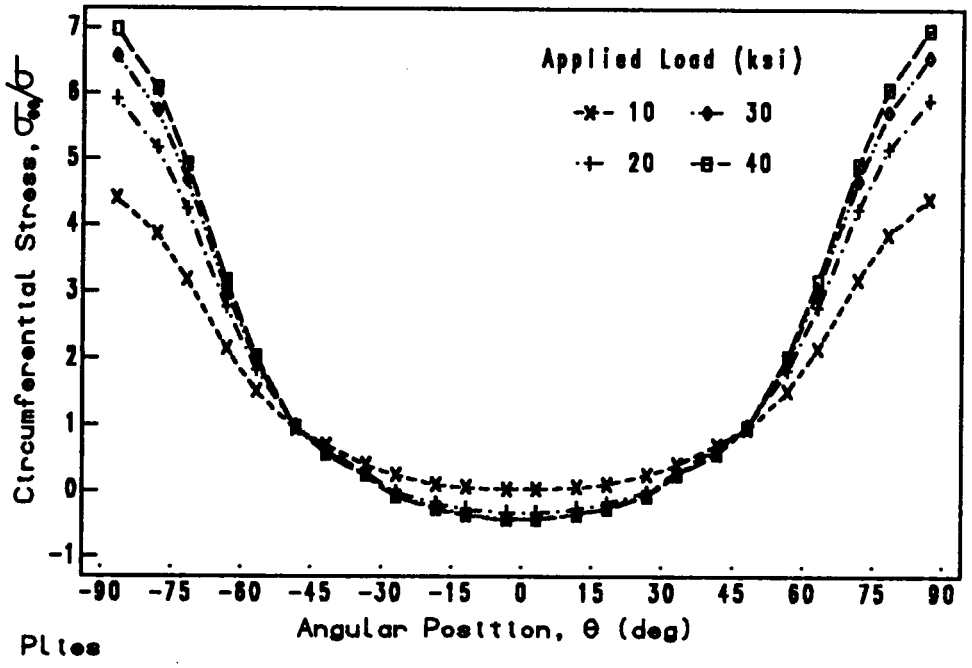

(a) 0° Plies

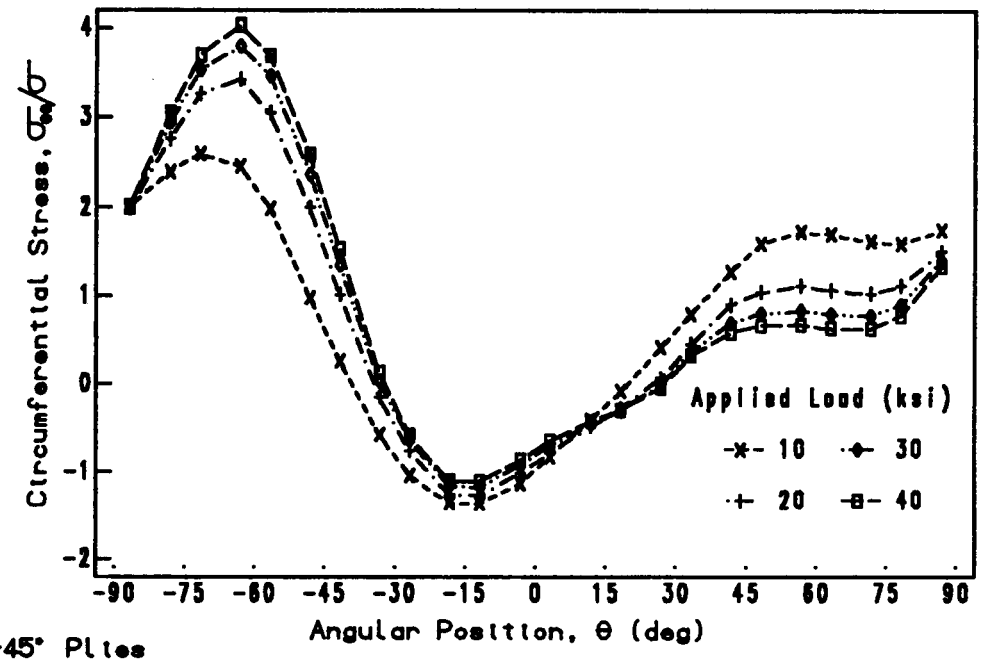

(b) +45° Plies

Figure 4.33. Circumferential Stresses at Edge of Hole in [0/±45/90]s Boron/Aluminum Laminate for the 0° and +45° Plies

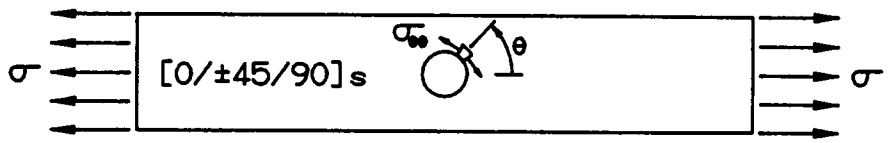

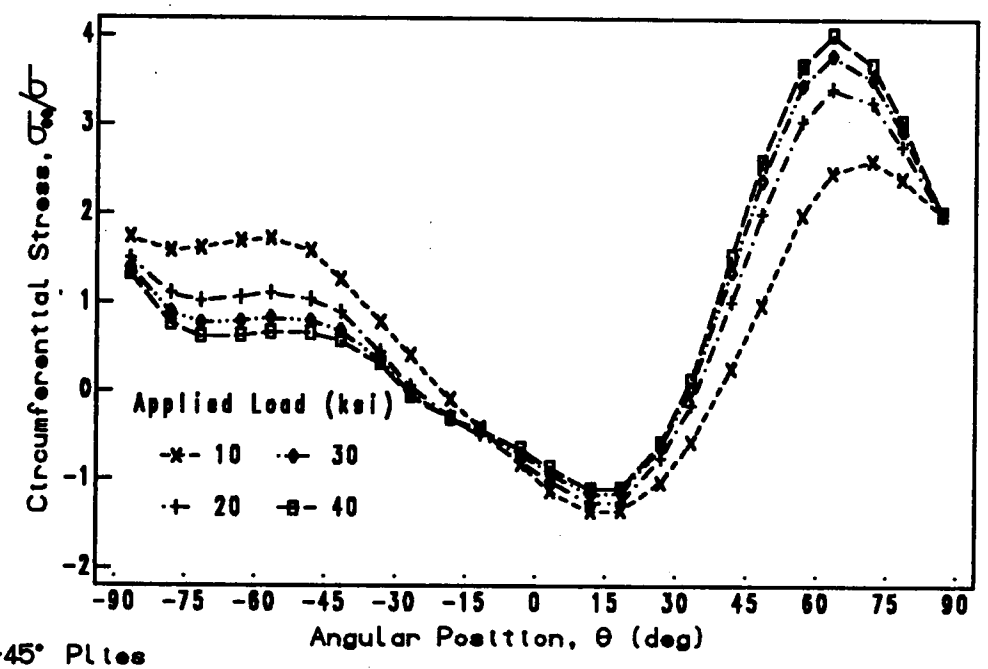

(c) -45° Plies

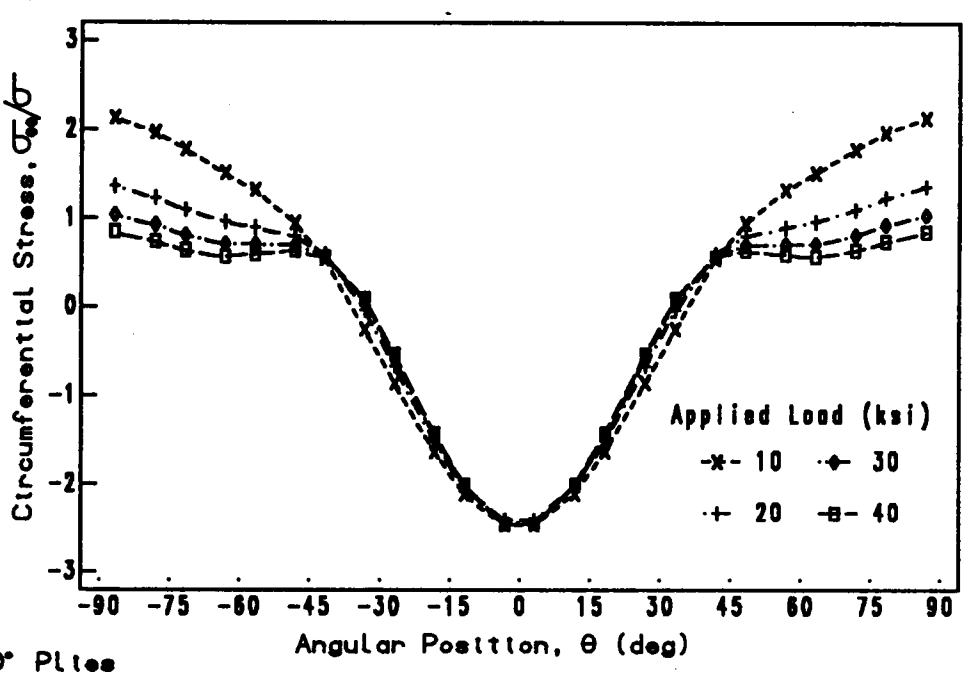

(d) 90° Plies

Figure 4.34. Circumferential Stresses at Edge of Hole in [0/±45/90]s Boron/Aluminum Laminate for the -45° and 90° Plies

configurations along with the finite element meshes are shown in Fig. 4.35.

The finite element stiffness matrices are integrated using a selective integration technique. The selective integration technique consists of using a 3 x 3 Gauss rule for all terms in the stiffness matrices with the exception of the terms associated with the transverse shear strain energy which are integrated using a 2 x 2 Gauss rule. The nodal forces resulting from plastic stress resultants are evaluated using a 2 x 2 Gauss rule. The plastic stress resultants are computed using a (2 x 3) integration rule (see section 4.3 for an explanation of this notation).

Two types of boundary conditions are considered, simply supported and clamped. The simply supported boundary conditions consist of restraining the w displacement components at the supported perimeter. The clamped boundary conditions consist of restraining the w displacements in addition to the rotations ψ_x and ψ_y at the supported perimeter. For both the boundary conditions, the in-plane displacements u and v are restrained in order to remove rigid body motion. These restraints are needed to allow free thermal expansion during the initial thermal conditioning of the plates which is used to approximate the residual stress state in the composite.

The center displacement as a function of the applied transverse load for both the square and circular plates is shown in Fig. 4.36. The plates are loaded until failure based on a maximum stress failure theory. This failure criterion limits the maximum transverse load to 12 psi for all plate configurations except the clamped circular plate which

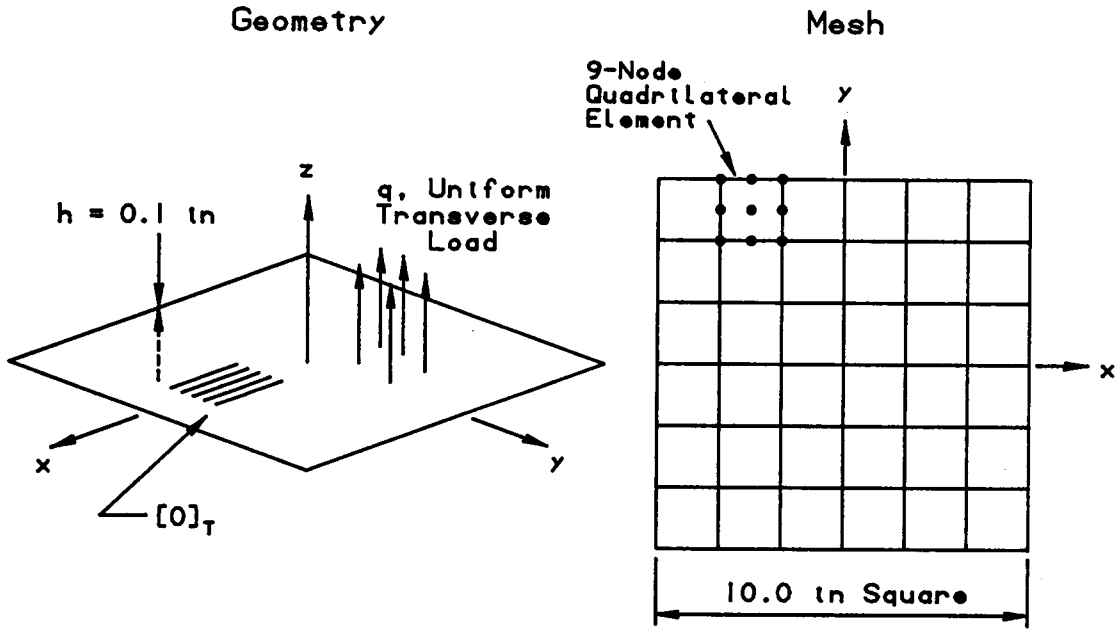

(a) Square Plate

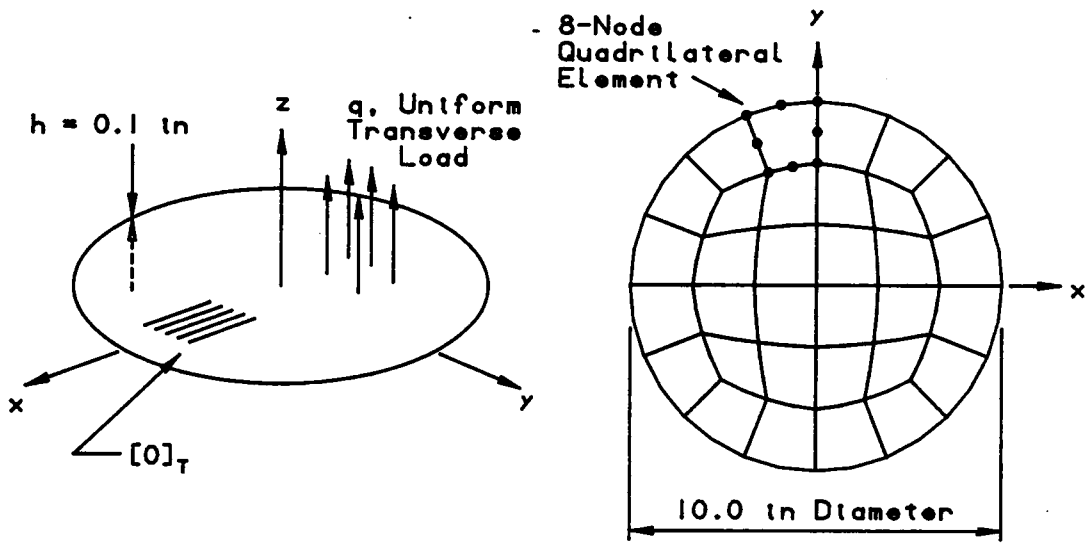

(b) Circular plate

Figure 4.35. Plate Geometry and Finite Element Mesh

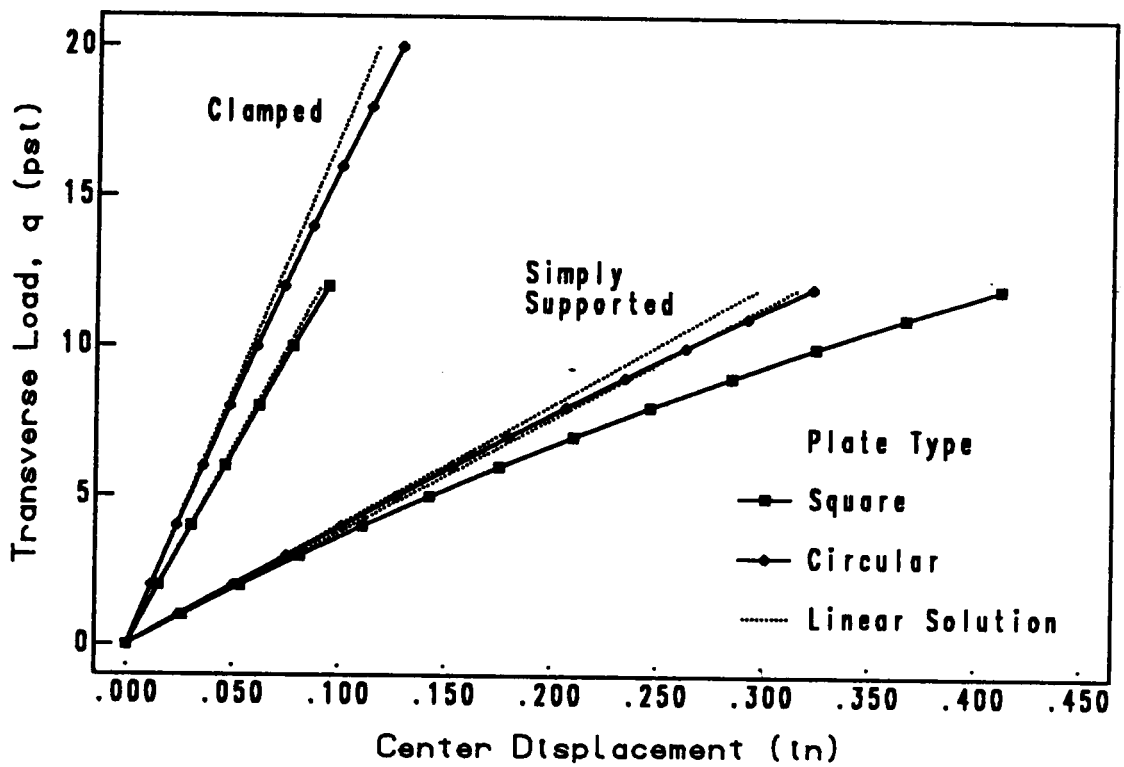

Figure 4.36. Center Displacements of Circular and Square Unidirectional Plates for Simply Supported and Clamped Boundary Conditions

is limited to a 20 psi load. All four plate configurations exceeded an approximate transverse tensile allowable stress of 20 ksi. The allowable tensile stress used is based on the experimental work by Becker [94] for a similar boron/aluminum material system. Becker reported a maximum transverse tensile stress of 17 ksi, for the work reported here this value is simply rounded to 20 ksi.

In general the load/displacement response of the plates exhibited relatively little to moderate deviation from the linear elastic behavior. Among the four plate configurations, the simply supported square plate provided the most nonlinear response.

The evolution of plastic regions at the top and bottom surfaces are shown in Figs. 4.37 through 4.40. The equivalent uniaxial plastic strain which is defined by (4.1) is used as a measure of plastic deformation. In the simply supported square plate, Fig. 4.37, the plastic zone initially forms at the center of the plate. Following this, plastic zones begin to form in each corner of the plate. As the load increases, the plastic zones at the center and the corners continue to grow primarily along the diagonals of the plate.

The plastic zones in the clamped square plate, Fig. 4.38, begin to form initially at the edges $y = \pm 5.0"$. As the load increases, the plastic regions remain concentrated along the same edge with the addition of a smaller zone located at the center of the plate. The large plastic zones at the edges of the plate are due to the rotational restraints there which cause significant bending moments.

The plastic zones which form in the circular plates share basic similarities to the square plates with the same type of boundary

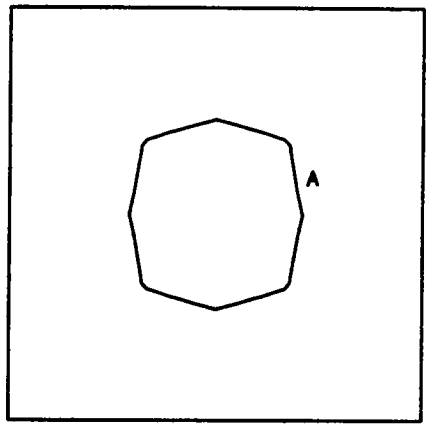

(a) Load q = 3.0 psi

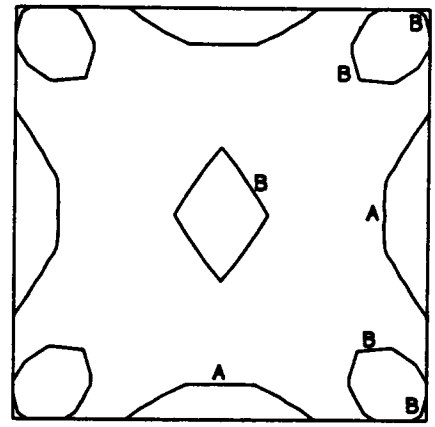

(b) Load q = 6.0 psi

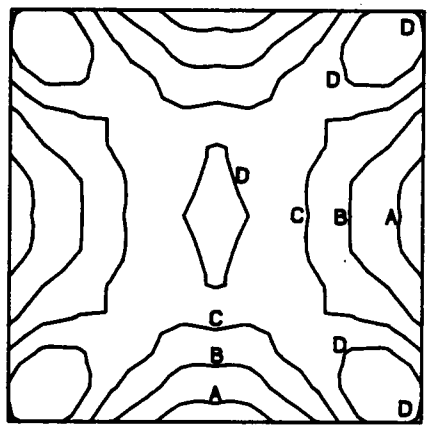

(c) Load q = 9.0 psi

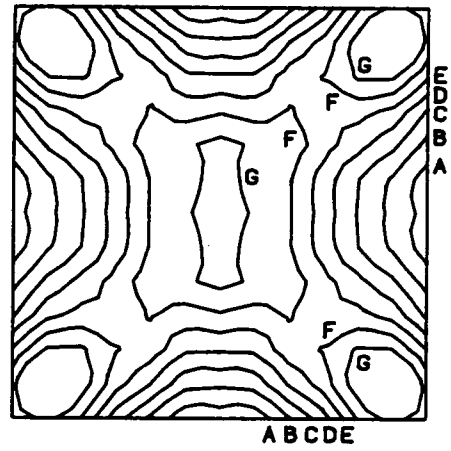

(d) Load q = 12.0 psi

Label	Strain (in/in)
A	3.0E-4
B	5.0E-4
C	7.0E-4
D	9.0E-4
E	11.0E-4
F	13.0E-4
G	15.0E-4

Figure 4.37. Equivalent Uniaxial Plastic Strain at z = ±0.05 in a Unidirectional Simply Supported Square Plate

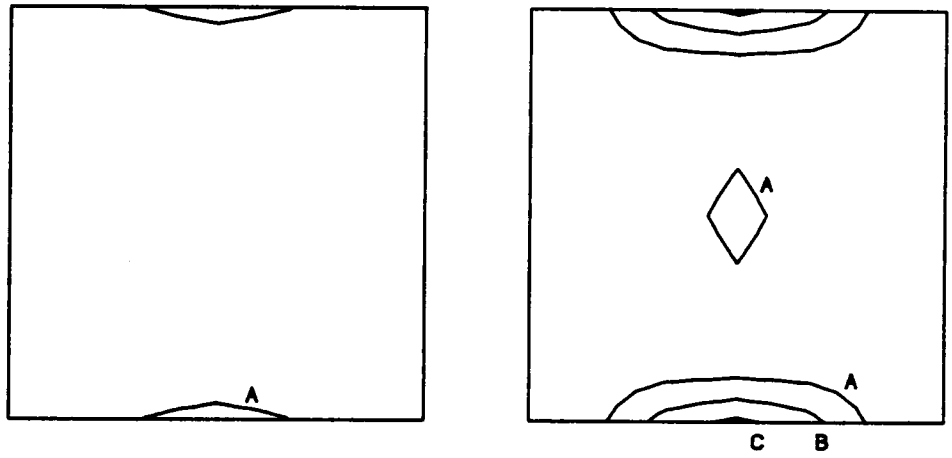

(a) Load q = 3.0 psi

(b) Load q = 6.0 psi

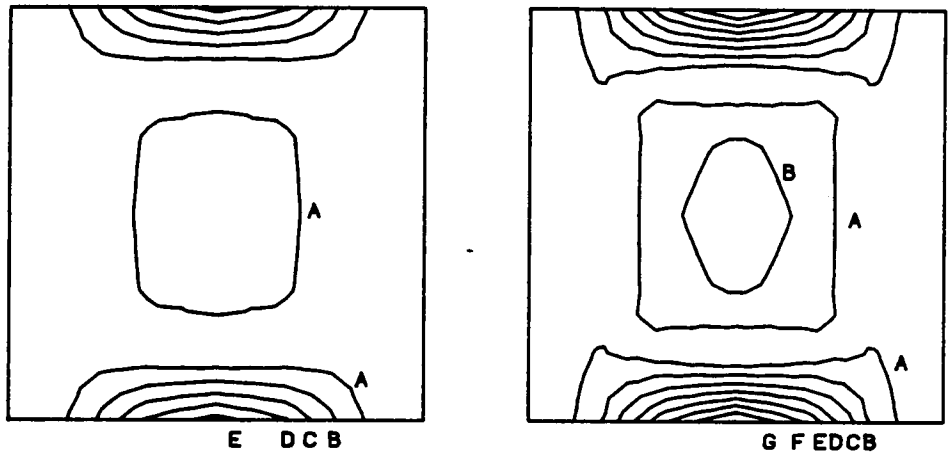

(c) Load q = 9.0 psi

(d) Load q = 12.0 psi

Label	Strain (in/in)
A	3.0E-4
B	4.0E-4
C	5.0E-4
D	6.0E-4
E	7.0E-4
F	8.0E-4
G	9.0E-4

Figure 4.38. Equivalent Uniaxial Plastic Strain at z = ±0.05 in a Unidirectional Clamped Square Plate

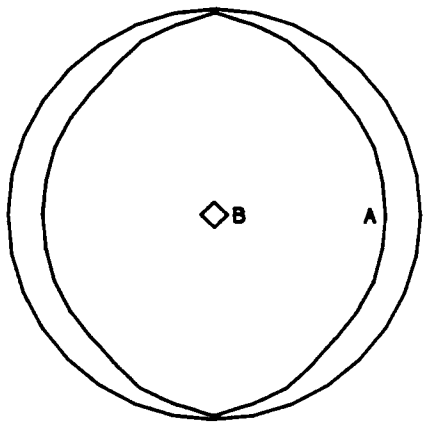

(a) Load q = 3.0 psi

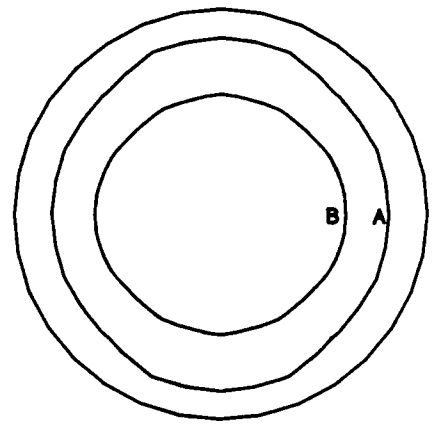

(b) Load q = 6.0 psi

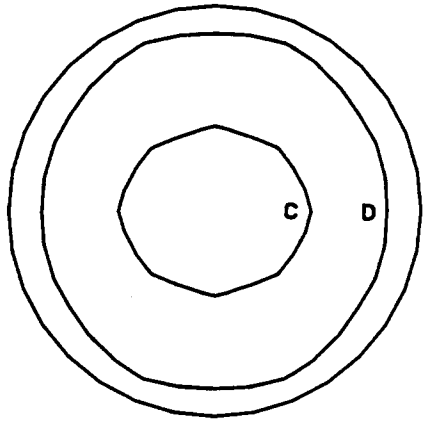

(c) Load q = 9.0 psi

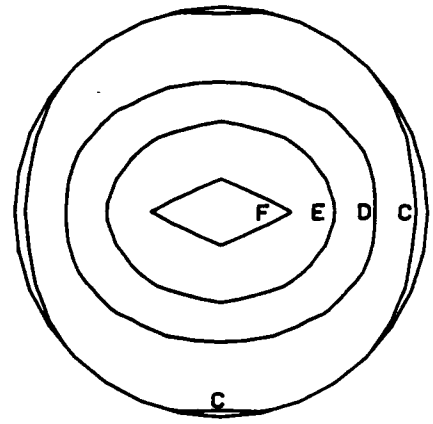

(d) Load q = 12.0 psi

Label	Strain (in/in)
A	2.50E-4
B	3.25E-4
C	4.00E-4
D	7.00E-4
E	10.00E-4
F	13.00E-4

Figure 4.39. Equivalent Uniaxial Plastic Strain at z = ±0.05 in a Unidirectional Simply Supported Circular Plate

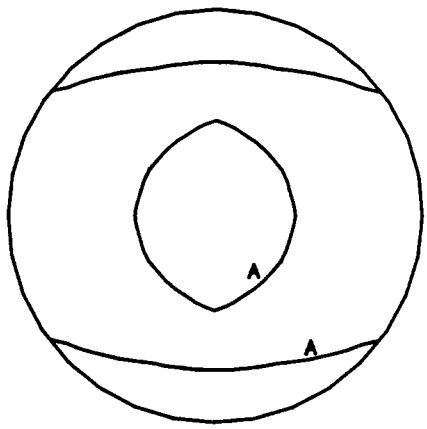

(a) Load q = 5.0 psi

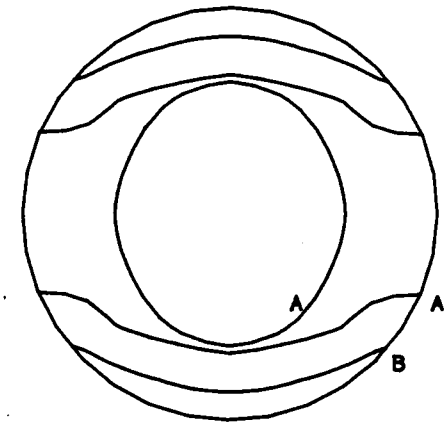

(b) Load q = 10.0 psi

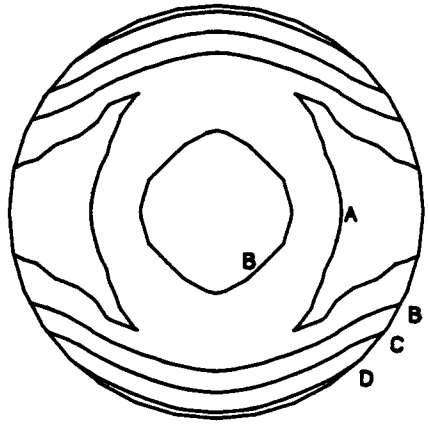

(c) Load q = 15.0 psi

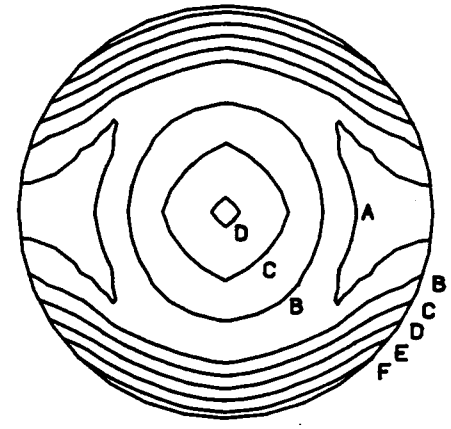

(d) Load q = 20.0 psi

Label	Strain (in/in)
A	2.5E-4
B	4.0E-4
C	5.5E-4
D	7.0E-4
E	8.5E-4
F	10.0E-4

Figure 4.40. Equivalent Uniaxial Plastic Strain at z = ±0.05 in a Unidirectional Clamped Circular Plate

conditions. The simply supported circular plate has oval shaped plastic zones which emanate from the center. The oval shape is a result of the orthotropy of the composite. The clamped circular plate is dominated by the bending moments at the edge of the plate. The edge moments transverse to the fiber orientation form large plastic zones there in many ways like those found in the square plate.

The maximum stress, as a function of applied load at the top surface of the plate (z = 0.05"), is shown in Figs. 4.41 through 4.44 for the various plate configurations. The figures show the absolute value of the maximum stress for the σ_{11}, σ_{22} and σ_{12} stress components. Contour plots are also included which show the stress distributions as a percentage of the maximum value of the stress component for the maximum applied load. On the contour plots, a star (*) is placed to indicate the location of the maximum stress for the respective stress component.

The location of the maximum stress for the σ_{11} and σ_{22} stress components for the simply supported square and circular plates is at the center of the plate. For the clamped plates, the location of the maximum stress occurs at the edge of the plate due to the rotational restraint there. The shear stress σ_{12} has a similar distribution among the simply supported square plate and both circular plates. In these plates, the shear stress has four distinct regions of alternating sign. The maximum shear stress occurs at the edge of the plate at four equally spaced locations around the perimeter. In the case of the simply supported square plate, the maximum stress is at the corner of the plate. For the clamped square plate, the location of the maximum

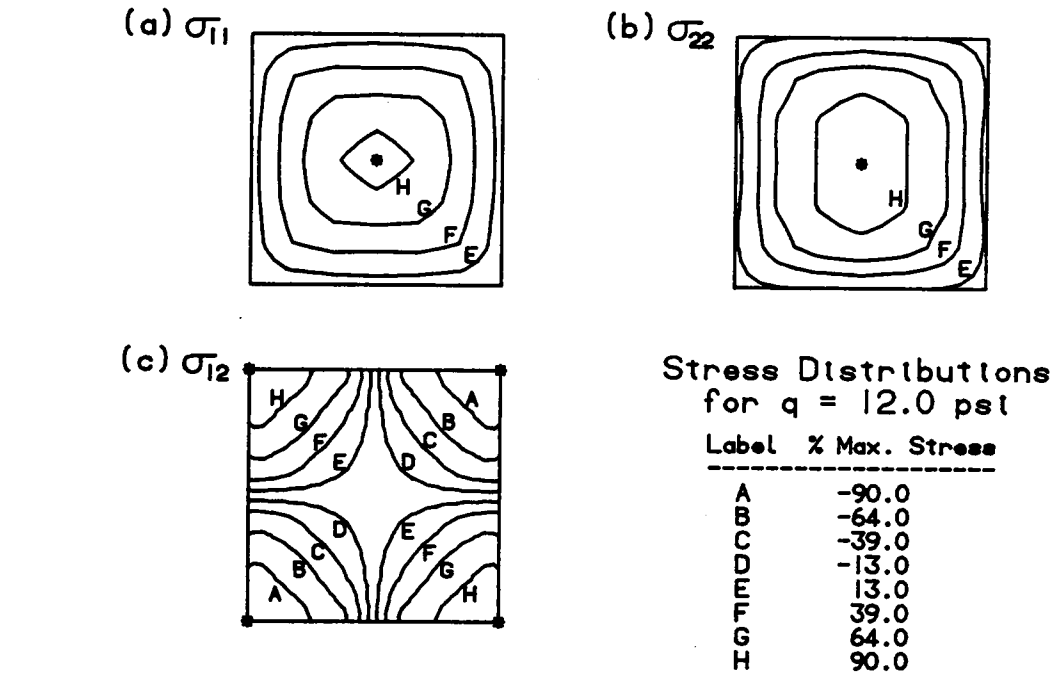

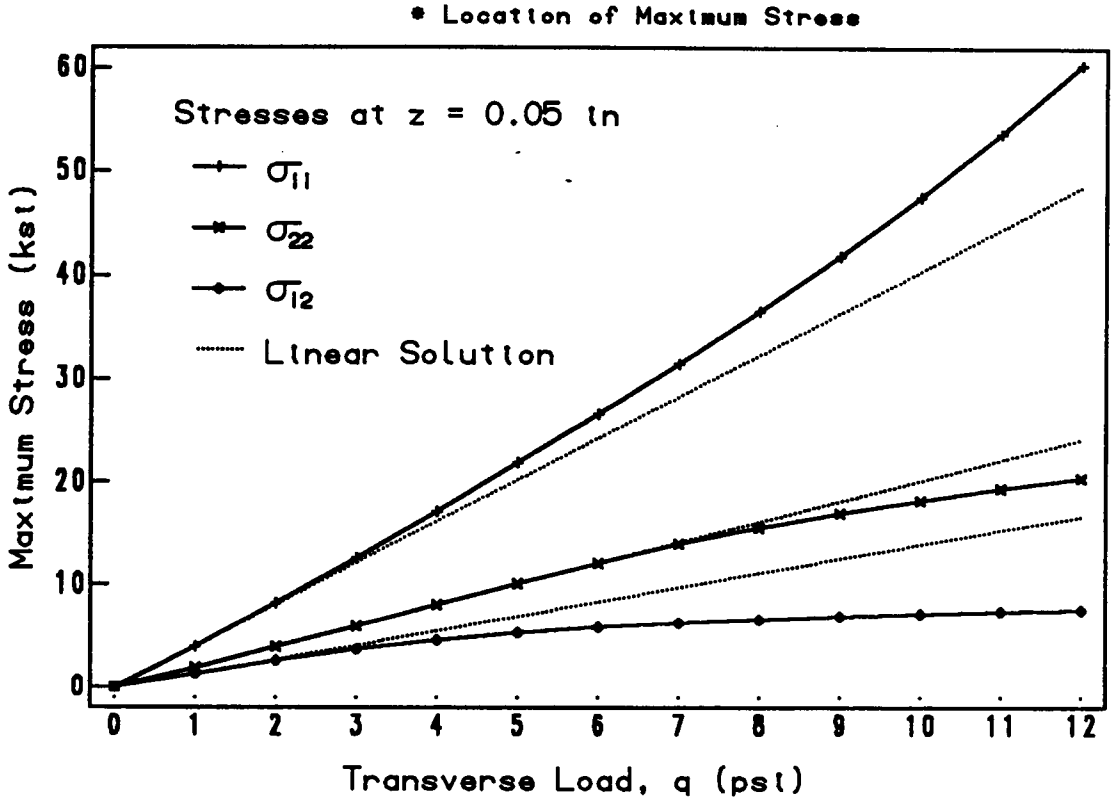

Figure 4.41. Stresses in a Simply Supported Unidirectional $[0]_T$ Square Plate Subjected to a Uniform Transverse Load

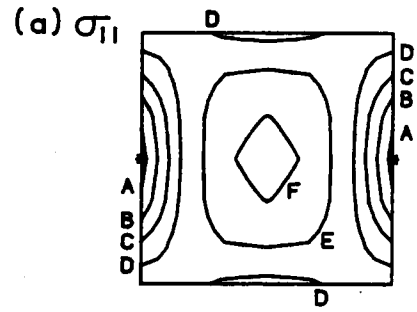

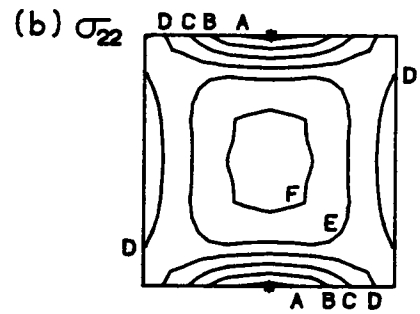

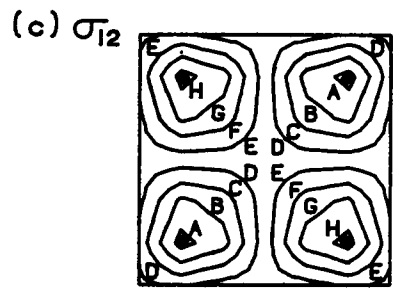

Stress Distributions for q = 12.0 psi

Label	% Max. Stress
A	-90.0
B	-64.0
C	-39.0
D	-13.0
E	13.0
F	39.0
G	64.0
H	90.0

* Location of Maximum Stress

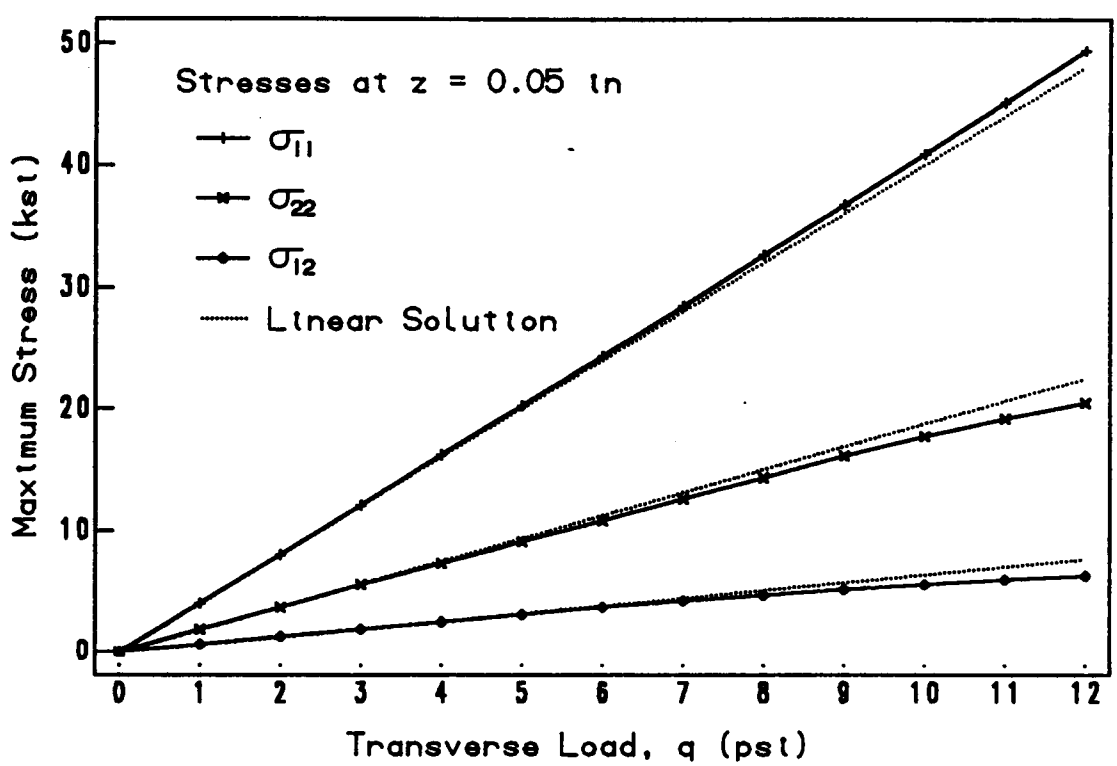

Figure 4.42. Stresses in a Clamped Unidirectional $[0]_T$ Square Plate Subjected to a Uniform Transverse Load

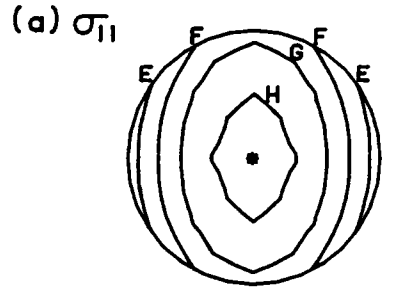

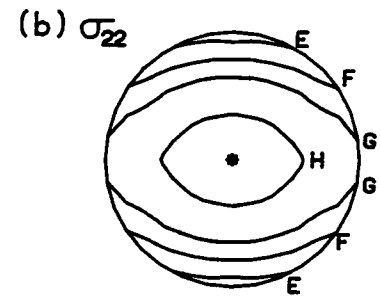

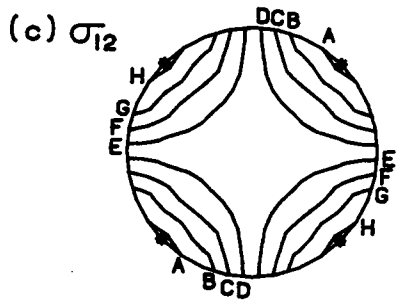

Stress Distributions for q = 12.0 psi

Label	% Max. Stress
A	-90.0
B	-64.0
C	-39.0
D	-13.0
E	13.0
F	39.0
G	64.0
H	90.0

* Location of Maximum Stress

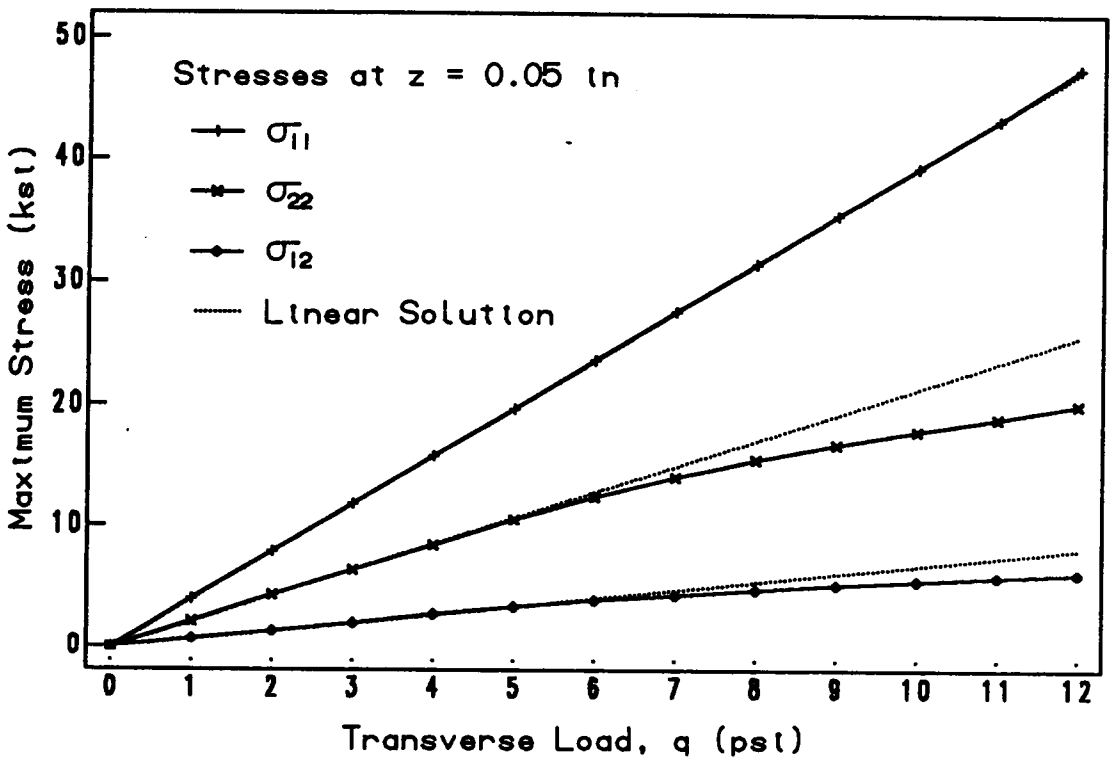

Figure 4.43. Stresses in a Simply Supported Unidirectional $[0]_T$ Circular Plate Subjected to a Uniform Transverse Load

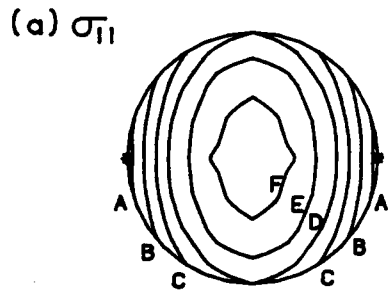

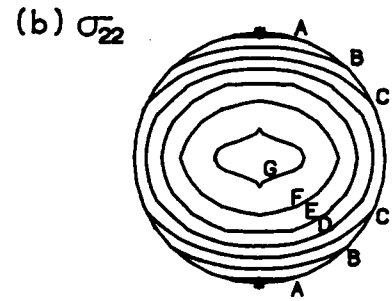

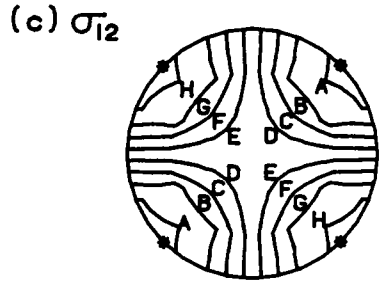

Stress Distributions for q = 20.0 psi

Label	% Max. Stress
A	-90.0
B	-64.0
C	-39.0
D	-13.0
E	13.0
F	39.0
G	64.0
H	90.0

* Location of Maximum Stress

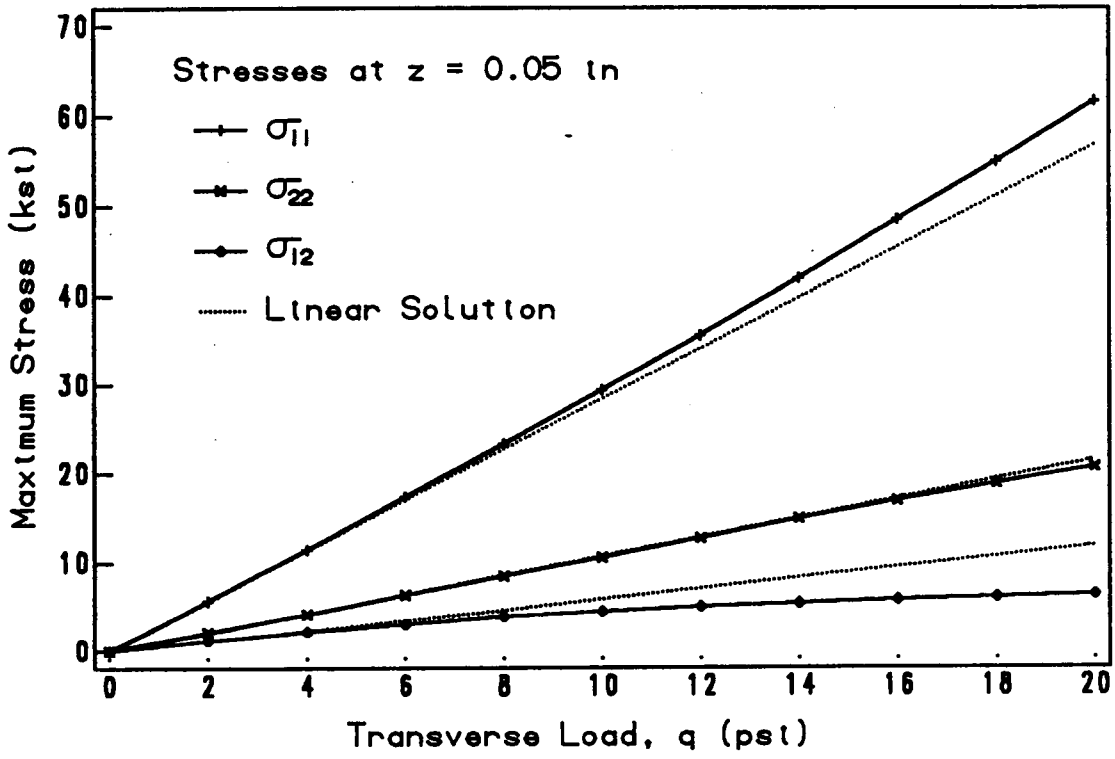

Figure 4.44. Stresses in a Clamped Unidirectional $[0]_T$ Circular Plate Subjected to a Uniform Transverse Load

shear stress is in from the corners located along the diagonals of the plate.

For the four plate configurations, a redistribution of the stresses is again observed. Due to yielding in the matrix material, the maximum stress predicted by the elastic-plastic solution for the σ_{22} and σ_{12} components is less than that predicted by the linear elastic solution while the maximum stress in the σ_{11} component is slightly larger for the elastic-plastic solution. In the plate as the matrix begins to yield, the composite cannot carry as much load transverse to the fibers or in shear. As a result, the composite begins to carry larger portions of the load in the fiber direction which explains the larger σ_{11} stresses compared to the linear elastic solution.

4.7 Additional Capabilities of the Material Model

In this closing section of applications, several additional capabilities of the micromechanics model are demonstrated. Examples illustrating the effect of fiber/matrix debonding, rate dependence and creep behavior are presented. These capabilities highlight the overall versatility of the Aboudi micromechanics model and Bodner-Partom plasticity theories. Thorough examination of these phenomena are beyond the scope of the current research, however, they are included at this point as an indication of possible future work.

The first example which is addressed is the effect of imperfect fiber/matrix bonding. We shall examine the effect of the tangential bonding parameter R_t. For this example the axial response of two off-axis test coupons are considered. The coupons are boron/aluminum with

material properties from Table 4.5. The effect of residual stresses is not considered in this example and the thermal preconditioning is not performed (i.e. $\Delta T_p = 0$). Additionally, we should note for this analysis that the normal bonding parameter $R_n = 0$ is used, which implies perfect bonding normal to the fiber/matrix interface.

The axial response as a function of the tangential debonding parameter is shown in Fig. 4.45. The tangential bonding parameter R_t ranges from 0 to 10^{-2} these values reflect perfect bonding to near perfect lubrication or debonding, respectively. For the case of near perfect lubrication, the main load transfer mechanism between the fiber and matrix is disabled and prevents the fiber from carrying any load longitudinally. For both the 15° and the 45° off-axis test coupon, we see a significant reduction in the initial modulus and overall softening behavior of the material as the quality of the fiber/matrix interface is degraded to near perfect debonding.

The ability to adjust the adhesion between the fiber and matrix phases provides an alternate means of modeling the interphase region. Aboudi [78] suggests the bonding parameters R_n and R_t could be interpreted as the thickness of the interphase region divided by Young's modulus or the shear modulus depending the direction of the bonding parameter. The final component needed in order to utilize the adhesion model is a suitable damage growth law which could describe the evolution of the bonding parameters as a function of the load history.

The final examples considered are the effect of rate dependence and creep. The boron/aluminum material systems which have been considered so far do not exhibit significant creep or rate dependence. In order to

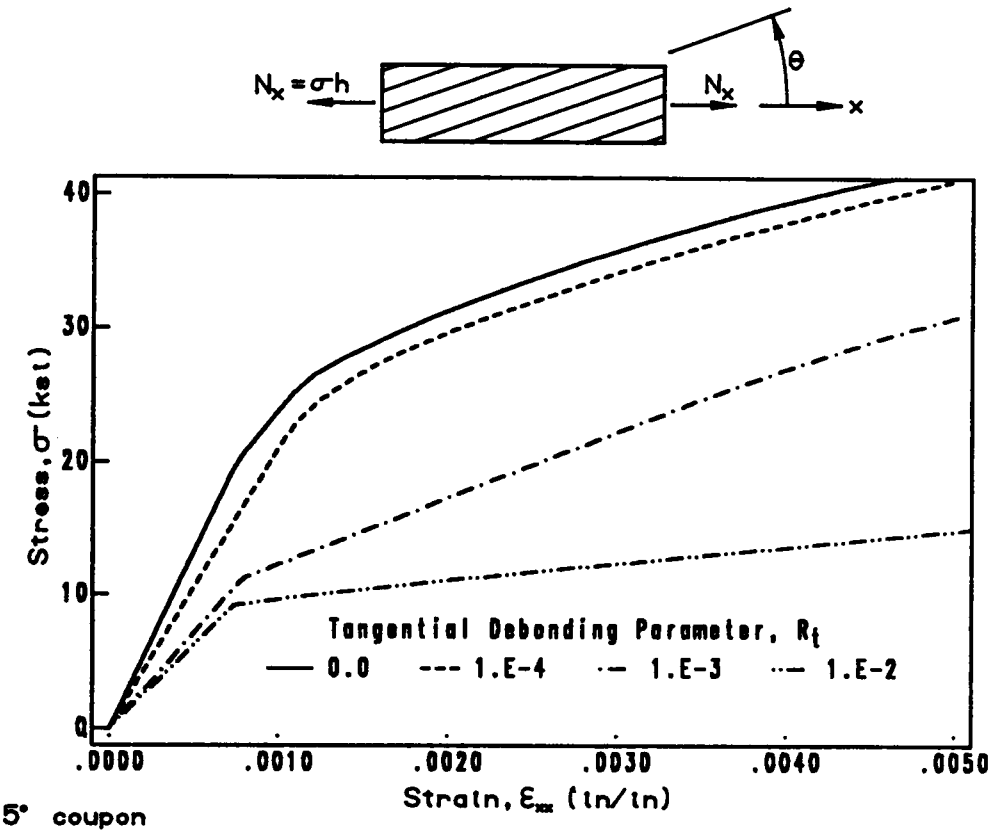

(a) 15° coupon

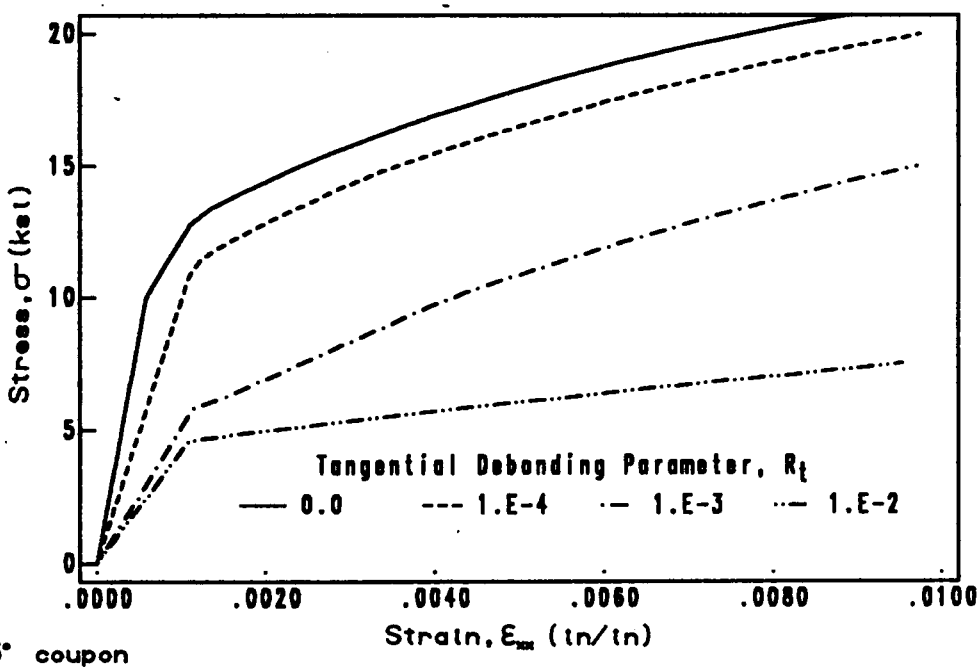

(b) 45° coupon

Figure 4.45. Effect of Tangential Fiber/Matrix Debonding on the Response of Off-Axis Test Coupons

examine these effects we shall consider the response of a boron/2024-T4 aluminum material system at 400°F. The constituent material properties used are given in Table 4.8. The boron properties are not significantly altered at this temperature so the room temperature properties from Table 4.5 are used. The 2024-T4 aluminum properties are from Ref. [47].

The effect of loading rate on a $[\pm 45]_S$ laminate is shown in Fig. 4.46. The rate of loading $\dot{\sigma}$ of the laminate ranges from 10^{-2} to 10^{2} ksi/sec. The effect of the loading rate displays a pronounced difference in maximum load by approximately 5 ksi. This effect is expected to be more significant at higher temperatures.

The creep response of a $[\pm 45]_S$ boron/aluminum laminate is shown in Fig. 4.47. A load of magnitude σ is applied to the laminate in the form of a step function at time, $t = 0$. For applied loads up to 38 ksi the observed creep behavior appears to be minimal. For loads greater than 38 ksi, the creep behavior becomes more apparent and is especially significant for loads greater than 44 ksi. Like rate dependent effects, creep behavior becomes more apparent at elevated temperatures.

The use of the Bodner-Partom unified plasticity theory adds considerable flexibility to the constitutive model presented in this research. The most notable attributes of this plasticity theory are its capabilities to predict rate dependence and creep response. Considering the current interest in metal matrix composites for high temperature structural applications, the Aboudi micromechanics theory used in conjunction with a unified plasticity theory such as the Bodner-Partom model produces a powerful analysis tool for these complex structures.

Table 4.8

Constituent Material Properties for
Boron/Aluminum at 400°F

Boron Properties

$E = 58.0$ msi

$\nu = 0.2$

Aluminum Properties

$E = 9.53$ msi

$\nu = 0.33$

$D_0 = 10^4$ sec^{-1}

$m = 300$

$n = 4$

$z_0 = 49.0$ ksi

$z_1 = 63.0$ ksi

Composite Properties

Viber Volume Fraction, $V_f = 0.45$

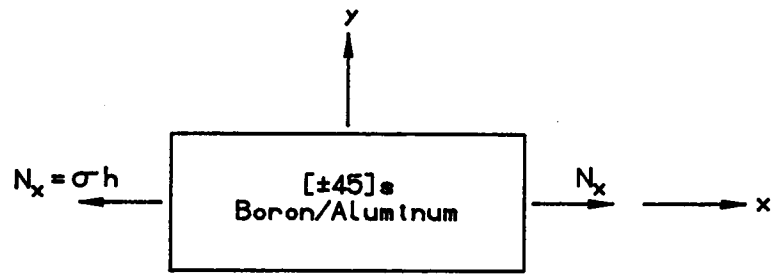

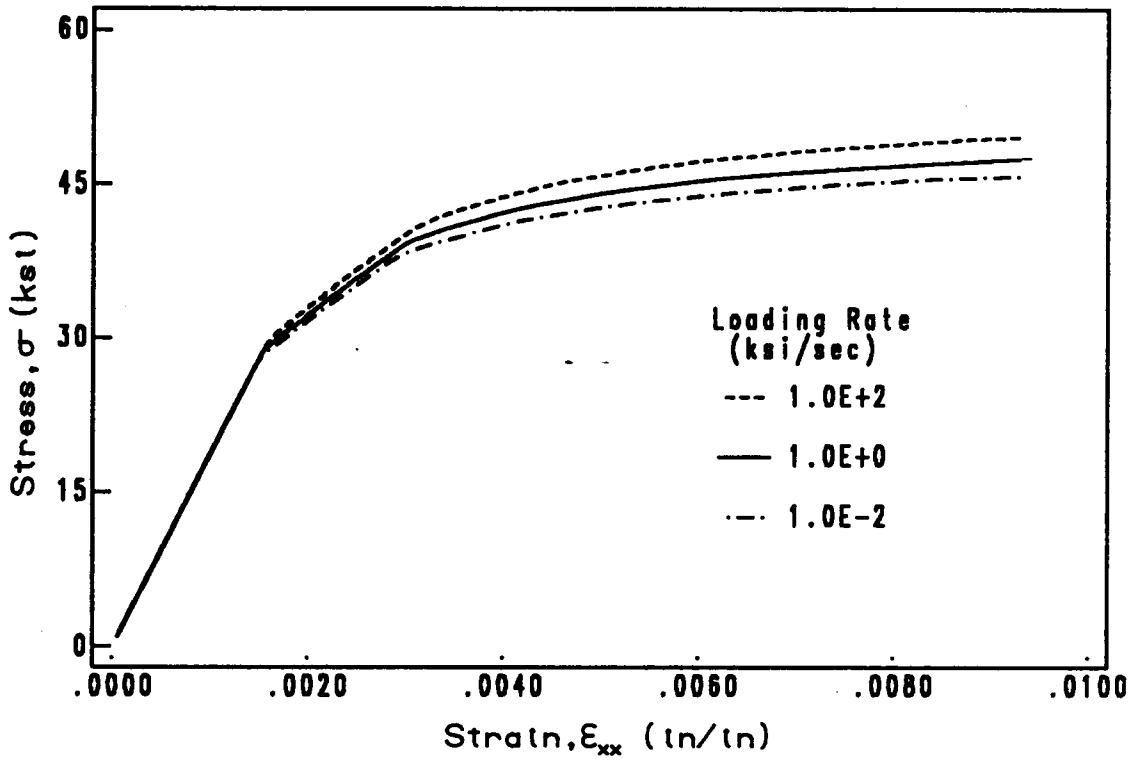

Figure 4.46. Effect of Loading Rate on a Boron/Aluminum Laminate

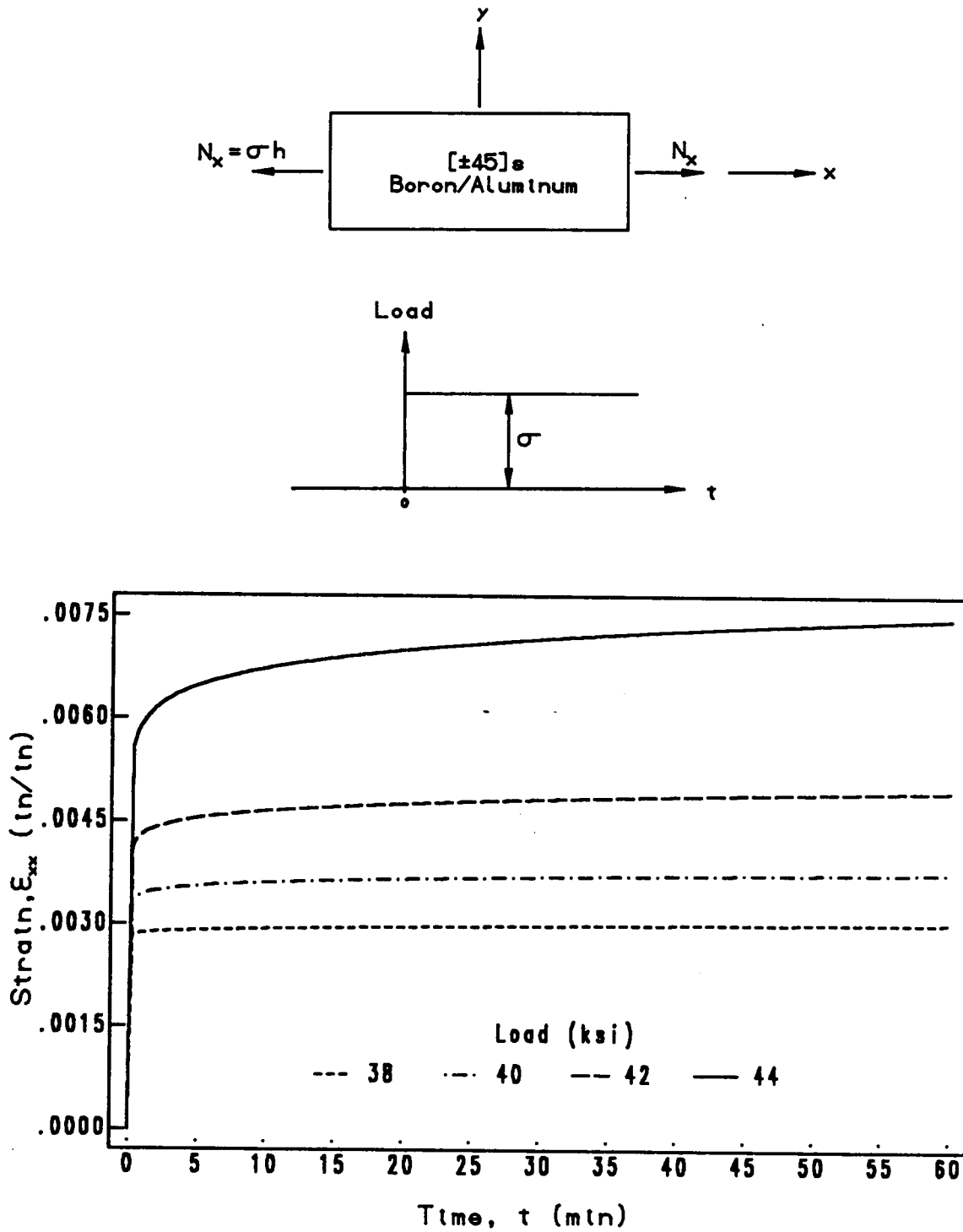

Figure 4.47. Creep Response of a Boron/Aluminum Laminate

Models such as these will be the focus of extensive research for the next several years.

5. SUMMARY AND CONCLUSIONS

A new formulation of the laminated plate constitutive relations is presented which are based on the Aboudi micromechanics theory in conjunction with the unified plasticity theory of Bodner and Partom. The resulting constitutive relations are incorporated into a finite element model by using a first-order shear deformation plate theory. This effort is the first implementation of the Aboudi micromechanics theory for the purpose of analyzing the inelastic behavior of composite structures.

The finite element solution is based on an initial strain formulation. The integration of the inelastic strains is performed by using either Euler's method or a predictor/corrector scheme. Numerical results indicate the Euler's method requires less computations for solutions requiring only moderate accuracy. Integration of the plastic stress resultants is performed by using Gauss-Legendre quadrature. For bending problems the quadrature method converges in a nonuniform manner, thus requiring additional care in selecting a suitable integration rule.

Several analyses are presented which illustrate the extensional and bending response of a metal matrix composite. In the analysis of a notched boron/aluminum test coupon very good correlation is observed between the analytical predictions and experimental data. The analysis of square and circular plates subjected to a transverse load shows a matrix failure transverse to the fibers which limited the response so that only small to moderate nonlinearities are observed. Other capabilities of the material model are demonstrated including the effects of fiber/matrix debonding, rate effects and creep response.

The Aboudi micromechanics theory provides a rational means for modeling the complex behavior typical of composite materials. The results presented indicate the Aboudi micromechanics theory has considerable potential and deserves continued investigation.

6. RECOMMENDATIONS FOR FUTURE WORK

Recommendations for future work are suggested in two general areas: the material model and the finite element model of the structure. Regarding the material model, the following areas could be considered for future work.

1. Further comparisons between the micromechanics model and experimental results for several additional material systems are needed to assess the overall accuracy of the micromechanics model.
2. Investigate the influence of the interphase region using the simple fiber/matrix interface model presented in this study. A significant portion of this work would consist of developing evolution type expressions which would describe the state or condition of the interphase as a function of the load history.
3. Failure theories could be included into the material model to predict post-first-ply failure. Using the micro-stress information provided by the micromechanics theory, suitable failure theories could be selected which are better suited for the individual constituents. Additionally the micromechanics theory could be extended to address compressive instabilities usually termed microbuckling or fiber kinking.

Concerning the finite elements model of the structure, several possible areas could be addressed for future work. Some of the more promising areas are listed below.

1. In order to address a larger class of aerospace type structures, the micromechanics model could be incorporated into a suitable shell theory.

2. If unified plasticity theories are to be used, improved solution strategies are required.
3. The structural model could be extended to include geometrically nonlinear and inertia effects for the purpose of analyzing the structural stability and transient response of metal matrix composite structures.
4. Considering the interest in metal matrix composites for structures at elevated temperatures, a suitable finite element model for the coupled thermal-structural response could be very valuable.

References

1. Christensen, R. M., Mechanics of Composite Materials, Wiley, New York, 1979.

2. Hashin, Z., Theory of Fiber Reinforced Materials, NASA CR-1974, March 1972.

3. Hill, R., "Theory of Mechanical Properties of Fiber-Strengthened Materials: II. Inelastic Behavior," J. Mech. Phys. Solids, Vol. 12, 1964, p. 213.

4. Hill, R., "Theory of Mechanical Properties of Fiber-Strengthened Materials: III. Self-Consistent Model," J. Mech. Phys. Solids, Vol. 13, 1965, p. 189.

5. Mulhern, J. F., Roger, T. G. and Spencer, A. J. M., "A Continuum Model for Fibre-Reinforced Plastic Materials," Proc. Roy. Soc., Series A, Vol. 301, 1967, p. 473.

6. Mulhern, J. F., Roger, T. G. and Spencer, A. J. M., "Cyclic Extension of an Elastic Fibre with an Elastic-Plastic Coating," J. Inst. Maths. Applics., Vol. 3, 1967, p. 21.

7. Mulhern, J. F., Roger, T. G. and Spencer, A. J. M., "A Continuum Theory of a Plastic-Elastic Fibre-Reinforced Material," Int. J. Engr. Sci., Vol. 7, 1969, p. 129.

8. Spencer, A. J. M., "A Continuum Theory of a Plastic-Rigid Solid Reinforced by Two Families of Inextensible Fibres," Q. J. Mech. Appl. Math., Vol. 23, 1970, p. 489.

9. Spencer, A. J. M., "Dynamics of Ideal Fibre-Reinforced Rigid-Plastic Beams," J. Mech. Phys. Solids, Vol. 22, 1974, p. 147.

10. Pipkin, A. C. and Rogers, T. G., "Plane Deformations of Incompressible Fiber-Reinforced Materials," J. Appl. Mech., Vol. 38, 1971, p. 634.

11. Rogers, T. G. and Pipkin, A. C., "Small Deflections of Fiber-Reinforced Beams and Slabs," J. Appl. Mech., Vol. 38, 1971, p. 1047.

12. Adams, D. F. and Doner, D. R., "Longitudinal Shear Loading of a Unidirectional Composite," J. Composite Materials, Vol. 1, January 1967, p. 4.

13. Adams, D. F., "Inelastic Analysis of a Unidirectional Composite Subjected to Transverse Normal Loading," J. Composite Materials, Vol. 4, July 1970, p. 310.

14. Adams, D. F., "Practical Problems Associated with the Application of the Finite Element Method to Composite Material Micromechanical Analyses," Fiber Science and Technology, Vol. 7, No. 2, 1974, p. 111.

15. Adams, D. F., "A Micromechanical Analysis of Crack Propagation in an Elastoplastic Composite Material," Fiber Science and Technology, Vol. 7, No. 4, 1974, p. 237.

16. Adams, D. F. and Miller, A. K., "Hygrothermal Microstresses in a Unidirectional Composite Exhibiting Inelastic Material Behavior," J. Composite Materials, Vol. 11, No. 3, 1977, p. 285.

17. Adams, D. F. and Miller, A. K., "Inelastic Finite Element Analysis of a Heterogeneous Medium Exhibiting Temperature and Moisture Dependent Material Properties," Fiber Science and Technology, Vol. 13, No. 2, 1980, p. 135.

18. Murphy, D. P. and Adams, D. F., "Energy Absorption Mechanisms During Crack Propagation in Metal Composites," Department Report UWME-DR-901-103-1, Department of Mechanical Engineering, University of Wyoming, Laramie, Wyoming, June, 1979.

19. Adams, D. F. and Crane, D. A., "Finite Element Micromechanics Analysis of a Unidirectional Composite Including Longitudinal Shear Loading," Computers and Structures, Vol. 18, No. 6, 1984, p. 1153.

20. Dvorak, G. J., Rao, M. S. M. and Tarn, J. Q., "Yielding in Unidirectional Composites Under External Loads and Temperature Changes," J. Composite Materials, Vol. 7, 1973, p. 194.

21. Dvorak, G. J., Rao, M. S. M. and Tarn, J. Q., "Generalized Initial Yield Surfaces for Unidirectional Composites," J. Appl. Mech., Vol. 41, 1974, p. 249.

22. Dvorak, G. J. and Rao, M. S. M., "Axisymmetric Plasticity Theory of Fibrous Composites," Int. J. Engng. Sci., Vol. 14, 1976, p. 361.

23. Dvorak, G. J. and Rao, M. S. M., "Thermal Stress in Heat-Treated Fibrous Composites," J. Appl. Mech., Vol. 43, 1976, p. 619.

24. Dvorak, G. J. and Bahei-El-Din, Y. A., "Elastic-Plastic Behavior of Fibrous Composites," J. Mech. Phys. Solids, Vol. 27, 1979, p. 51.

25. Dvorak, G. J. and Bahei-El-Din, Y. A., "Plasticity of Composite Laminates," Proceedings of the Research Workshop on Mechanics of Composite Materials, Dvorak, G. J., ed., Duke University, October 1978, p. 32.

26. Dvorak, G. J. and Bahei-El-Din, Y. A., "Plasticity Analysis of Fibrous Composites," J. Appl. Mech., Vol. 49, 1982, p. 327.

27. Bahei-El-Din, Y. A., Dvorak, G. J. and Utku, S., "Finite Element Analysis of Elastic-Plastic Fibrous Composite Structures," Computers and Structures, Vol. 13, 1981, p. 321.

28. Bahei-El-Din, Y. A. and Dvorak, G. J., "Plastic Yielding at a Circular Hole in a Laminated FP-Al Plate," Modern Development in Composite Materials and Structures, Vinson, J. R., ed., The American Society of Mechanical Engineers, 1979, p. 123.

29. Bahei-El-Din and Y. A. Dvorak, "Plasticity Analysis of Laminated Composite Plates," J. Appl. Mech., Vol. 49, 1982, p. 740.

30. Hutchinson, J. W., "Elastic-Plastic Behavior of Poplycrystalline Metals and Composites," Proc. Roy. Soc., Series A, Vol. 319, 1970, p. 247.

31. Bahei-El-Din, Y. A., Plasticity Analysis of Metal-Matrix Composite Laminates, Ph.D. Dissertation, Duke University, 1979.

32. Rao, M. S. M., Plasticity Theory of Fiber-Reinforced Metal Matrix Composites, Ph.D. Dissertation, Duke University, 1974.

33. Min, K. B. and Crossman, F. W., "History-Dependent Thermomechanical Properties of Graphite/Aluminum Unidirectional Composites," Composite Materials: Testing and Design [Sixth Conference], ASTM STP 787, Danial, I. M., ed., Americal Society for Testing and Materials, 1982, p. 371.

34. Min, K. B. and Flaggs, D. L., "A Non-Isothermal Plasticity Analysis of Composite Laminates," Mechanics of Composite Materials - 1983, Proceedings of the Symposium, Boston, MA, November 13-18, 1983, American Society of Mechanical Engineers, p. 51.

35. Min, K. B. and Flaggs, D. L., "A Thermomechanical Elastoplastic Analysis of Fibrous Composite Laminates," to appear in J. Mech. Phys. Solids.

36. Hunsaker, B., Jr., Vaughan, D. K., Stricklin, J. A. and Haisler, W. E., "A Comparison of Current Work-Hardening Models Used in the Analysis of Plastic Defrmation," TEES-RPT-2926-73-3, October 1973, Aerospace Engineering Department, Texas A&M University, College Station, Texas.

37. Wolf, E. G., Min, K. B. and Kural, M. H., "Thermal Cycling of a Unidirectional Graphite/Magnesium Composites," J.Materials Science, Vol. 20, April 1985, p. 1141.

38. Ruffin, A. C., Rimbos, P. G. and Bigelow, S. D., "Point-Stress Analysis of Continuous Fiber-Reinforced Composite Materials With an Elastic-Plastic Matrix," Computers and Structures, Vol. 20, 1985, p. 375.

39. Aboudi, J., "A Continuum Theory for Fiber-Reinforced Elastic-Viscoplastic Composites," Int. J. Engng. Sci., Vol. 20, 1982, p. 605.

40. Aboudi, J., "Effective Constitutive Equations for Fiber-Reinforced Viscoplastic Composites Exhibiting Anisotropic Hardening," Int. J. Engng. Sci., Vol. 21, 1983, p. 1081.

41. Aboudi, J., "Effective Moduli of Short-Fiber Composites," Int. J. Solids and Structures, Vol. 19, 1983, p. 693.

42. Aboudi, J., "Effective Behavior of Inelastic Fiber-Reinforced Composites," Int. J. Engng. Sci., Vol. 22, 1984, p. 439.

43. Aboudi, K. and Benveniste, Y., "Constitutive Relations for Fiber-Reinforced Inelastic Laminated Plates," J. Appl. Mech., Vol. 51, 1984, p. 107.

44. Benveniste, Y. and Aboudi, J., "A Continuum Model for Fiber Reinforced Materials with Debonding," Int. J. Solids and Structures, Vol. 20, 1984, p. 935.

45. Aboudi, J., "Effective Thermomechanical Behavior of Inelastic Fiber-Reinforced Materials," Int. J. Engng. Sci., Vol. 23, 1985, p. 773.

46. Aboudi, J., "Inelastic Behaviour of Metal-Matrix Composites at Elevated Temperature," Int. J. Plasticity, Vol. 1, 1985, p. 359.

47. Aboudi, J., "Elastoplasticity Theory for Composite Materials," Solid Mech. Arch., Vol. 11, 1986, p. 141.

48. Aboudi, J., "Damage in Composites: Modeling of Imperfect Bonding," Composite Sci. Tech., to appear.

49. Bodner, S. R. and Partom, Y., "Constitutive Equations for Elastic-Viscoplastic Strain-Hardening Materials," J. Appl. Mech., Vol. 42, 1975, p. 385.

50. Foye, R. L., "Theoretical Post-Yielding Behavior of Composite Laminates Part I - Inelastic Micromechanics," J. Composite Materials, Vol. 7, 1973, p. 178.

51. Hashin, Z. and Humphreys, E. A., Material Science Corporation TPR 1130/1502, 1980 and TFR 1214/1502, 1981.

52. Petit, P. H. and Waddoups, M. E., "A of Predicting the Nonlinear Behavior of Laminated Composites," J. Composite Materials, Vol. 3, 1969, p. 2.

53. Hahn, H. T. and Tsai, S. W., "Nonlinear Elastic Behavior of Unidirectional Composite Laminate," J. Composite Materials, Vol. 7, 1973, p. 102.

54. Hahn, H. T., "Nonlinear Behavior of Laminated Composites," J. Composite Materials, Vol. 7, 1973, p. 257.

55. Hashin, Z., Rosen, B. W. and Bagchi, D., "Non-Linear Behavior of Fiber Composite Laminates," NASA CR-2313, April 1974.

56. Jones, R. M. and Nelson, D. A. R., Jr., "A New Material Model for the Nonlinear Biaxial Behavior of ATJ-S Graphite," J. Composite Materials, Vol. 9, January 1975, p. 10.

57. Jones, R. M. and Morgan, H. S., "Analysis of Nonlinear Behavior of Fiber-Reinforced Composites," J. Composite Materials, Vol. 15, December 1977.

58. Hill, R., "A Theory of the Yielding and Plastic Flow of Anisotropic Metals," Proc. Roy. Soc., Vol. 193, No. 1033, 1948, p. 189.

59. Hill, R., The Mathematical Theory of Plasticity, Oxford University Press, 1950.

60. Hu, L. W., "Studies on Plastic Flow of Anisotropic Metals," J. Appl. Mech., September 1956.

61. Jensen, W. R., Falby, W. E. and Prince, N., "Matrix Analysis for Anisotropic Inelastic Materials," AFFDL-TR-65-220, 1966.

62. Dubey, R. N. and Hillier, M. J., "Yield Criteria and Bauschinger Effect for a Plastic Solid," J. Basic Engineering, Paper No. 711-MET-p., March 1972.

63. Shih, C. F. and Lee, D., "Further Developments in Anisotropic Plasticity," J. Engineering Materials and Technology, Vol. 100, July 1978, p. 294.

64. Pifko, P., Levine, H. S. and Armen, H., Jr., "PLANS-A Finite Element Program for Nonlinear Analysis of Structures," NASA CR-2568, 1975.

65. Chou, P. C. and Chou, D. K., "Plastic Flow Rule of Laminated Composites," J. Composite Materials, Vol. 10, January 1976, p. 55.

66. Chou, P. C., Carleone, J. and Hsu, C. M., "Elastic Constants of Layered Media," J. Composite Materials, Vol. 6, 1972, p. 80.

67. Renieri, G. D. and Herakovich, C. T., "Nonlinear Analysis of Laminated Fibrous Composites," VPI-E-76-10, Engineering Science and Mechanics Department, Virginia Polytechnic Institute and State University, Blacksburg, Virginia, 1976.

68. Griffin, O. H., "Three-Dimensional Inelastic Finite Element Analysis of Laminated Composites," Ph.D. Dissertation, Virginia Polytechnic Institute and State University, Blacksburg, Virginia, 1980.

69. Chandrashekhara, K., "Geometric and Material Nonlinear Analysis of Laminated Composite Plates and Shells," Ph.D. Dissertation, Virginia Polytechnic Institute and State University, Blacksburg, Virginia, 1985.

70. Pindera, M. J. and Herakovich, C. T., "An Endochronic Model for the Response of Unidirectional Composites Under Off-Axis Tensile Loads," Mechanics of Composite Materials: Recent Advances, Proceedings of the IUTAM Symposium on Mechanics of Composite Materials, Hashin, Z. and Herakovich, C. T., eds., Virginia Polytechnic Institute and State University, Blacksburg, Virginia, August 1982.

71. Valanis, K. C., "Fundamental Consequences of a New Intrinsic Time Measure: Plasticity as a Limit of the Endochronic Theory," Arch. of Mech., Vol. 32, 1980, p. 171.

72. Zinov'ev, P. A. and Sarbaev, B. S., "Endochronic Theory of Nonlinear Deformation of Laminated Composite Materials," Mechanics of Composite Materials, (Translated from Russian), Vol. 21, No. 3, 1985, p. 278.

73. Wren, G. and Allen, D. H., "Development of a Theoretical Framework for Constitutive Equations for Metal Matrix Composites with Damage," MM 4875-85-9, June 1985, Mechanics and Materials Center, Texas A&M University, College Staion, Texas.

74. Jones, J. P. and Whittier, J. S., "Waves at a Flexably Bonded Interface," J. Appl. Mech., Vol. 34, 1967, p. 905.

75. Benveniste, Y., "The Effective Mechanical Behavior of a Composite Material With Imperfect Contact Between the Constituents," Mech. Mater., Vol. 4, 1985, p. 197.

76. Bodner, S. R., "Review of a Unified Elastic-Viscoplastic Theory," in Unified Constitutive Equations for Plastic Deformations and Creep of Engineering Alloys, Miller, A. K. (Ed.), Elsevier Applied Sciences Pubishers, 1986.

77. Aboudi, J., "Closed Form Constitutive Equations for Metal Matrix Composites," Int. J. Engng. Sci., Vol. 25, 1987, p. 1229.

78. Aboudi, J., "Constitutive Equations for Elastoplastic Composites with Imperfect Bonding," Int. J. Plasticity, June, 1988.

79. Pindera, M-J., Aboudi, J. and Herakovich, C. T., "Nonlinear Response of Boron/Aluminum Under Combined Loading," Proceedings of the IUTAM/ICM Symposium on Yielding, Damage and Failure of Anisotropic Solids, Grenoble, France, August, 1987.

80. Hildebrand, F. B., Reissner, E. and Thomas, G. B., "Notes on the Foundations of the Theory of Small Displacements of Orthotropic Shells," NACA Technical Note No. 1833, March 1949.

81. Mindlin, R. D., "Influence of Rotary Inertia and Shear on Flexural Motions of Isotropic, Elastic Plates," J. Appl. Mech., Vol. 18, 1951, p. 31.

82. Whitney, J. M., Structural Analysis of Laminated Anisotropic Plates, Technomic, Lancaster, Pennsylvania, 1987.

83. Jones, R. M., Mechanics of Composite Materials, McGraw-Hill, New York, 1975.

84. Reddy, J. N., Energy and Variational Methods in Applied Mechanics, Wiley, New York, 1984.

85. Zienkiewicz, O. C., The Finite Element Method, 3rd ed., McGraw-Hill, London, 1977.

86. Stroud, A. H. and Secrest, D., Gaussian Quadrature Formulas, Prentice-Hall, Englewood Cliffs, N.J., 1966.

87. Cormeau, I. C., Viscoplasticity and Plasticity in the Finite Element Method, Ph.D. Thesis, University of Wales, Swansea, March, 1976.

88. Banthia, V. and Mukherjee, S., "On an Improved Time Integration Scheme for Stiff Constitutive Models of Inelastic Deformation," J. Eng. Mat. Tech., V. 107, October, 1985, p. 282.

89. Shampine, L. F. and Gordon, M. K., Computer Solution of Ordinary Differential Equations, Freeman and Company, San Francisco, 1975.

90. Shampine, L. F. and Watts, H. A., "DEPAC-Design of a User Oriented Package of ODE Solvers," Report No. SAND79-2374, Sandia Laboratories, Alburquerque, New Mexico.

91. Pindera, M-J. and Lin, M. W., "Micromechanical Analysis of the Elastoplastic Response of Metal Matrix Composites," ASME Pressure Vessels and Piping Conference, Pittsburg, PA, June 19-23, 1988.

92. Prager, W. and Hodge, P. G., Theory of Perfecty Plastic Solids, Wiley, New York, 1951.

93. Shukow, S. I., Acoustic/Mechanical Characterization of Boron/Aluminum Composite Laminates, M. S. Thesis, University of Delaware, June, 1978.

94. Becker, W., Mechanical Response of Undirectional Boron/Aluminum Under Combined Loading, M.S. Thesis, Virginia Polytechnic Institute and State University, Blacksburg, Virginia, 1987.

APPENDIX A

The element equations for the finite element model are

$$[K^e]\{\Delta^e\} = \{\hat{F}^e\} + \{F_p^e\} + \{F_T^e\}$$

where

$$[K^e] = \begin{bmatrix} \underset{\sim}{K}^{11} & \underset{\sim}{K}^{12} & \underset{\sim}{K}^{13} & \underset{\sim}{K}^{14} & \underset{\sim}{K}^{15} \\ & \underset{\sim}{K}^{22} & \underset{\sim}{K}^{23} & \underset{\sim}{K}^{24} & \underset{\sim}{K}^{25} \\ & & \underset{\sim}{K}^{33} & \underset{\sim}{K}^{34} & \underset{\sim}{K}^{35} \\ & & & \underset{\sim}{K}^{44} & \underset{\sim}{K}^{45} \\ \text{(symmetric)} & & & & \underset{\sim}{K}^{55} \end{bmatrix}$$

$$\{\Delta^e\} = \begin{Bmatrix} \underset{\sim}{u}^e \\ \underset{\sim}{v}^e \\ \underset{\sim}{w}^e \\ \underset{\sim}{\psi}_x^e \\ \underset{\sim}{\psi}_y^e \end{Bmatrix}, \qquad \{\hat{F}^e\} = \begin{Bmatrix} \underset{\sim}{\hat{F}}^1 \\ \underset{\sim}{\hat{F}}^2 \\ \underset{\sim}{\hat{F}}^3 \\ \underset{\sim}{\hat{F}}^4 \\ \underset{\sim}{\hat{F}}^5 \end{Bmatrix}$$

$$\{F_p^e\} = \begin{Bmatrix} \underset{\sim}{F}_P^1 \\ \underset{\sim}{F}_P^2 \\ \underset{\sim}{F}_P^3 \\ \underset{\sim}{F}_P^4 \\ \underset{\sim}{F}_P^5 \end{Bmatrix}, \qquad \{F_T^e\} = \begin{Bmatrix} \underset{\sim}{F}_T^1 \\ \underset{\sim}{F}_T^2 \\ \underset{\sim}{F}_T^3 \\ \underset{\sim}{F}_T^4 \\ \underset{\sim}{F}_T^5 \end{Bmatrix}$$

The elements of these are defined as

$$\underset{\sim}{K}^{11} = \underset{\sim}{S}^{xx}A_{11} + (\underset{\sim}{S}^{xy} + \underset{\sim}{S}^{yx})A_{13} + \underset{\sim}{S}^{yy}A_{33}$$

$$\underset{\sim}{K}^{12} = \underset{\sim}{S}^{xx}A_{13} + \underset{\sim}{S}^{xy}A_{12} + \underset{\sim}{S}^{yx}A_{33} + \underset{\sim}{S}^{yy}A_{23}$$

$$\underset{\sim}{K}^{14} = \underset{\sim}{S}^{xx}B_{11} + (\underset{\sim}{S}^{xy} + \underset{\sim}{S}^{yx})B_{13} + \underset{\sim}{S}^{yy}B_{33}$$

$$\underset{\sim}{K}^{15} = \underset{\sim}{S}^{xx}B_{16} + \underset{\sim}{S}^{xy}B_{12} + \underset{\sim}{S}^{yx}B_{33} + \underset{\sim}{S}^{yy}B_{23}$$

$$\underset{\sim}{K}^{22} = \underset{\sim}{S}^{xx}A_{33} + (\underset{\sim}{S}^{xy} + \underset{\sim}{S}^{yx})A_{23} + \underset{\sim}{S}^{yy}A_{22}$$

$$\underset{\sim}{K}^{24} = \underset{\sim}{S}^{xx}B_{13} + \underset{\sim}{S}^{xy}B_{33} + \underset{\sim}{S}^{yx}B_{12} + \underset{\sim}{S}^{yy}B_{23}$$

$$\underset{\sim}{K}^{25} = \underset{\sim}{S}^{xx}B_{33} + (\underset{\sim}{S}^{xy} + \underset{\sim}{S}^{yx})B_{23} + \underset{\sim}{S}^{yy}B_{22}$$

$$\underset{\sim}{K}^{33} = \underset{\sim}{S}^{xx}A^{s}_{11} + (\underset{\sim}{S}^{xy} + \underset{\sim}{S}^{yx})A^{s}_{12} + \underset{\sim}{S}^{yy}A^{s}_{22}$$

$$\underset{\sim}{K}^{34} = \underset{\sim}{S}^{xo}A^{s}_{11} + \underset{\sim}{S}^{yo}A^{s}_{12}$$

$$\underset{\sim}{K}^{35} = \underset{\sim}{S}^{xo}A^{s}_{12} + \underset{\sim}{S}^{yo}A^{s}_{22}$$

$$\underset{\sim}{K}^{44} = \underset{\sim}{S}^{xx}D_{11} + (\underset{\sim}{S}^{xy} + \underset{\sim}{S}^{yx})D_{13} + \underset{\sim}{S}^{yy}D_{33} + \underset{\sim}{S}^{oo}A^{s}_{11}$$

$$\underset{\sim}{K}^{45} = \underset{\sim}{S}^{xx}D_{13} + \underset{\sim}{S}^{xy}D_{12} + \underset{\sim}{S}^{yx}D_{33} + \underset{\sim}{S}^{yy}D_{23} + \underset{\sim}{S}^{oo}A^{s}_{12}$$

$$\underset{\sim}{K}^{55} = \underset{\sim}{S}^{xx}D_{66} + (\underset{\sim}{S}^{xy} + \underset{\sim}{S}^{yx})D_{23} + \underset{\sim}{S}^{yy}D_{22} + \underset{\sim}{S}^{oo}A^{s}_{22}$$

$$\underset{\sim}{K}^{13} = \underset{\sim}{K}^{23} = \underset{\sim}{\theta} \quad \text{(zero matrix)}$$

$$\hat{F}_3 = \underset{\sim}{S}^{o}q$$

$$\hat{\underset{\sim}{F}}_1 = \hat{\underset{\sim}{F}}_2 = \hat{\underset{\sim}{F}}_4 = \hat{\underset{\sim}{F}}_5 = \underset{\sim}{0} \quad \text{(zero vector)}$$

$$\underset{\sim}{F}^{1}_{P} = \underset{\sim}{S}^{x}\, N^{P}_{x} + \underset{\sim}{S}^{y}\, N^{P}_{xy}$$

$$\underset{\sim}{F}^{2}_{P} = \underset{\sim}{S}^{x}\, N^{P}_{xy} + \underset{\sim}{S}^{y}\, N^{P}_{y}$$

$$\underset{\sim}{F}^{3}_{P} = \underset{\sim}{S}^{x}\, Q^{P}_{x} + \underset{\sim}{S}^{y}\, Q^{P}_{y}$$

$$\underset{\sim}{F}_P^4 = \underset{\sim}{S}^x M_x^P + \underset{\sim}{S}^y M_{xy}^P + \underset{\sim}{S}^o Q_x^P$$

$$\underset{\sim}{F}_P^5 = \underset{\sim}{S}^x M_{xy}^P + \underset{\sim}{S}^y M_y^P + \underset{\sim}{S}^o Q_y^P$$

$$\underset{\sim}{F}_T^1 = \underset{\sim}{S}^x N_x^T + \underset{\sim}{S}^y N_{xy}^T$$

$$\underset{\sim}{F}_T^2 = \underset{\sim}{S}^x N_{xy}^T + \underset{\sim}{S}^y N_y^T$$

$$\underset{\sim}{F}_T^3 = \underset{\sim}{0}$$

$$\underset{\sim}{F}_T^4 = \underset{\sim}{S}^x M_x^T + \underset{\sim}{S}^y M_{xy}^T$$

$$\underset{\sim}{F}_T^5 = \underset{\sim}{S}^x M_{xy}^T + \underset{\sim}{S}^y M_y^T$$

where $\underset{\sim}{S}^{\xi\eta}$ and $\underset{\sim}{S}^{\xi}$ are the integral operators

$$S_{ij}^{\xi\eta}(\cdot) = \int_{R^e} (\cdot) \frac{\partial \phi_i}{\partial \xi} \frac{\partial \phi_j}{\partial \eta} \, dxdy \quad , \quad \xi, \eta = 0,x,y$$

$$S_i^{\xi}(\cdot) = \int_{R^e} (\cdot) \frac{\partial \phi_i}{\partial \xi} \, dxdy \quad , \quad i, j = 1,2,3,\ldots,r$$

These operate on the term which follows immediately, for example

$$\underset{\sim}{S}^{xx} A_{11} = \int_{R^e} A_{11} \frac{\partial \phi_i}{\partial x} \frac{\partial \phi_j}{\partial x} \, dxdy$$

The vita has been removed from the scanned document